

DESIGN OF A HIGH PRECISION HYBRID AM MACHINE

A THESIS SUBMITTED TO
THE GRADUATE SCHOOL OF NATURAL AND APPLIED SCIENCES
OF
MIDDLE EAST TECHNICAL UNIVERSITY

BY

YUNUS EMRE YILMAZ

IN PARTIAL FULFILLMENT OF THE REQUIREMENTS
FOR
THE DEGREE OF MASTER OF SCIENCE
IN
MECHANICAL ENGINEERING

AUGUST 2019

Approval of the thesis:

DESIGN OF A HIGH PRECISION HYBRID AM MACHINE

submitted by **YUNUS EMRE YILMAZ** in partial fulfillment of the requirements for the degree of **Master of Science in Mechanical Engineering Department, Middle East Technical University** by,

Prof. Dr. Halil Kalıpçılar
Dean, Graduate School of **Natural and Applied Sciences**

Prof. Dr. M. A. Sahir Arıkan
Head of Department, **Mechanical Engineering**

Assoc. Prof. Dr. Melik Dölen
Supervisor, **Mechanical Engineering, METU**

Assist. Prof. Dr. Ulaş Yaman
Co-Supervisor, **Mechanical Engineering, METU**

Examining Committee Members:

Prof. Dr. Ender Ciğeroğlu
Mechanical Engineering, METU

Assoc. Prof. Dr. Melik Dölen
Mechanical Engineering, METU

Assist. Prof. Dr. Ulaş Yaman
Mechanical Engineering, METU

Assist. Prof. Dr. A. Buğra Koku
Mechanical Engineering, METU

Assist. Prof. Dr. Kutluk Bilge Arıkan
Mechanical Engineering, TED University

Date: 29.08.2019

I hereby declare that all information in this document has been obtained and presented in accordance with academic rules and ethical conduct. I also declare that, as required by these rules and conduct, I have fully cited and referenced all material and results that are not original to this work.

Name, Surname: Yunus Emre Yılmaz

Signature:

ABSTRACT

DESIGN OF A HIGH PRECISION HYBRID AM MACHINE

Yılmaz, Yunus Emre
Master of Science, Mechanical Engineering
Supervisor: Assoc. Prof. Dr. Melik Dölen
Co-Supervisor: Assist. Prof. Dr. Ulaş Yaman

August 2019, 149 pages

Precision requirements in fused deposition modelling (FDM) processes have been increasing in recent years, especially after recognizing the potential of FDM process to produce complex and functional components. In order to increase precision of FDM process, 6-axis hybrid manufacturing system, which can carry out additive- and subtractive manufacturing processes in one manufacturing system platform, is designed. During design, kinematic analysis of the machine is done, axial- and angular errors are estimated by Monte Carlo simulation and components of linear- and rotary bearings are selected based on the model constructed to identify the axial and radial errors of the linear- and rotary axis. Furthermore, other machine components such as structures and transmission and actuation as well as sensor selection processes are explained. The components of the structure, four linear axes and the rotary stage components are manufactured and assembled, while spindle and extruder head planned to be manufactured in near future.

Keywords: Precision Machine Design, Hybrid Manufacturing, Error Budget, Modular Design, Additive and Subtractive Manufacturing

ÖZ

YÜKSEK HASSASİYETLİ MELEZ EKLEMELİ İMALAT MAKİNESİ

Yılmaz, Yunus Emre
Yüksek Lisans, Makina Mühendisliği
Tez Danışmanı: Doç. Dr. Melik Dölen
Ortak Tez Danışmanı: Dr. Öğr. Üyesi Ulaş Yaman

Ağustos 2019, 149 sayfa

Birleştirmeli yığılma modellemesi işlemlerinde hassasiyet gereksinimleri son yıllarda, özellikle birleştirmeli yığılma modellemesi işleminin karmaşık ve fonksiyonel bileşenler üretme potansiyeli tanındıktan sonra artmaktadır. Birleştirmeli yığılma modellemesi işleminin hassasiyetini arttırmak için, tek bir üretim sistemi platformunda katkı ve çıkarma üretim işlemlerini gerçekleştirebilen 6 eksenli hibrit üretim sistemi tasarlanmıştır. Tasarım sırasında, makinenin kinematik analizi yapıp, Monte Carlo simülasyonu ile aksel ve açısal hatalar tahmin edilmiş ve lineer ve döner aksellerin aksel ve radyal hatalarını bulmak için yapılan modele göre doğrusal ve döner yatakların bileşenleri seçilmiştir. Ayrıca, karkas yapı, tahrik ve iletim sistemleri gibi diğer makine bileşenleri ile sensör seçim süreçleri açıklanmaktadır. Yapının bileşenleri, dört doğrusal eksen ve döner eksen bileşenleri üretilip ve monte edilirken, iş mili ve ekstrüder kafasının yakın gelecekte üretilmesi planlanmaktadır.

Anahtar Kelimeler: Hassas Makine Tasarımı, Hibrit Üretim, Modüler Tasarım, Eklemeli ve Çıkarmalı Üretim

Dedicated with love to my grandmother.

ACKNOWLEDGEMENTS

I would like to deeply thank my supervisor Assoc. Prof. Dr. Melik Dölen and co-supervisor Assist. Prof. Dr. Ulaş Yaman for their continuous support, guidance and encouragement along my thesis work. They have motivated me to work hard and complete my thesis.

I would also like to thank the Scientific and Technological Research Council of Turkey (TÜBİTAK) for financially supporting my thesis project under the code 117M429 as well as Modesis Makina Elektronik & Bilişim Teknolojileri and their hard-working employees, especially Onur Yarkınoğlu, for continuous and valuable help in design and manufacturing.

Finally, I would never be able to complete my thesis without strong support of my closest family members and friends, especially Maja Maver, who have helped and assisted me along the way.

TABLE OF CONTENTS

ABSTRACT	v
ÖZ	vi
ACKNOWLEDGEMENTS	viii
TABLE OF CONTENTS	ix
LIST OF TABLES	xiv
LIST OF FIGURES.....	xvi
LIST OF ABBREVIATIONS	xx
LIST OF SYMBOLS	xxi
CHAPTERS	
1. INTRODUCTION	1
1.1. Motivation and Goals	1
1.2. Scope of the Thesis.....	2
2. LITERATURE SURVEY	3
2.1. Introduction	3
2.2. Structures.....	5
2.2.1. Cast Structures	5
2.2.2. Welded Structures.....	5
2.2.3. Bolted Structures.....	7
2.2.4. Glued Structures	7
2.2.5. Composite Structures.....	8
2.2.5.1. Granite Structures.....	8
2.2.5.2. Polymer Concrete Structures.....	9

2.2.5.3. Concrete Structures.....	10
2.2.5.4. Carbon Fiber	10
2.3. Linear Stages.....	10
2.3.1. Linear Bearing Systems.....	10
2.3.1.1. Hydrodynamic	10
2.3.1.2. Hydrostatic.....	11
2.3.1.3. Aerodynamic.....	13
2.3.1.4. Aerostatic	13
2.3.1.5. Roller Bearing Systems	14
2.3.1.6. Magnetic Bearings	15
2.3.2. Actuation and Transmission System	15
2.3.2.1. Linear Motor	16
2.3.2.2. Lead Screw	17
2.3.2.3. Ball Screw.....	17
2.3.2.4. Rack and Pinion in Combination with Motor.....	18
2.3.2.5. Belt Drive.....	18
2.3.2.6. Planetary Roller Screw	18
2.3.2.7. Friction Drives	19
2.3.3. Sensor Systems.....	20
2.3.3.1. Direct Measurement.....	20
2.3.3.2. Indirect Measurement	23
2.4. Rotary Stages	24
2.4.1. Rotary Bearing Systems	24
2.4.1.1. Hydrodynamic	24

2.4.1.2. Hydrostatic	24
2.4.1.3. Aerodynamic	25
2.4.1.4. Aerostatic	25
2.4.1.5. Roller Bearing Systems.....	26
2.4.1.6. Magnetic Bearings	27
2.4.2. Actuation and Transmission System.....	28
2.4.2.1. Direct Drive.....	28
2.4.2.2. Gearbox	29
2.4.2.3. Belt Drive and Motor	31
2.4.2.4. Roller Gear Cam	31
2.4.2.5. Friction Drives	33
2.4.3. Sensor Systems	35
2.4.3.1. Optical Position Systems.....	35
2.5. Spindles	35
2.6. Hybrid Printer Systems.....	39
3. DESIGN OF HYBRID MANUFACTURING SYSTEM	43
3.1. Introduction	43
3.2. Concept Selection.....	44
3.3. Dimensional Analysis.....	47
3.3.1. Dimensional Analysis along X Direction	47
3.3.2. Dimensional Analysis along Y Direction	48
3.3.3. Dimensional Analysis along Z Direction.....	49
3.4. Kinematic Analysis and Error Budget.....	50
3.4.1. Error Budget	54

3.5. Structures	56
3.5.1. Static- and Modal Analysis	57
3.6. Linear Stages.....	62
3.6.1. Structures.....	62
3.6.2. Actuation and Transmission.....	62
3.6.2.1. Feed Screw Bearing System	67
3.6.3. Linear Bearing System	68
3.6.3.1. Accuracy of the Linear Bearings	68
3.6.3.2. Force Analysis of Horizontal Linear Bearings	76
3.6.3.3. Force Analysis of Vertical Linear Bearings	78
3.6.3.4. Life of the Linear Bearings.....	80
3.6.4. Final Design	81
3.7. Rotary Stages	82
3.7.1. Structures.....	82
3.7.2. Actuation and Transmission.....	82
3.7.2.1. Force Analysis of Actuation and Transmission System	83
3.7.3. Rotary Bearing System.....	85
3.7.3.1. Accuracy of the Rotary Bearings.....	85
3.7.3.2. Force analysis of C axis.....	91
3.7.3.3. Force Analysis of B axis.....	96
3.7.3.4. Life of the Rotary Bearings	98
3.7.4. Sensors.....	99
3.7.5. Final Design	99
3.8. Spindle Design	101

3.9. Extruder Head Design	104
3.10. Workpiece Holding	108
3.11. Closure.....	110
4. PRODUCTION OF HYBRID MANUFACTURING SYSTEM	111
4.1. Production.....	111
4.2. Production of the Structure.....	111
4.3. Production of Linear Stages	114
4.4. Production of Rotary Stages.....	116
4.5. Final Assembly	117
4.6. Closure.....	118
5. CONCLUSIONS AND FUTURE WORK.....	119
5.1. Conclusion.....	119
5.2. Future Works	120
REFERENCES.....	123
APPENDICES	
A. Monte Carlo Simulation for Kinematic Analysis	131
B. Linear Bearings Accuracy Analysis Function	134
C. Monte Carlo Simulation for Linear Bearings Accuracy Analysis.....	137
D. Rotary Bearings Accuracy Analysis Function.....	138
E. Monte Carlo Simulation for Rotary Bearings Accuracy Analysis	147
F. Center Forces	148
CURRICULUM VITAE	149

LIST OF TABLES

TABLES

Table 2.1. Commercially available products that can carry out extrusion type additive manufacturing and subtractive manufacturing at the same time	42
Table 3.1. Machine specifications	43
Table 3.2. Dimensions of hybrid manufacturing system.....	47
Table 3.3. Representation of coordinate frame shown in Figure 3.7.....	51
Table 3.4. Joint variables	51
Table 3.5. Results of error budget analysis.....	55
Table 3.6. Results of modal analysis	61
Table 3.7. Speed and force requirements for different operations.....	63
Table 3.8. Torque and force requirements for different operations.....	63
Table 3.9. Speed and force requirements for different conditions in terms of feed ..	64
Table 3.10. Pitch of the feed screws	64
Table 3.11. Speed and torque requirements for different conditions	64
Table 3.12. Torque requirements and motor torque comparison.....	65
Table 3.13. Required torque and motor torque comparison for vertical axis	66
Table 3.14. Running accuracy for HG [71]	69
Table 3.15. Geometric parameters for linear bearings of horizontal axis	77
Table 3.16. External forces for linear bearings of horizontal axis.....	77
Table 3.17. Reaction forces for linear bearings of horizontal axis	77
Table 3.18. Comparison of reaction forces and load capacities	78
Table 3.19. Geometric parameters for linear bearings of Z axis	79
Table 3.20. External forces for linear bearings of Z axis	79
Table 3.21. Reaction forces for linear bearings of horizontal axis	79
Table 3.22. Comparison of reaction forces and load capacities	80
Table 3.23. Life of the linear bearings for horizontal and vertical axis.....	81

Table 3.24. Components of the rotary stage	82
Table 3.25. Speed and torque values of rotary platform	82
Table 3.26. Speed and torque values of stepper motor	82
Table 3.27. Formulas for worm gear forces	83
Table 3.28. Properties of worm gear	84
Table 3.29. Results of worm gear force analysis	84
Table 3.30. Accuracy grades of angular contact bearing [72]	85
Table 3.31. Magnitudes of the external forces for C axis	91
Table 3.32. Reaction forces in X- and Y directions for C axis	93
Table 3.33. Radial reaction forces for C axis	94
Table 3.34. Axial reaction forces for C axis	94
Table 3.35. Bearing calculation parameters and load rating (C).....	94
Table 3.36. Reaction forces for C axis	95
Table 3.37. Magnitudes of the external forces for B axis	96
Table 3.38. Reaction forces in X- and Y directions for B axis	96
Table 3.39. Radial reaction forces for B axis.....	98
Table 3.40. Axial reaction forces for B axis	98
Table 3.41. Reaction forces for B axis	98
Table 3.42. Encoder and stepper motor parameters	99

LIST OF FIGURES

FIGURES

Figure 2.1. The organizational diagram of the literature survey	3
Figure 2.2. The organizational diagram of the precision machine system components	4
Figure 2.3. The effect of applying a theoretical bending load with different ribbings and displacements [6]	6
Figure 2.4. A slide construction based on the results from Figure 2.3. [6]	7
Figure 2.5. Glued structures [9]	8
Figure 2.6. Functional parts of the linear hydrostatic guideways [20]	12
Figure 2.7. Hydrostatic bearing system [19]	12
Figure 2.8. A-110 Physics Instruments glide LC linear stage with air bearings [22]	13
Figure 2.9. Preload types [23].....	14
Figure 2.10. Caged ball LM Guide model SHS [24]	15
Figure 2.11. Schematic diagram of electro-hydraulic system to derive the dynamic model [25].....	16
Figure 2.12. Ball screw contact area (above) vs planetary roller screw contact area (below) [27]	19
Figure 2.13. Capstan drives [10].....	19
Figure 2.14. Components of the linear scale [31].....	21
Figure 2.15. Absolute position (left) and incremental position (right) [31]	22
Figure 2.16. The components of the hydrostatic rotary bearing and its fluid circuit [19]	25
Figure 2.17. Aerostatic rotary table made by Zollern GmbH [35]	26
Figure 2.18. Torque motor made by Kollmorgen Co. [37]	28
Figure 2.19. Planetary gear system [38]	29
Figure 2.20. Components of harmonic drive [42]	31

Figure 2.21. Velocity diagrams of roller Gear Cam (left) and worm drive (right) [44]	32
Figure 2.22. The roller gear cam and its components [44]	32
Figure 2.23. The PCB motor [45]	33
Figure 2.24. The properties of drive system being a power transmitter [46]	34
Figure 2.25. The RMI drive [47]	35
Figure 2.26. Demands of spindle performance according to branches [29]	36
Figure 2.27. Conventional and motor spindles [48]	37
Figure 2.28. Performance of bearings [29]	37
Figure 2.29. Air bearing spindle [53]	39
Figure 3.1. Some conceptual machine designs	44
Figure 3.2. Swiveling tool configuration	46
Figure 3.3. Final design	46
Figure 3.4. X direction dimensional analysis	48
Figure 3.5. Y direction dimensional analysis	49
Figure 3.6. Z direction dimensional analysis	49
Figure 3.7. a) Solid view of hybrid manufacturing system. b) Coordinate frames of hybrid manufacturing system	50
Figure 3.8. The results of Monte Carlo simulation	55
Figure 3.9. The result of static structural analysis	58
Figure 3.10. Natural frequencies and deflections from 1 st to 6 th mode	59
Figure 3.11. Natural frequencies and deflections from 7 th to 12 th mode	60
Figure 3.12. Natural frequencies and deflections from 13 th to 15 th mode	61
Figure 3.13. Torque/output power and speed of X axis [69]	65
Figure 3.14. Torque/output power and speed of Y, Z and W axes [69]	66
Figure 3.15. Feed screw bearing configurations [71]	67
Figure 3.16. Linear bearings datum and dimensions [71]	68
Figure 3.17. Geometric tolerances on mounting plate	70
Figure 3.18. Force balance on the linear guide	71
Figure 3.19. Force system of contact points in a) Y direction, b) Z direction	71

Figure 3.20. Geometric tolerances of the mounting surface after analysis.....	74
Figure 3.21. Axial- and radial errors generated by Monte Carlo simulation. a) axial error in Y direction, b) axial error in Z direction, c) angular error in X direction, d) angular error in Y direction, e) angular error in Z direction.....	75
Figure 3.22. Force condition for horizontal axis [71].....	76
Figure 3.23. Force condition for vertical axis [71].....	78
Figure 3.24. Mounting rails and block [71].....	81
Figure 3.25. X axis normal and exploded view.....	81
Figure 3.26. Speed vs torque plot for rotary stages [69].....	83
Figure 3.27. Forces on worm gear and worm wheel [72].....	84
Figure 3.28. Geometric tolerances for bearing seat and shaft [72].....	85
Figure 3.29. Forces on the bearing surface for rotary axes.....	86
Figure 3.30. Force system of contact points in a) radial direction, b) Z direction.....	87
Figure 3.31. Geometric tolerances for bearing seat and shaft after analysis [72].....	89
Figure 3.32. Axial and radial errors generated by Monte Carlo simulation. a) axial error in X direction, b) axial error in Y direction, c) axial error in Z direction, d) angular error in X direction, e) angular error in Y direction.....	90
Figure 3.33. Force condition for C axis.....	92
Figure 3.34. Moments affecting bearings for C axis. a) Effect of M_x on bearings b) Effect of M_y on bearings. A stands for the upper bearing and B for the lower bearing.	93
Figure 3.35. Force condition for B axis.....	97
Figure 3.36. Exploded view of actuation system of the rotary stage.....	100
Figure 3.37. Exploded view of the rotary stage.....	100
Figure 3.38. Spindle structure [74].....	102
Figure 3.39. Internal components of the drilling machine.....	103
Figure 3.40. Fin structure aluminum base.....	103
Figure 3.41. Location of rotary sensor in the spindle.....	104
Figure 3.42. Variable bead width [75].....	105
Figure 3.43. Exploded view of the extruder.....	106

Figure 3.44. Left side shows the bottom view of the extruder and the right side indicates the detailed view of the region within the detail A.....	107
Figure 3.45. Top view of the extruder.....	107
Figure 3.46. Work holders on B/C axis a) universal type, b) collet type, c) dove tail, d) details of the dove tail.....	109
Figure 3.47. Final design.....	110
Figure 4.1. Production and assembly stages of the system: a) Sigma profile contact surfaces after grinding, b) columns after grinding, c) epoxy on ground surfaces, d) connection of sigma profiles, e) assembled bottom structure, f) bottom and columns assembled before Bohrwerk operation, g) masking before painting, h) assembly of overall structure.....	113
Figure 4.2. Components of the linear stages	114
Figure 4.3. Assembly stages of the axes: a) preloading linear bearings and removing the empty space with set screw, b) tightened bolts, c) pushing the bearings left, d) pushing the bearings right, e) isometric view, f) applying nested force and tightening bolts with the given order, g) taking empty space with a setscrew, h) tightening bolts to connect carriage and feed screw nut	115
Figure 4.4. Assembly of rotary stage a) C axis b) B axis.....	116
Figure 4.5. The final assembly	117

LIST OF ABBREVIATIONS

ABBREVIATIONS

ABS	Acrylonitrile Butadiene Styrene
AM	Additive Manufacturing
CNC	Computer Numerical Control
CPR	Count per Revolution
DC	Direct Current
FEM	Finite Element Method
FDM	Fused Deposition Modelling
HTM	Homogenous Transformation Matrices
LM	Linear Motion
PCB	Printed Circuit Board
PLA	Polylactic Acid
RMI	Rolling Motion Industries
RPM	Revolution per Minute

LIST OF SYMBOLS

SYMBOLS

i	Gear ratio
z_r	Number of gear teeth of the ring
z_s	Number of gear teeth of the sun
fP_p	Position vector of point P in the coordinate frame f
fT_x	Homogenous transformation matrices from the f coordinate frame to the x coordinate frame
E	Error vector
ε	Error matrix
ε_x	Angular error around X axis
ε_y	Angular error around Y axis
ε_z	Angular error around Z axis
δ_x	Axial error in X axis
δ_y	Axial error in Y axis
δ_z	Axial error in Z axis
A	Accuracy
f	Frequency
δ	Deflection
σ	Standard deviation
n	Rotational speed
V_a	Axial speed
h	Pitch
μ	Efficiency
k	Stiffness
r_p	Position of the point P
F_p	Forces on point P

CHAPTER 1

INTRODUCTION

1.1. Motivation and Goals

Additive manufacturing, which is a relatively a new production method compared to traditional production methods, has various advantages in terms of the nature of the process. Layer by layer production enables production of parts which cannot be produced by other conventional manufacturing methods. However, chordal error, staircase effect, minimum slice height, support structure, build shape change of the extruded filaments that are all due to thermal instability affect the quality of the printing negatively [1]. As a result of increasing demand on high quality printing, researchers and people working in additive manufacturing field have begun to focus on improving quality of the printing. For these reasons, surface roughness and dimensional correctness of the product, repeatability of the process and so on have become important concern of this field.

Processes used in addition to layered production to improve product quality can be examined in three sections for the method of application: (i) pre-treatment prior to printing; (ii) integrated applications during printing; (iii) post-printing enhancement [2].

Pre-treatment prior to printing (mentioned as the first method of application) is one of the most common solutions. Accordingly, the determination of some variables affecting the production process (layer thickness, manufacturing direction of the part, etc.) by using optimization methods can partially correct the defects that may arise. Nevertheless, the application of several secondary methods as integrated or post-processing may be necessary for a complete solution.

In this thesis, it is anticipated to improve the quality of the products produced by the material extrusion method by applying integrated and post-processing enhancements. In this thesis, it is aimed to create a hybrid production platform which enables the efficient use of fused deposited method and machining processes together. It is planned that the designed hybrid platform will have the capability of integrated application or finishing application mentioned in the second and third articles.

1.2. Scope of the Thesis

The focus of this thesis is a mechanical design of a 6-axis hybrid manufacturing system, which can do additive and subtractive manufacturing processes in one manufacturing system platform. For better understanding of hybrid manufacturing system, possible components of precision manufacturing systems and state of art studies in precision manufacturing systems are presented in Chapter 2. Furthermore, Chapter 3 will provide information about the requirements of the hybrid system and design and analysis of the components that constitute the system. In Chapter 4 production of hybrid manufacturing system will be explained. Finally, Chapter 5 will provide discussion about the overall machine and future works.

CHAPTER 2

LITERATURE SURVEY

2.1. Introduction

This literature review describes the components of recent precision manufacturing systems, overall precision manufacturing systems and hybrid printer systems. In Section 2.2 structures of the precision manufacturing systems are described. Section 2.3 focuses on components of linear stages that include bearings, actuation and transmission and sensor systems. In Section 2.4 components of rotary stages are described. These involve bearings, actuation and transmission and sensor systems. The following Section 2.5 discusses spindles, which are very similar to the rotary stages described earlier. In Section 2.6 general features of precision manufacturing systems are briefly mentioned. Finally, in Section 2.7 hybrid printer systems are outlined with some of their characteristics. Figure 2.1 indicates the focus of literature review. Hybrid printer systems have 6 subtopics in literature. However, focus of hybrid printer systems is on material extrusion hybrid machines. Details of precision machine system components are described in Figure 2.2.

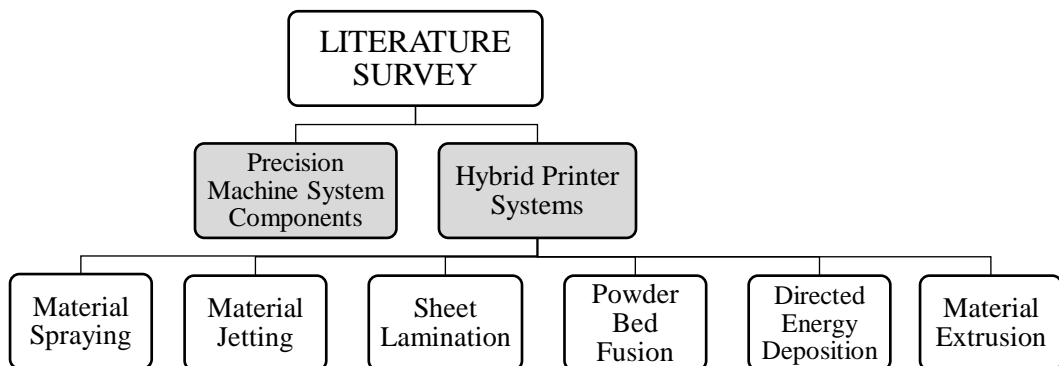


Figure 2.1. The organizational diagram of the literature survey

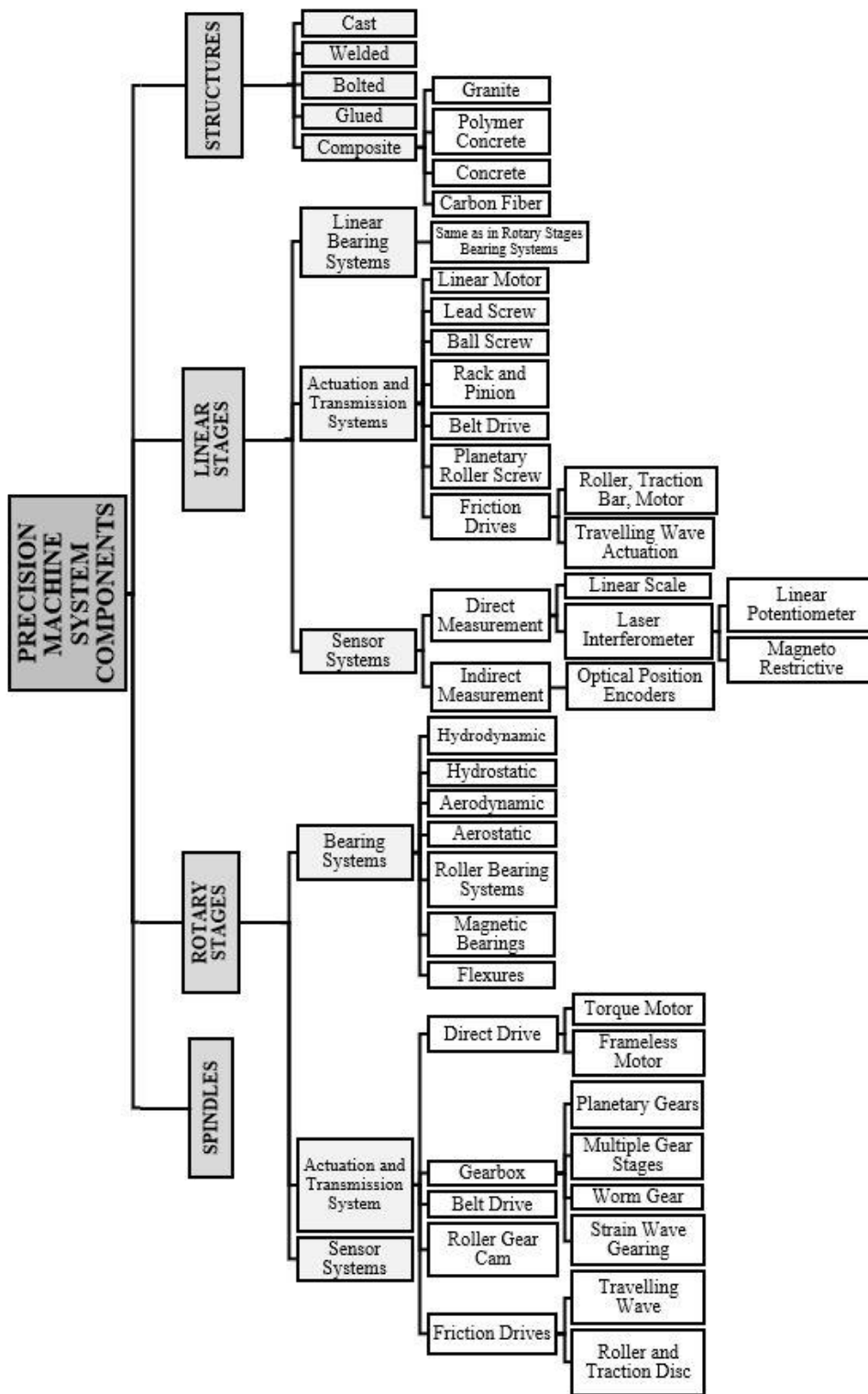


Figure 2.2. The organizational diagram of the precision machine system components

2.2. Structures

Structures are the fundamental components of the precision machine tools. Performance of the structure influences the overall performance of the machine tools. Ideal structures should be rigid under static, dynamic and thermal load conditions. Moreover, they should have high damping properties to absorb unwanted vibration and other disturbances. Material properties, assembly methods and manufacturing of the structure affects the performance of the structure. In the following section the structures which are most commonly used in precision machine construction are described.

2.2.1. Cast Structures

Cast structures are commonly used materials for machine construction. The complicated parts, which can be manufactured by milling or other processes can be produced by casting. Also, very complex ribbings can be manufactured by casting. As Möhring et al. [3] discussed, because of its low coefficient of thermal expansion and high internal damping properties, cast iron is one of the most chosen materials for a machine structure. Rapid cooling of casting causes residual stress. According to Slocum [4], in order to remove residual stress from rapid cooling, vibration or heat treatments should be applied to the structure. In order to obtain precision products, reference surfaces must be milled or grinded after casting process. Locating surfaces must be considered to clamp and fixture the casted structure for machining. Moreover, various design rules must be followed to prevent hot spots and increase material stability.

As Wills et al. [5] suggested, two main ways to improve damping properties of the casting involve keeping the sand cores inside of the casted structure and packing the machine structure with glass balls.

2.2.2. Welded Structures

One of the methods used to construct the structure of the precision machine is by combining profiles, tubes and plates by welding. Especially steel sheet metal components are mostly constructed by welding. As a result of heat generation in

welding, bending, distortion and residual stresses are induced. In order to prevent this, additional production steps such as grinding, milling and heat treatment should be applied.

Furthermore, in his paper Möhring [3] found that welding structures have low damping properties, but they can be improved with shear dampers. Moreover, it is cheaper to combine the structures by welding than buying complete material and then removing it by machining. To sum up, it is important to optimize the overall structure.

Munirathnam [6] presents the effect of applying a theoretical bending load, which can be seen in Figure 2.3. This involves different ribbings and displacements. In Figure 2.4 a slide was constructed based on the outcome of this effect.

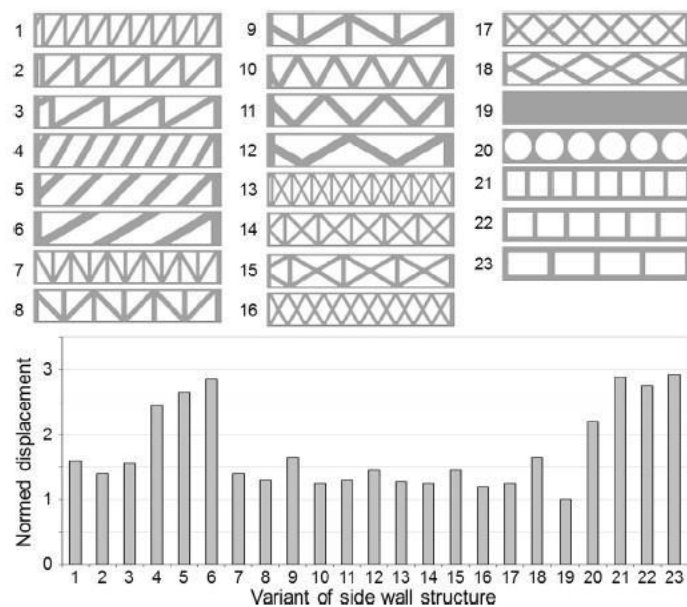


Figure 2.3. The effect of applying a theoretical bending load with different ribbings and displacements [6]

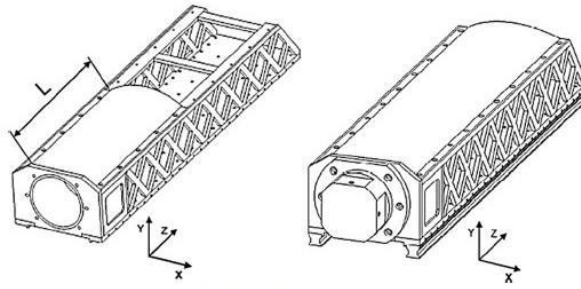


Figure 2.4. A slide construction based on the results from Figure 2.3. [6]

2.2.3. Bolted Structures

One of the most widely used methods to attach several parts of the machine to each other is by using bolted joint. It is popular both in machine tools as well as in industrial machines. As described by Ito [7], the main factor that affects the structure's damping and stiffness property is tightening of the bolts. In fact, by increasing the tightening, bending stiffness increases. At the same time, damping decreases. Moreover, the characteristic of damping increases when there is lubrication over the joint surface.

By Zaman et al. [8] it was studied how dynamic response of structures is affected by the bolted joints. The results showed that by adding the bolted joints, the structure increases in mass, because of which the structure's natural frequency is lowered. Moreover, the damping ratio was considerably elevated as the bolted joints were used for the construction of the structure. Finally, by comparing monolithic structures with jointed structures, Zaman et al. has shown that the stiffness is greater in monolithic structures, whereas damping is greater in jointed structures.

2.2.4. Glued Structures

According to Adams et al. [9], adhesively bonded joints can accommodate high shear stress. Moreover, adhesive bonding increases the damping of the structure. Bonding strength of the joint decreases as temperature gets higher. Thanks to adhesive bonding wide variety of structures can be combined and superior structures can be obtained.

For instance, steel inserts can be combined with granite to provide mechanical interfaces. Figure 2.5 shows how steel inserts are combined with granite surfaces to obtain mechanical interfaces.



Figure 2.5. Glued structures [9]

2.2.5. Composite Structures

By combining different fiber and matrix materials different mechanical properties can be achieved. Moreover, by optimizing the fiber direction very high values of specific stiffness and specific strength can be obtained. However, the process of joining can be challenging and costly [3].

2.2.5.1. Granite Structures

Not being subjected to residual stresses makes granite a very stable material. Granite structures have high hardness, low thermal conductivity (3.2 [W/m K]), high damping properties and low thermal expansion coefficient (0.005–0.006 [mm/m K]). [10] They are used as reference planes in precision instruments. [11] Granite is shaped by drilling, sawing and grinding. In order to make mechanical connections, glued metal can be combined with granite base.

Grotz [12] talks about screwing and conglutination, the two processes being generally used for the construction of several granite components. Because of granite's property to absorb moisture, a thin epoxy resin must be sealed with it. In the study by Abdin et

al. [13] and de Bruin [14] dimensional stabilities of cast iron, granite, graphite composites and polymer concrete were used to identify the limitation of granite's stability over a long period of time. They found that moisture affects sensitivity to high extent. Therefore, additional care must be taken to prevent granite from absorbing water.

2.2.5.2. Polymer Concrete Structures

After cold-curing reaction, resins became available in 1970s and the polymer concrete structures started to be used for constructing frame of precision machines [3]. Polymer concrete is composed of polymeric resin and aggregate mixture. In his study, Bedi et al. [15] states that approximately 75-80% of the mixture is made of aggregates and fillers. Epoxy and polyester are the most used resins, but epoxy is mostly used in the construction of precision machine frames due to having better mechanical properties. Polymer and aggregate content, addition of fibers, micro fillers and curing regimes are factors affecting the mechanical properties of a polymer concrete.

Haddad and Al Kobaisi [16] studied six different aggregates while keeping resin volume fraction the same. The results revealed that basalt, spodumene and fly ash make up the most optimum composition to obtain the highest flexural stress and minimum coefficient of thermal expansion. Polymer concrete structures are preferred due to their superior damping properties, high stiffness, low residual stress (produced at room temperature) and low thermal expansion.

Do Suh and Lee [17] used polymer concrete combined with welded steel frame as a machine base for their high-speed CNC (computer numerical control) milling machine. They analyzed the natural frequency and damping properties of the machine bed structure both with FEM (finite element method) as well as experimentally. They found the damping factor in the range of 2.93-5.69%, which is much more superior compared to the steel-based structure which is 0.2-0.3%. Damping coefficients observed in the experiment were more than the results obtained from FEM.

2.2.5.3. Concrete Structures

Since 1944, concrete structures are used in machine structures [3]. Combination of cast iron and concrete structures have improved damping properties. Static stiffness of the concrete structures combined with the cast iron plates is comparable with cast iron structure. On the other hand, thermal conductivity is lower compared to cast iron. In their study about development of a high-speed CNC cutting machine using linear motors, Gordon and Hillery [18] used steel reinforced concrete as machine chassis.

2.2.5.4. Carbon Fiber

Carbon fiber has superior strength to weight property. It is inexpensive as a raw material. However, process employed to make carbon fiber usable is expensive, but producing tube shape structures from carbon fiber is relatively easy and inexpensive. It is important that carbon fibers do not get in touch with any liquid. Similarly, humidity should be avoided [4].

2.3. Linear Stages

Linear stages are fundamental components of the machine tools. They provide linear motion in high accuracy. Bearing systems, actuation and transmission systems and sensors are the components of the precision linear stages described in this section.

2.3.1. Linear Bearing Systems

Linear bearings are machine components that provide accurate free motion in linear direction. There are different linear bearings to guide the linear stage accurately. In the following section these different kinds of linear bearings are described.

2.3.1.1. Hydrodynamic

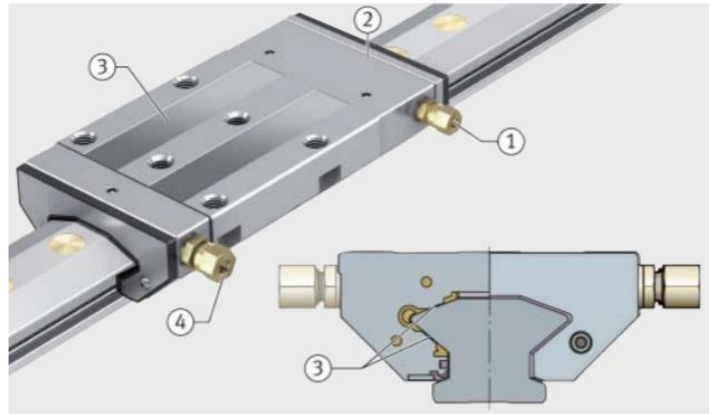
Working principle of hydrodynamic bearings, which are well described by Harnoy [19], is the prevention of metal to metal contact in machine elements by a thin film of liquid, which provides the dynamic action of contact surfaces. In order to provide

complete separation in between metals by the hydrodynamic bearing, high relative speed in-between components is desired. During start and stop processes, hydrodynamic bearings cannot provide complete full film lubrication, because of which the bearing and moving element get damage. Furthermore, design engineer should always consider vibration and disturbances which can lead to the contact between surface impurities of the bearing and moving component. The surface impurities should always be 10 to 100 times lower than minimum lubrication-film thickness. Moreover, proper oil should be provided continuously to prevent overheating.

2.3.1.2. Hydrostatic

Hydrostatic linear bearings are widely used in precision machine systems because of their high stiffness, superior damping and very low friction in between guideway and carriage. Harnoy [19] further describes that surface irregularities of guideway and carriage should be always less than fluid film in between the surfaces.

Pressurized liquid is placed in between guideway and carriage which causes constant full film lubrication even when there is no motion. In order to pressurize the liquid, pump must be included in the system which makes the system more expensive compared to other types of bearings. Compared to hydrodynamic bearings, hydrostatic linear bearing has higher stiffness, which makes it applicable for precision machinery. To increase radial stiffness of the bearing, recesses and flow restrictors are included in the bearing system. Fluid comes to the recesses through flow restrictors. Furthermore, film lubricant layer is much thicker in hydrostatic than in hydrodynamic bearings. Therefore, manufacturing errors are not bottleneck issue for hydrostatic bearings. Figure 2.6 indicates the functional parts of the linear hydrostatic guideways.



1- Pressure side 2- Integrated choke 3- Pressure pockets 4- Extraction side

Figure 2.6. Functional parts of the linear hydrostatic guideways [20]

As seen from Figures 2.6 and 2.7, from the pressure side, pressured lubricant is supplied, which then passes through pressure pockets and from the extraction side unpressurised lubricant moves to the reservoir. Then, the gear pump makes the lubricant pressurized and sends it to the flow divider. During circulation of the lubricant, heat is removed from the system and unwanted dirt and dust are filtered.

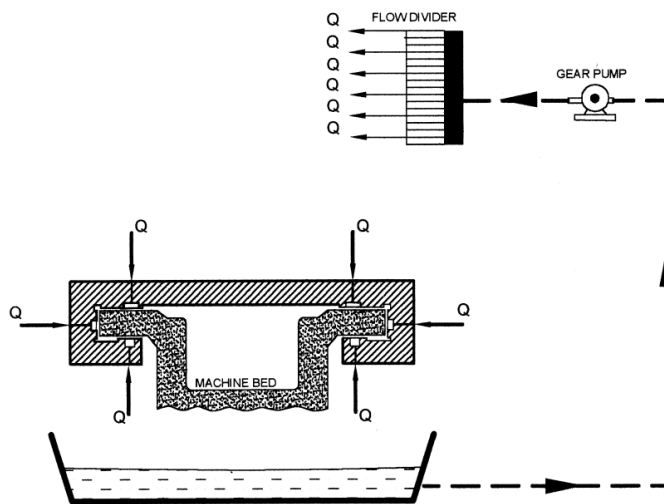


Figure 2.7. Hydrostatic bearing system [19]

2.3.1.3. Aerodynamic

Working principle of the aerodynamic linear bearing is similar to the hydrodynamic bearings. The only major difference is using air instead of liquid. It is mostly not applicable in the linear machinery.

2.3.1.4. Aerostatic

Working principle of the aerostatic linear bearings is similar to the hydrostatic linear bearings. The only difference is that there is air instead of liquid. Rowe [21] explains that the supplied pressure should be higher than the recessed pressure in order to allow for carriage of different loads. Unlike aerostatic, hydrostatic bearings are much smaller and shallower. This is for the purpose of reducing the response time from the load application to the recess pressure change. Moreover, compared to the hydrostatic, aerostatic bearings have lower loading capacity.

Aerostatic linear bearings are commercially available. They are also called as air bearings. Physics Instruments Co. [22] has different air bearing stages which can achieve less than 1 [μm] accuracy over 200 [mm] distance, such as a product shown in Figure 2.8.



Figure 2.8. A-110 Physics Instruments glide LC linear stage with air bearings [22]

Ro et al. [23] described in his study that stiffness of the air bearing depends on air gap thickness, air gap pressure and surface area of the bearing. By preloading, stiffness of the bearing can increase. Common methods for preloading are magnet, mass, vacuum or 2 opposite sided air bearings, as seen from Figure 2.9.

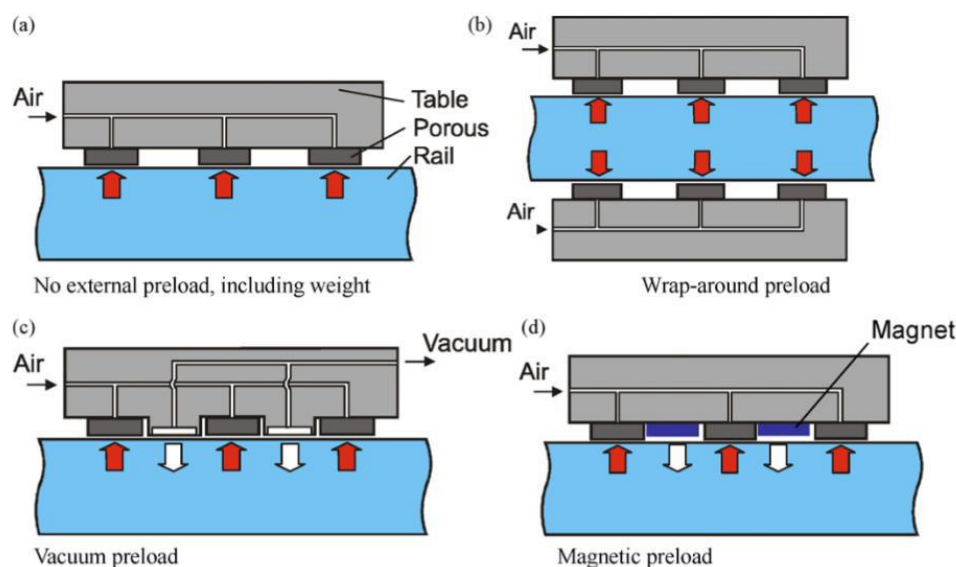


Figure 2.9. Preload types [23]

When working with aerostatic bearings the environment should be kept clean and vacuum environment should be avoided.

2.3.1.5. Roller Bearing Systems

Their general properties are similar to rotary roller bearings. In fact, they both contain roller components to guide the motion. Figure 2.10 indicates the components of linear bearings. Linear motion blocks move on the linear motion rail. Linear roller bearings can accommodate radial loads and moments as well as provide smooth motion in linear direction. Quality of the balls, rail and block influence the precision of the system. Roller elements prevent the sliding contact, the end seals prevent lubrication

going out of the block and the ball cage that is covering the balls prevents contact in between the balls and reduces noise [24].

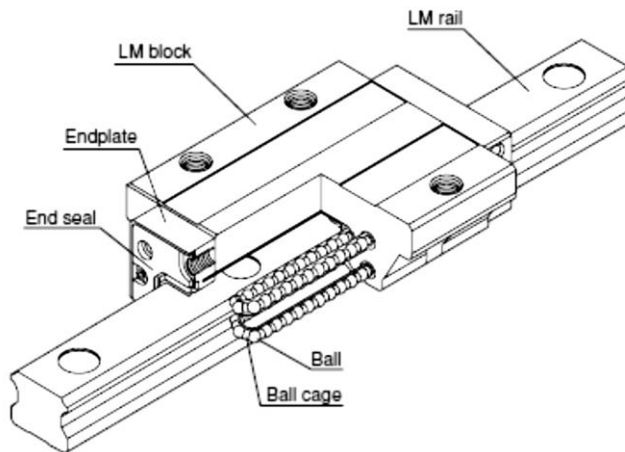


Figure 2.10. Caged ball LM Guide model SHS [24]

2.3.1.6. Magnetic Bearings

Basic working principle of magnetic bearings is applying a magnetic field in order to carry the bearing load. This type of bearing is also called as magnetic levitation active feedback control. In order to generate the same load capacity as hydrostatic bearings they need to be much bigger in size [19].

2.3.2. Actuation and Transmission System

In precision linear stages one of the fundamental components is actuation and transmission system. If the linear motor is used in the system, there is no need to use additional transmission. In fact, the linear motor directly generates the linear motion. However, in many cases a motor which generates the rotary motion is used. Using transmission systems, the rotary motor can be converted into linear motion. In the following section different kinds of actuation and transmission systems are described.

2.3.2.1. Linear Motor

2.3.2.1.1. Hydraulic

Hydraulic actuator is used in high load application. Fluid pressure generated by pump moves the output member. By using limit switches, the end and beginning positions of the cylinder can be controlled, as seen from Figure 2.11. In order to control the position, the system should contain the control system and a measurement instrument, such as linear potentiometer. Furthermore, hydraulic actuator system requires pump, reservoir and release valve.

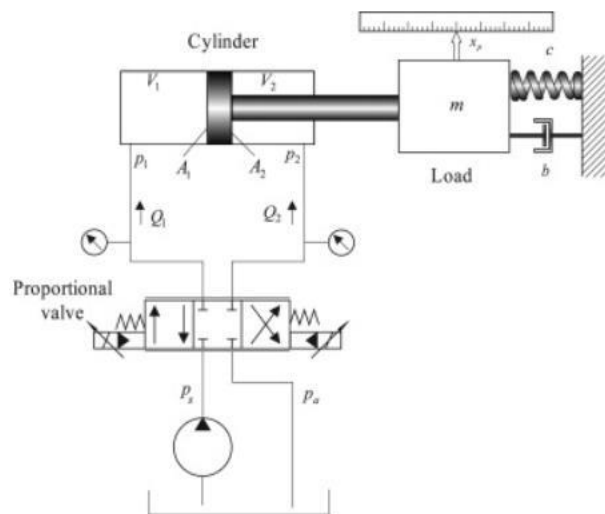


Figure 2.11. Schematic diagram of electro-hydraulic system to derive the dynamic model [25]

2.3.2.1.2. Pneumatic

Working principle of pneumatic actuators is very similar to hydraulic actuators. The main difference is that, instead of fluid, compressed air is being used in pneumatic actuators, which has more compressibility compared to liquids. Compared to hydraulic system with the same size, pneumatic systems have much lower load capacity. Furthermore, leaking of the air can be problem when there is no proper

sealing. However, it does not cause dirt, which is the case in hydraulic systems. Finally, measurement and control system should be included in the system to control the position.

2.3.2.1.3. Electromagnetic Motor

Linear stages can be actuated directly by electromagnetic motor without any need for transmission system. Therefore, transmission errors and inefficiencies are eliminated. They are widely used when quick acceleration performance is required.

One of the most important drawbacks of linear bearing are attraction forces generated by the linear axis. The forces produced in other than feed directions are 10 times larger than the forces produced in feed direction. These forces should be carried by the linear guides, carriages and machine structure. Furthermore, the resulting magnetic fields can have a disruptive effect on machine-integrated sensors and cause problems in the attraction of ferromagnetic chips.

2.3.2.2. Lead Screw

By using lead screw in combination with motor, the rotary motion can be converted into linear motion. The power transmission efficiency of this combination is less than in ball screws. If the efficiency of the lead screw is less than 50%, system will be self-locked and linear force acting on the lead screw cannot move the system.

2.3.2.3. Ball Screw

By using this combination, motor generated rotary motion can be converted into linear motion. Balls moving inside the nut make rolling contact instead of sliding contact. The efficiency of ball screw is typically more than 80%. When the axial load approaches the preload, mechanical efficiency of the ball screw decreases with increasing rotational speed [26]. Less energy is wasted and, compared to lead screw, less heat is generated. Nevertheless, in precision machine system heat of the ball-screw can be a problem. One of the ways to eliminate the ball screw thermal stress is

by using fixed-fixed bearing arrangement and pre-tensioning ball screw. Another way is by using active cooling system passing inside of the ball screw.

2.3.2.4. Rack and Pinion in Combination with Motor

Rotary motion generated by motor is conducted to rack via pinion. One method of doing so is by fixing the rack on the stationary plate which results in linear motion of pinion with motor. By using another method, it is also possible to fix the pinion on the stationary plate and make the rack move linearly. The first method provides cost effective solution for long range linear motion. Backlash in between rack and pinion can be eliminated by using split 2 pinions which are torsionally preloaded between each other [10].

2.3.2.5. Belt Drive

When belts are used for linear motion. They are called as belt drive and have both low stiffness as well as low load capacity. In contrast to flat belts, there is no slipping in timing belts. [27]

Belts can be used to drive the pulleys. The motor drives one of the pulleys, while another pulley is connected to the bearing on the other side of the system and rotates freely. Linear motion in between the pulleys can be obtained and this motion can be conducted to the connected components. Connection to the belts can be made by clamp plates which have a matching profile with the belts.

2.3.2.6. Planetary Roller Screw

Rotary motion produced by the motor can be converted into linear motion by using planetary roller screw. Cylindrical nuts and flanged nuts are the most common choices. Number of contact points increases by its special geometry and can withstand very large loads. Figure 2.12 indicates the contact area in-between shaft and nut in the ball screw and planetary roller screw mechanisms. It can be seen that the planetary roller screw has higher contact area than the ball screw.

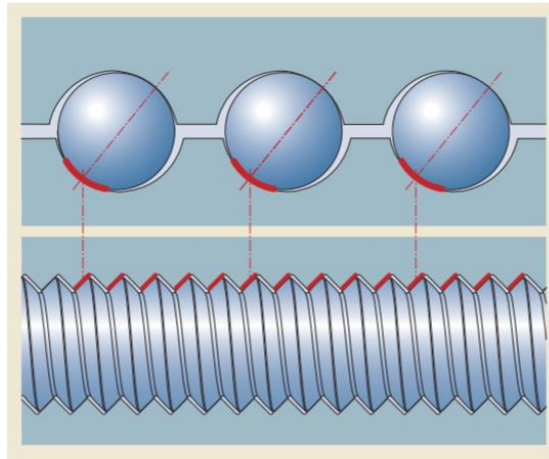


Figure 2.12. Ball screw contact area (above) vs planetary roller screw contact area (below) [27]

2.3.2.7. Friction Drives

2.3.2.7.1. Roller, Traction Bar and Motor

As seen from Figure 2.13 and explained by Venkatesh and Izman [29], friction drives use a drive roll element to move traction bar, which is plain hardened. Drive roll should be preloaded against thrust bearing to obtain better stiffness and adequate friction for the drive. Since the slip is inevitable, direct measurement of the position is required. There is no backlash in the system and very little amount of mechanical vibration.



Figure 2.13. Capstan drives [10]

2.3.2.7.2. Travelling Wave Actuation

Piezo walking drives are composed of several preloaded piezo actuators against guided runner. Linear feed motion can be obtained by walking motion of piezo actuators. Thanks to its very small walking steps, resolution below 1 [nm] can be achieved [30]. Runner has a self-locking property, which is the result of the preloading piezo walk actuators against it. Therefore, when the system is switched off, there is no power consumption, which causes heat in the system to lock the system.

2.3.3. Sensor Systems

In order to obtain position or velocity information from the moving system, sensors are used. For the linear stage, if the position of the moving platform is directly measured by the sensors, it is called as direct measurement. If the position of the moving platform is measured from the transmission system, such as from the rotation of the feed screw, it is called as indirect measurement.

2.3.3.1. Direct Measurement

Measuring the position directly eliminates the possible thermal and geometrical errors during measurement. It is more precise compared to indirect measurement. The equipment used for the direct measurement of precision linear motion that is discussed here involves linear scale, laser interferometer, linear potentiometer and magneto restrictive.

2.3.3.1.1. Linear Scale

Incremental or absolute linear scales are available. Some errors during motion of linear stages, such as positioning error because of thermal expansion, geometry and others, can be eliminated by using linear scales. It is not possible to predict all the errors in open loop system. By using linear scale, these errors can be detected for every position and can be corrected by control system and electronics.

Linear encoders are composed of mounting block, sealing lips, scanning carriage, and linear scale. As seen from Figure 2.14, presented by Heidenhain Co. [31], scanning carriages and linear scale remain inside of the housing during the measurement. Sealing lips protect the measurement inside the housing from dust, contamination and coolant.

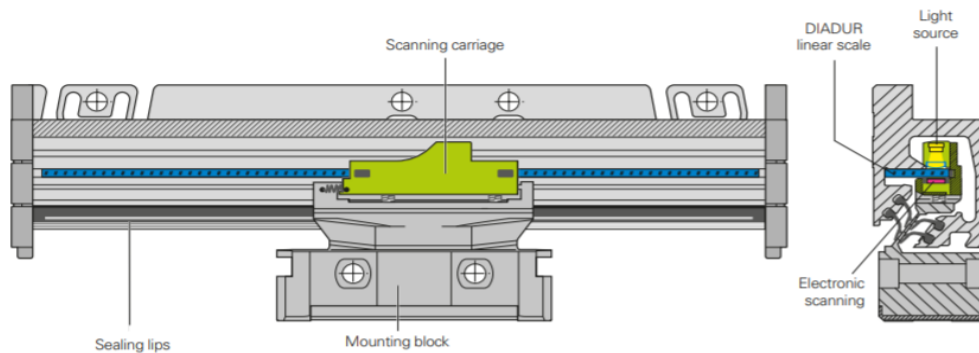


Figure 2.14. Components of the linear scale [31]

Further mentioned in [31], linear scale should be rigid in the measuring direction. By having no contact in the scanning process and having ball bearings to guide scanning carriage motion, friction can be eliminated. Thermal properties of the linear encoder should be chosen based on the measured object or workpiece. Commercial companies offer different materials of linear scale based on application.

Subsequent electronic can provide convenient turning on of the encoder that determines the position value by using absolute measurement. In order to define the reference point, the location of the axes does not have to be changed. For obtaining the scale graduation, the structure of serial absolute code is required, which then allows for the determination of the absolute position [31]. Moreover, both position value as well as incremental signal can be obtained from an incremental track. This is done by, first determining a certain point of origin and, then, measuring the amount of separate increments from that point. To make sure that the obtained position is correct,

absolute reference is used, because of which an extra reference mark is required on a scale tape. After scanning the reference mark, the absolute position is obtained, which defines 1 signal period specifically. Absolute and incremental positions are shown in Figure 2.15.

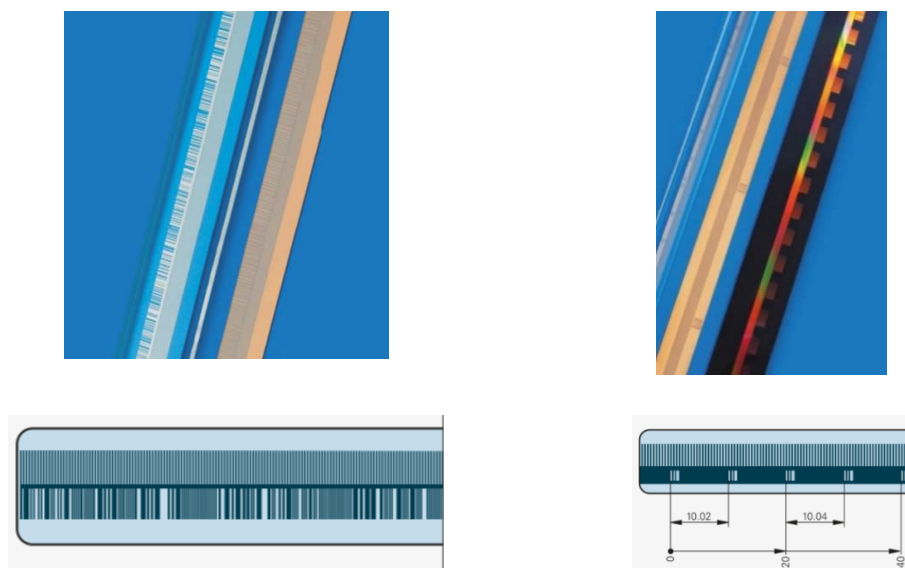


Figure 2.15. Absolute position (left) and incremental position (right) [31]

2.3.3.1.2. Laser Interferometer

Working principle of laser interferometer is based on the superposition of light waves. Different path length lights cause different phases. The resulting interference can be obtained by digital analysis. There are two kinds of detection. One is homodyne detection in which reference beams in the measurement have the same frequencies. In this type of detection, from the interference of the light sources, intensity information can be obtained. This information is used to obtain DC output signal. By counting the intensity changes, position information is obtained. In case of another detection method, called as heterodyne detection, polarized light source has 2 different signals with close frequencies. Frequency of each signal is too fast to be responded by

electronics. However, beat frequency, which is the difference between the two signals, is in order of [MHz] and can be processed by electronics. The advantage of heterodyne techniques over homodyne detection is having two orders higher magnitude of resolution. [10, 11]

2.3.3.1.2.1. Linear Potentiometer

Sliding contact inside the linear potentiometer moves with the motion on resistor. As the position changes, the resistance changes as well. Voltage changes based on the difference in resistance. Therefore, distance can be obtained from the changed voltage. [10]

2.3.3.1.2.2. Magneto Restrictive

Working principle of magneto strictive sensor is obtaining position information by measuring the time of the pulse while it is travelling from magnet to sensor and is described by Temposonics Co. [32]. Typically, moving object is connected to the magnet to which the sensor sends pulse. In the moment when the radial magnetic field interacts with the magnet, torsional strain pulse occurs. By measuring the travelling time of the pulse, position of the object can be estimated. Moreover, magneto strictive sensor is durable to pressure, so it has many applications in hydraulic cylinders.

2.3.3.2. Indirect Measurement

Indirect measurement does not involve measuring the position of the object directly. Instead, it measures other mechanical components and estimates the desired objects' location from the physical relationship point of view. Compared to direct measurement, indirect measurement is less reliable. However, due to place restriction it is widely used in machinery.

2.3.3.2.1. Optical Position Encoders

Optical position encoder is composed of transmitter, receiver and counting disk. The transmitter transmits light, while the receiver collects transmitted light behind the counting disk, as explained in the data sheet by Avago Technologies [33]. Based on

the counting disk structure optical position encoder can be absolute or incremental. Absolute optical encoder holds information about position continuously. However, in case of incremental encoder, after electricity is plugged in, the system should first go to the reference position [33].

2.4. Rotary Stages

Rotary stage is a mechanical component which provides precision rotary motion. Similar to linear stages, rotary stages are also composed of bearings, actuation and transmission system and sensor. In the following sections, these components will be described.

2.4.1. Rotary Bearing Systems

There are various rotary bearings to guide the rotary motion. In the following section, these components will be explained.

2.4.1.1. Hydrodynamic

Their general properties are described in “linear hydrodynamic bearings” section. In addition to that, they are applicable in high-speed operation. However, radial hydrodynamic bearings are not preferred in precision machinery due to their low stiffness in radial direction [19].

2.4.1.2. Hydrostatic

Its working principle is as described in the “hydrostatic linear bearing” section. Figure 2.16 indicates the components of the hydrostatic rotary bearing and its fluid circuit, as it is explained by Harnoy [19]. The upper diagram of Figure 2.16 involves a hydrostatic rotary bearing. From the reservoir, liquid is sent to the hydrostatic bearings by pumps. In order to control the pressure, pressure gauge and pressure relief valve should be part of the system. The below diagram of Figure 2.16 shows interaction

between the journal surface and the hydrostatic pad. The recess inside of the hydrostatic bearing provides even pressure distribution on the journal.

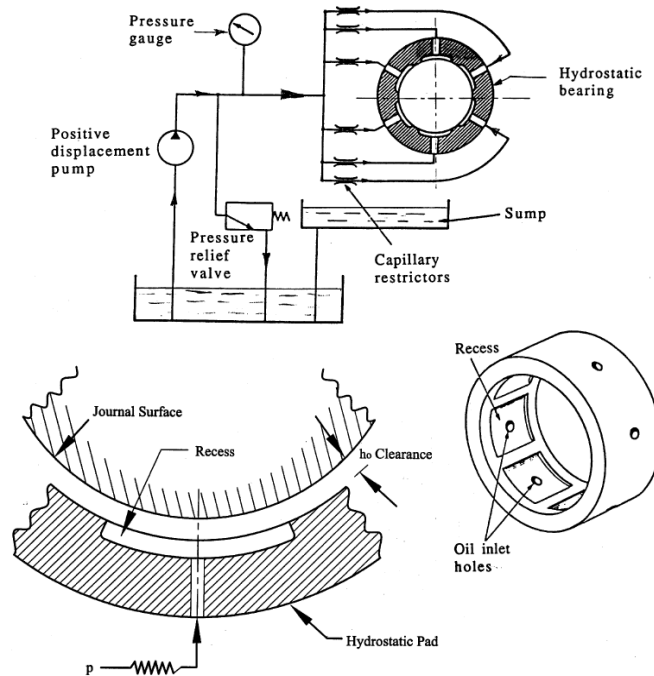


Figure 2.16. The components of the hydrostatic rotary bearing and its fluid circuit [19]

2.4.1.3. Aerodynamic

Studied by Delhaes et al. [34], aerodynamic bearing working principle is similar to the hydrodynamic rotary bearings, except that there is air between the journal and the house instead of liquid. It is applicable in high speed applications such as spindle.

2.4.1.4. Aerostatic

Their working principle is similar to the aerostatic linear bearings. Aerostatic rotary bearings are commercially available. Zollern Co. [35] made a direct driven motor with aerostatic rotary bearing stage. An example of their product (aerostatic rotary table) is shown in Figure 2.17.



Figure 2.17. Aerostatic rotary table made by Zollern GmbH [35]

2.4.1.5. Roller Bearing Systems

This type of bearing is also called as antifriction bearing. Studied by Harnoy [19], rolling action of the rolling elements provides less friction and low wear compared to the sliding bearings. Fatigue life and point contact in between balls and races should be considered during design. At very high-speed fatigue life of rotary roller bearings is reduced considerably. Moreover, at high speed the inner ring heats up and becomes hotter than the outer rings. The temperature difference in between inner and outer rings causes thermal stress, which also increases the contact stress. Lubricant is used in most of the applications to reduce or prevent the point contact as well as improves the fatigue life. Motion of the roller elements causes vibration and noise.

In his study, Stone [36] came up with the following report. Firstly, since roller bearings have longer contact length, they have higher stiffness compares to the ball bearings. Secondly, he reported that preload increases the stiffness and damping significantly. However, higher preload decreases the bearing life. His third finding referred to the clearance. Increasing clearance decreases stiffness and most of the times increases the damping, which is most likely due to the “joint” properties that have more important role when looking at the stiffness generally. Fourthly, Stone reported that an increase in the thickness of the oil film is most likely the cause of the increasing speed that

leads to increased stiffness and constant or reduced damping from the zone of entry until the ball or roller. Moreover, rise in stiffness and drop in damping can be affected by a decrease in joint clearance. Lastly, Stone reported his finding about the lubricant. Even by considerably affecting the running temperature, there will be almost no difference in stiffness and damping. Moreover, the lubricant's type will have almost no effect, if clearance and the temperature are not changed. On the other hand, clearance has an effect on stiffness and damping, by increasing and decreasing them, respectively. This is due to clearance affecting the high viscosity oil that rises damping in the joints and reduces deflection across the joint. Hence, energy dissipation will drop.

In contrast to the linear roller bearings, as described by [19], rotary bearings have centrifugal forces. These forces are joined to the external load and thermal stresses, which results in the rise of the contact stress located between the outer ring race and a rolling element.

2.4.1.6. Magnetic Bearings

Basic working principle of magnetic bearings is applying a magnetic field in order to carry the bearing load. In his study, Harnoy [19] found that there should be active feedback control to prevent any contact of journal with the bearing. During the feedback control, displacement of the shaft from the bearing centre is measured and information is sent to the controller. Then, by adjusting bearing forces produced by magnetic field, shaft is kept in the centre of the bearing.

Compared to other non-contact bearings such as hydrostatic bearings, magnetic bearings are more expensive and have fewer damping properties. In order to generate the same load capacity as hydrostatic bearings they need to be much bigger in size. Power supply should be uninterrupted such that when the power is off there should not be any sudden contact between the journal and the bearing. Instead, next to the magnetic bearings, large clearance rolling bearings can be used.

2.4.2. Actuation and Transmission System

2.4.2.1. Direct Drive

2.4.2.1.1. Torque Motor

Torque motor is composed of wound armature and permanent magnet. Its function is to convert electrical power into torque. Since it does not use mechanical transmission element, it is very efficient, and has low weight. Hollow structure of torque motor, as seen from the Figure 2.18, enables cabling from the middle [37].



Figure 2.18. Torque motor made by Kollmorgen Co. [37]

2.4.2.1.2. Frameless Motor

Frameless motors lack output shaft or bearing unit, which would be required for torque transmission. Its rotor and stator are directly integrated with the machine. Moreover, it has high stiffness and frictionless structure. One of the applications of these types of motors is in actuation of high precision spindle.

2.4.2.2. Gearbox

2.4.2.2.1. Planetary Gears

Planetary gears provide high mechanical advantage. They can be driven in different modes.

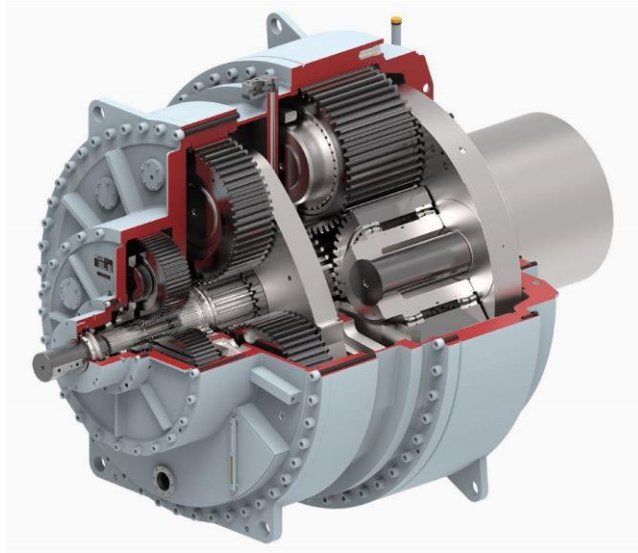


Figure 2.19. Planetary gear system [38]

Figure 2.19 indicates the components of the planetary gear system. By fixing different components, different transmission ratios can be obtained, as can be seen from the following equations [39]. If the ring gear is fixed, sun gear is driven and carrier is the output. Then, transmission ratio is

$$i = 1 + (z_r/z_s) \quad (2.1)$$

Where i is the gear ratio, z_r is the number of gear teeth of the ring and z_s is the number of gear teeth of the sun gear.

If the carrier is fixed, sun gear is driven and ring gear is the output. Then, sun gear and ring gear rotate in opposite directions. Transmission ratio is

$$i = -(z_r/z_s) \quad (2.2)$$

If the sun gear is fixed, ring gear is driven and carrier is the output. Transmission ratio is:

$$i = 1 + (z_s/z_r) \quad (2.3)$$

If direct drive configuration is used, transmission ratio is 1. Two or more sets of planetary gear can be used to obtain multiplication of gear ratios.

2.4.2.2.2. Multiple Gear Stages

Multiple gear stages can be used to get high transmission ratio. However, for each gear pair there will be some amount of inefficiencies and backlash.

2.4.2.2.3. Worm Gear

Worm gear is composed of worm and gear pair. Worm gear is driven by motor which can be connected by coupling. High transmission ratio in compact area can be obtained. Furthermore, worm gear has auto lock properties, because of which the gear cannot be driven by external forces. Therefore, even if cutting forces are too much and system cannot accommodate torque, system will not rotate in cutting force direction and will be locked [40].

2.4.2.2.4. Strain Wave Gearing

It is also called as harmonic drive. It is composed of wave generator, flex spline and circular spline. Wave generator is the input and the driven element of the transmission system. It has elliptical shape and is surrounded with ball bearing. Flex spline has high torsional stiffness and can transmit torque with external teeth. The circular spline has rigid construction and internal teeth as well as two additional teeth compared to the flex spline. Wave generator is placed inside of the flex spline. Flex spline then gets the shape of wave generator thanks to its flexibility and makes backlash free of contact with rigid circular spline [41]. Figure 2.20 indicates the components of harmonic drive.

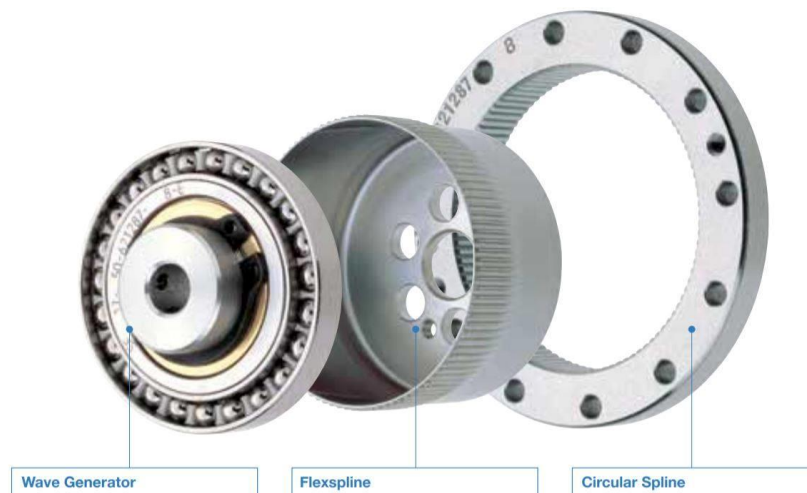


Figure 2.20. Components of harmonic drive [42]

2.4.2.3. Belt Drive and Motor

By using one pulley on the motor side and another on the output side, rotary motion can be conducted to the output side. By using pulleys of different diameters, different transmission ratios can be provided, as explained by Sandin [43]. In flat belts and V-belts slip is the problem. Therefore, proper amount of tensioning must be done by using tensioners. Moreover, timing belts can be used to prevent slippage. More than one output can be obtained by using belt drive. However, in rotary stages only one output belt drive is used.

2.4.2.4. Roller Gear Cam

Roller gear cam structure is similar to worm gear. However, instead of sliding, rolling contact decreases the friction and wear. Moreover, roller gear cam has high load capacity.

By adapting the cam shape, smooth starting and stopping can be obtained. Figure 2.21, presented by Pascal Co. [44], compares roller gear cam with worm drive in terms of their velocity. It can be seen that the roller gear cam has smoother start and stop curve compared to the worm drive.

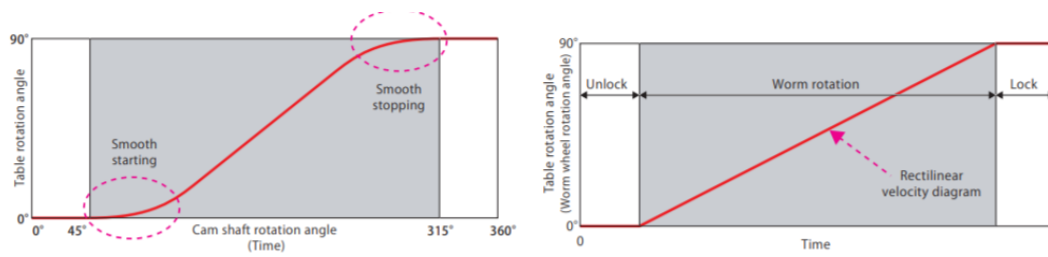


Figure 2.21. Velocity diagrams of roller Gear Cam (left) and worm drive (right) [44]

Figure 2.22 indicates the components of the roller gear cam. The cam shaft is actuated by the motor, while the rolling contact action between the cam shaft and the cam follower enables smooth motion of the turret.

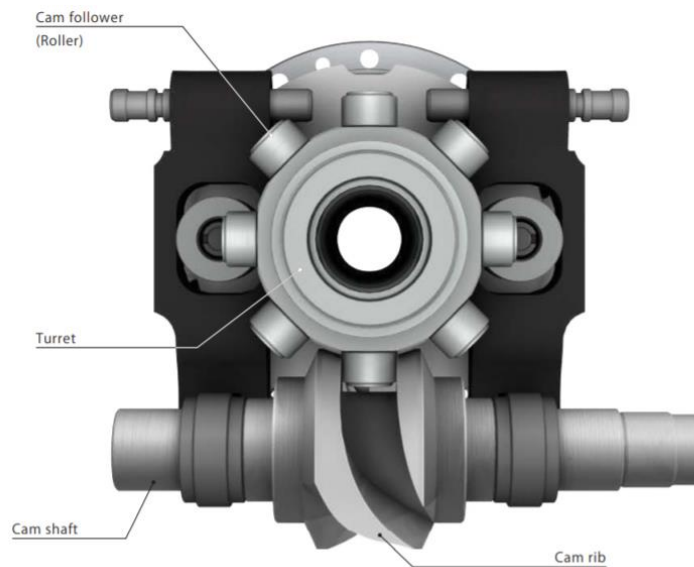


Figure 2.22. The roller gear cam and its components [44]

2.4.2.5. Friction Drives

In friction drives, friction is used to rotate the system. In the following section, different kinds of friction drives are explained.

2.4.2.5.1. Travelling Wave

Two main components of the printed circuit board (PCB) motors are the stator and the rotor. The stator functions in holding the electrical connecting circuit and the actuators, whereas the rotor has a role in providing the mechanical output while being tightly attached to the stator [45].

On the stator, traveling wave is produced. By aid of the wave, an easily movable ring is formed that triggers movement in the shape of ellipse on the rotor interface, as explained by [45]. This kind of motion causes the rotor with the attached drive shaft to start moving. In order to rise the rotational speed, the stator has teeth connected to it. Not only the friction between the moving rotor and the stator, but also amplitude of the wave that moves on the stator determine this process.

As seen from the Figure 2.23 of a PCB motor [45], two modes are initiated at the same time in order to produce a traveling wave inside of the stator. The drive circuit generates two signals that are required for this motion: cos and sin. The signals are located in a close proximity of the stator ring. In order to change the direction of the travelling wave, the drive signal's sign can be reversed.

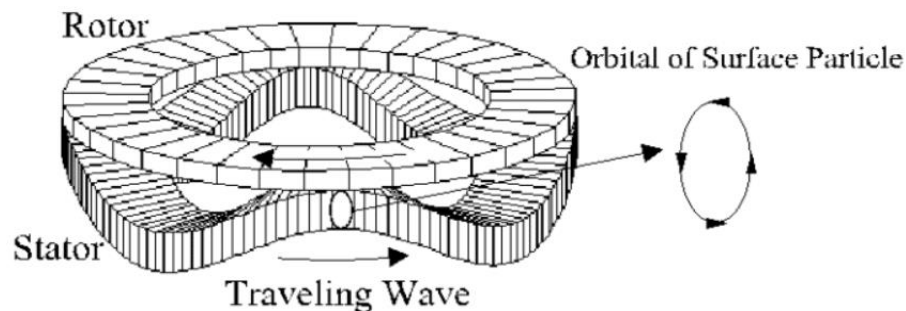


Figure 2.23. The PCB motor [45]

2.4.2.5.2. Roller and Traction Disc

Another method to convert rotary motion generated by a motor into a rotary motion with different reduction ratios is by using a roller, traction disk and a motor.

Power is transmitted by the shear force of a lubricant film which stands between 2 rotating components. The traction fluid is very thin and highly pressurized. Traction fluid is in the state of “hydrodynamic state”. Two rotating components should be preloaded against each other to increase the pressure of the lubricant in between each other, as seen on Figure 2.24 [46].

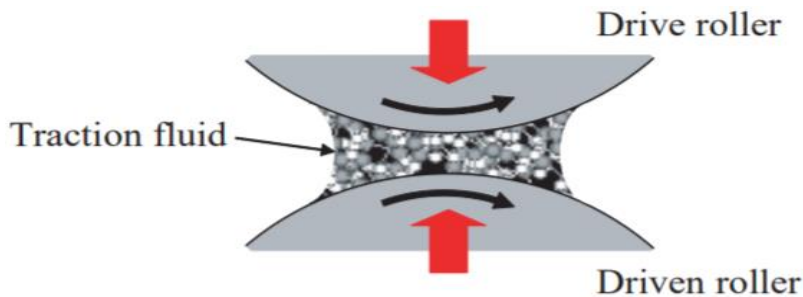


Figure 2.24. The properties of drive system being a power transmitter [46]

Commercial rolling motion industries (RMI) have a traction drive product (such as the one seen on Figure 2.25) [47] that is composed of five mechanical components as well as a lubricant between the rolling balls. Torque is transmitted from cup shaft to toroidal shaft via rolling balls. Therefore, there is rolling friction in between components.

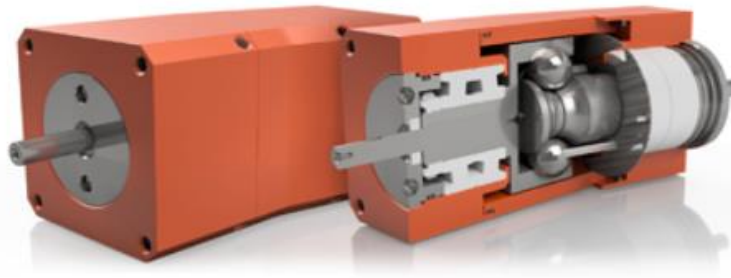


Figure 2.25. The RMI drive [47]

2.4.3. Sensor Systems

Sensor systems used in indirect measurement of linear stages can be used as a direct measurement sensor in rotary stages.

2.4.3.1. Optical Position Systems

Optical position systems in rotary motion's working principle is explained in the linear sensor system section.

2.5. Spindles

Spindle's working principle is like rotary tables, which must rotate without runout. Compared to the rotary tables, spindles generally work at very high speed of 5000-50000 [RPM] [48]. However, when printed circuit board is to be drilled by a spindle, the speed can be as high as 300000 [RPM] [48]. At this high speed, the spindle must withstand cutting forces with reasonable deflections.

Demands		Material	Speed	Power	Torque	Accuracy
Branches						
Job Shop		diverse	●	●	●	●
Mould and Die		steel	●	●	●	●
		Al alloys	●	●	●	●
Aerospace		Al alloys	●	●	●	●
		Ti alloys	○	●	●	●
		FRP	●	●	●	●
Automotive		cast alu.	●	●	●	●
		cast iron	●	●	●	●
Electronics (PCB)		FRP*	●	●	●	●

○ very low
 ◐ low
 ◑ medium
 ◒ high
 ● very high

Figure 2.26. Demands of spindle performance according to branches [29]

Figure 2.26 indicates the demands of spindle performance. For example, cutting of printed circuit boards requires very high speeds, cutting titanium alloys for aerospace requires high torque, and machining of mould and die requires high accuracy.

In order to obtain high precision under these cutting forces and high speeds, spindle must have very stiff, rigid and dynamically balanced construction.

Conventionally, spindles are driven externally via belt or via coupling, as seen from Figure 2.27 [48]. However, in order to eliminate transmission errors and inefficiencies and to obtain even better accuracy and precision, direct drive motors are used.

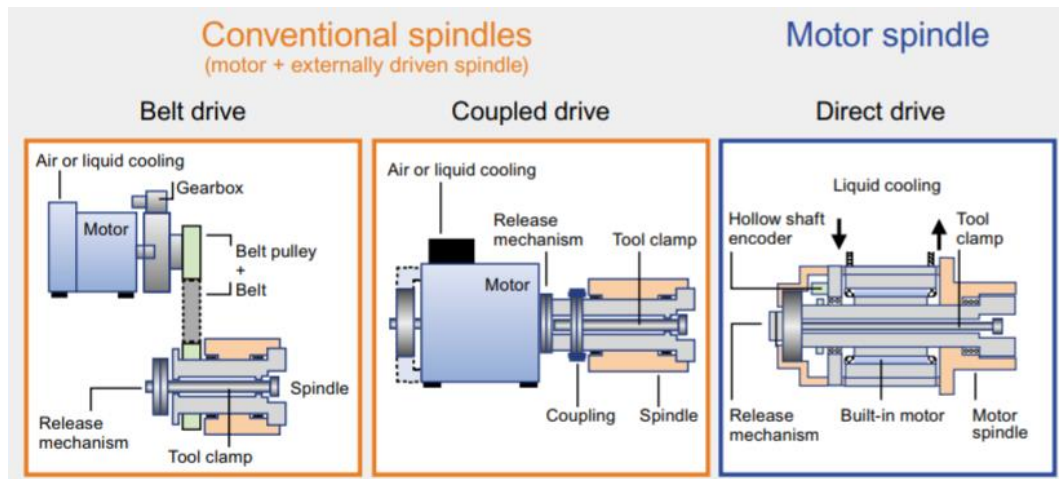


Figure 2.27. Conventional and motor spindles [48]

Rolling element bearings, air bearings, electromagnetic bearings, hydrodynamic and hydrostatic bearings can be used to support spindle in high speeds depending on the application and demands, as explained by [29] and show in Figure 2.28.

	rolling bearing	hydrod. bearing	hydrost. bearing	aerost. bearing	magn. bearing
speed coefficient $n \times d_m$	● ¹⁾	●	●	●	●
long life	●	●	● ²⁾	● ²⁾	● ²⁾
high running accuracy	●	●	●	●	●
high damping	○	●	●	●	●
high stiffness	●	●	●	●	●
low-cost/simple lubrication and lubrication systems	● ³⁾	●	○	●	○ ⁴⁾
low friction	●	○	○	●	●
low cost (Buying, Maintenance)	● ³⁾	●	●	●	○

● totally fulfilled
 ● fulfilled
 ● partly fulfilled
 ○ not fulfilled

1) depending on lubrication system and type of bearing
 2) unlimited lifetime under normal conditions
 3) partly fulfilled with oil-lubrication
 4) highly complex magnetic regulation

Figure 2.28. Performance of bearings [29]

In order to get high precision, components of the spindle should cool down and heat should be removed out from the system. In order to cool the motor, cooling liquid can be used. Yoshioka et al. [50] proposed a system where they control the temperature of the air in air bearing to cool down the system. For high speed application internal coolant system can be used as well.

Tool clamping and release mechanism of the spindle should be designed carefully. The clamping force mostly involves disk springs or spiral springs, which can affect the operation negatively by unbalancing it. In fact, masses may not be homogeneous. In order to avoid this and to provide distribution of masses homogeneously, Jakob and Sykora [51] suggested using gas-pressurized springs as an alternative to steel springs. However, gas springs have negative sides as well, since their pressure drops and causes clamping force to be lost. Therefore, the spring load should be always controlled.

Spindle tool interface is also very important for precision spindle. In order to connect tool and spindle, the tool holder is used. Such kind of an interface provides increased stiffness and sufficient damping, as explained by Rivin [52]. Moreover, by this system the process of changing tool is much faster and reliable.

Figure 2.29 presents an air bearing spindle. It has a frameless and brushless DC motor with an optical encoder. The motor decreases heat generation and is due to this highly efficient. Hence, it is very useful in processes that require high precision. Furthermore, the error of the motion of the spindle is below 25 [nm], even when the speed is around 10 000 [RPM] [53].

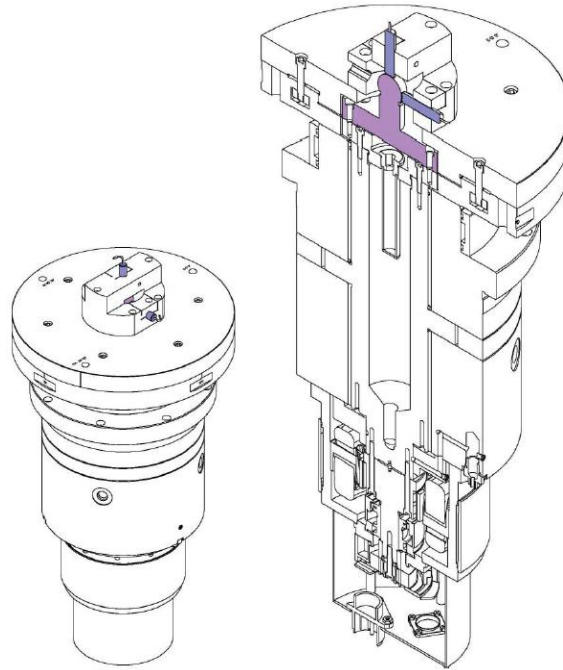


Figure 2.29. Air bearing spindle [53]

2.6. Hybrid Printer Systems

There are several commercially available hybrid machine tools that have a combination of additive and subtractive processes.

An example of a 5-axis machining that makes material spraying as an additive process is a product Hermle C-40 made by Hermle Co [54]. Another additive process is directed energy deposition. It is used by the products like Caybman Replicator made by Cybaman Technologies [55], Lasertec 65 3D by Dmg Mori [56], Hybrid HSTM 1000 by Hamuel Reichenbacher [57], Integrex I-400AM by Mazak [58], Lens 3D Hybrid 20 by Optomec [59], 3D Hybrid ARC, Laser and Cold Spray by 3D Hybrid Solutions [60], AMBIT Multitaks System by Hybrid Manuf. Tech. [61] and Add and Process Family by Ibarmia [62]. All of these products use 5-axis machining as a subtractive process, except for the Replicator that makes 6-axis machining. Replicator has epoxy resing fibre granite structure and working area of 170 [mm] in X-, Y- and Z direction. In addition to additive- and subtractive processes it also

provides some assistive processes such as robot welding and 3D scanning. The performance of Lasertec 65 3D is improved by using the combination of materials like Copper and Inconel. Moreover, its working area is 735 [mm] in X direction, 650 [mm] in Y direction and 560 [mm] in Z direction. It uses a highly controlled laser deposition for 5-axis milling. 5-axis milling at high speed is also an essential property of Hybrid HSTM 100 product. This product uses 3D scanning, deburring, laser cladding, laser marking and many other assistive processes to produce a workpiece on 45° inclined slide way that allows for the best mass distribution. Another product that uses laser marking as an assistive process is Integrex I-400AM. It makes 2 main subtractive processes: turning and 5-axis machining. The bed length of its feed axes is 615 [mm] in X axis, 260 [mm] in Y axis and 1585 [mm] in Z axis. A product with slightly smaller working area is Lens 3D Hybrid 20. Its working area is 500×300×500 [mm] in X-, Y- and Z directions respectively. This product, that is made of cast iron, uses atmospheric control to deliver metal powders like Inconel, Steel and Titanium. Moreover, it also uses heat treatment as an assistive process.

Next product that makes 5-axis milling comes from 3D Hybrid Solutions Co.. Their product is a combination of three metal additive manufacturing tools, which are 3D Hybrid ARC (utilizes electrical energy), 3D Hybrid Laser (optical energy) and 3D Hybrid Cold Spray (kinetic energy). With ARC technology, printing of feed-stock alloys, such as aluminum alloys, stainless steel alloys and nickel based super alloys can be performed. By 3D Hybrid Cold spray, materials like copper, nickel, aluminum, titanium and many others can be processed. The last two discussed products that make directed energy depositions an additive process are AMBIT Multitask system and Add & Process Family. The former one uses stress relieving and marking as assistive processes and can print on a working area of 120×40×30 [mm] in X-, Y- and Z directions respectively. In case of Add & Process Family product, the working area is much larger and can print a workpiece as large 1.6 [m].

Apart from the directed energy deposition, other additive processes can be used as well. These include material jetting, powder bed fusion, sheet lamination and material extrusion.

An example of a commercially available product that uses material jetting is a Solidscape family made by Solidscape Co. [63]. It performs high precision milling that is, unlike in most of other products, used especially for jewelry design and manufacturing. The Solidscape 3D printer creates wax models with high precision which are then casted into metals.

Powder bed fusion additive process is used by products such as Lumex Avance 25/60 made by Matsuura [64], Opm350L by Sodick [65] and M Line Factory by Concept Laser [66]. The first one makes 3-axis machining and, similarly to Lens 3D Hybrid 20, uses atmospheric control as an assistive process. It can work on a workpiece of a maximum 600 [mm] in width and depth and 500 [mm] in height. Opm350L can work on only half as big workpiece as Lumex Avance. However, unlike Lumex Avance, it can make 6-axis machining with assistive process of material recovery system. The product of the Concept Laser Co. performs CNC machining on an industrial scale. It can make powder bed fusion on a workpiece slightly smaller than the Lumex Avance machine.

Last product described here is SonicLayer4000 made by Fabrisonic Co. [67] that uses sheet lamination to add material. It performs 3-axis machining to which ultrasonic welding is integrated.

Finally, in material extrusion additive manufacturing systems material is liquified in extruder head and poured on flat surface layer by layer. Heat is required in order to liquify the material. Heating the material influences the dimensional stability of the material. When the material cools down, dimensions of the product change and some amount of warpage can be observed in the system. Drawback of the material extrusion additive manufacturing can be eliminated by using subtractive manufacturing in the same platform. This idea is also the main scope of this thesis.

There are commercially available hybrid manufacturing systems that combine for material extrusion and milling in one platform. One of the 5-axis hybrid manufacturing platforms is Enamoto. In the platform, extruder head is next to the spindle. Another hybrid commercially available product is Diabase and has turret type tool holders that can hold many other manufacturing and quality control systems on itself. Ethereal is

another recent commercial product. It is affordable desktop hybrid manufacturing system. However, its software is complex for user. Nscrypt is gantry type hybrid manufacturing system that has the advantage of high workpiece volume to machine dimensions. It has different products each of which has different accuracy level. Most accurate one, 3Dn-500, has accuracy 1.5 [μm] in X-, Y- and 3 [μm] in Z directions. Lastly, Hydra 16A has heated and enclosed build environment that can control the temperature of the manufacturing material.

Table 2.1. *Commercially available products that can carry out extrusion type additive manufacturing and subtractive manufacturing at the same time*

	Number of Axis	Accuracy [μm]
Enamoto	5-axis	X
Diabase	5-axis	50
Ethareal	5-axis	60
Nscrypt	3-axis	1.5×1.5×3 (X×Y×Z)
Hydra 16A	5-axis	60×60×10 (X×Y×Z)

CHAPTER 3

DESIGN OF HYBRID MANUFACTURING SYSTEM

3.1. Introduction

In this thesis it is desired to design a machine which has capability to do fused filament fabrication and machining at the same time. Mainly thermoplastics will be milled with this machine which can be as big as 300 [mm] in diameter and 300 [mm] in length. However, it is also desired to machine Al-6000 series, copper and others. Moreover, it is desired to eliminate support structures and staircase effect which are the bottleneck problems of conventional 3D printers. Furthermore, it is desired to produce complex slots/holes without support structure to obtain better surface quality. In fact, with conventional 3D printers this was not possible.

In order to eliminate the support structure, it is necessary to have two additional rotary axis that allow for the production of complex shapes. Moreover, it is desired to have variable bead width which provides variety of thicknesses during fused filament fabrication. The variable bead width will be accomplished by having rectangular shaped nozzle which can rotate around the centre of the rectangle. Initial specifications of the machine are listed in Table 3.1.

Table 3.1. *Machine specifications*

Working Volume Dimensions	300 [mm] × 300 [mm] × 300 [mm]
Materials Processed	Al series, Copper, ABS, PLA, Nylon, PETG, POM
Motion Control Method	RS-274-D Accepts Standard G Code
Accuracy [μm]	100

3.2. Concept Selection

System architecture is based on a 5-axis vertical CNC machine tool, and all possible alternatives are considered individually during the preliminary design process. In general, there are 2^N specific machine configurations for a machine with N independent (linear and rotary) axes. There are $2^5 = 32$ different alternative solutions on a machine with 5 degrees of freedom. The best architecture has been selected considering the technical advantages/disadvantages of all of the alternatives within the scope of this thesis. Figures 3.1 and 3.2 show some types of hybrid machines that have been considered and designed.

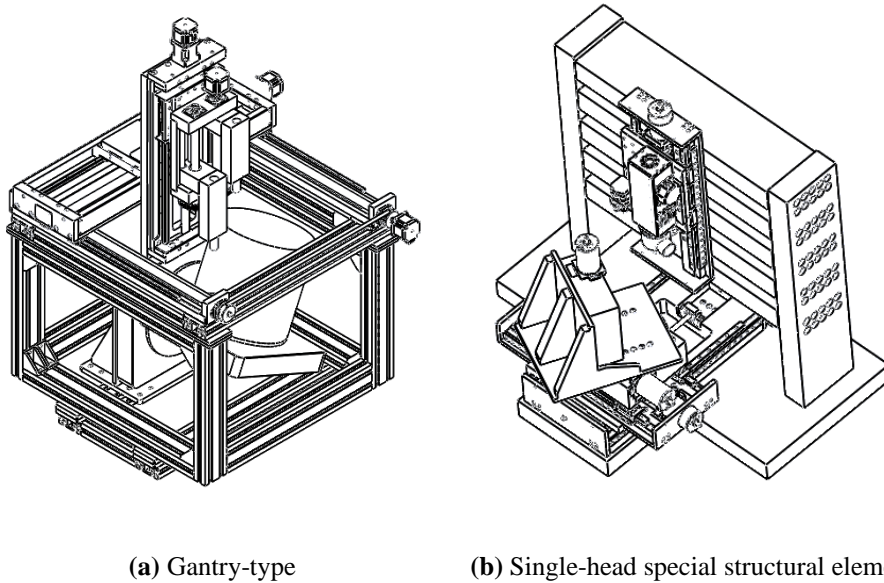


Figure 3.1. Some conceptual machine designs

For the concept selection the following properties have been considered:

- modularity,
- rigidity of the system,
- ease of manufacture,
- cost of manufacture,
- ratio of the producible workpiece volume to structure volume,
- Precision of the system.

Main problem of the designs in Figure 3.1 is having a spindle and extruder head on the same linear axes. Moreover, apart from spindle and extruder head, also systems like variable nozzle head, filament feeder mechanism and spindle vacuum mechanism will be in the hybrid manufacturing centre. Therefore, having all these components on the same axis makes the system complicated.

Highest producible workpiece volume to the structure volume ratio can be obtained by the gantry type structure which is shown in Figure-3.1a. However, this system needs additional mechanism to adjust position of the nozzle and spindle. Having extra position adjustment mechanism cannot solve the problem of having all mechanisms on a single axis. Furthermore, this mechanism brings additional cost and extra challenge to control the system.

Because of these reasons, extruder head and spindle are taken to different axes. This system enables independency of the spindle and extruder head. Furthermore, having symmetric system and modular design enables usability of different manufacturing systems other than extruder head and spindle.

Figure 3.2 indicates a system that has extruder head and spindle on different axis. It has eight axis to obtain 5 degrees of freedom, which is costly. Therefore, another configuration, which has 4 degrees of freedom for the workpiece, 1 degree of freedom for the spindle and 2 degrees of freedom for the nozzle, is selected and shown in Figure 3.3.

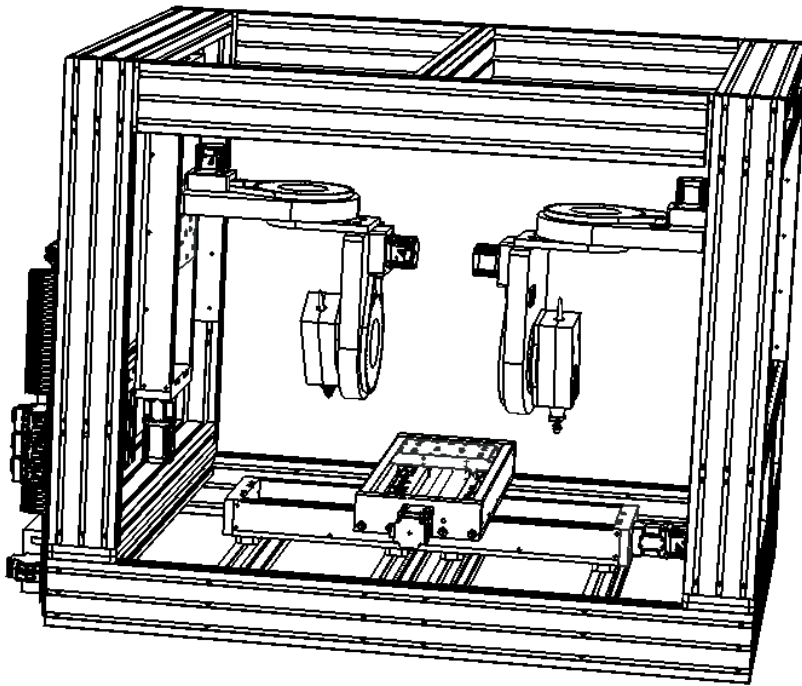


Figure 3.2. Swiveling tool configuration

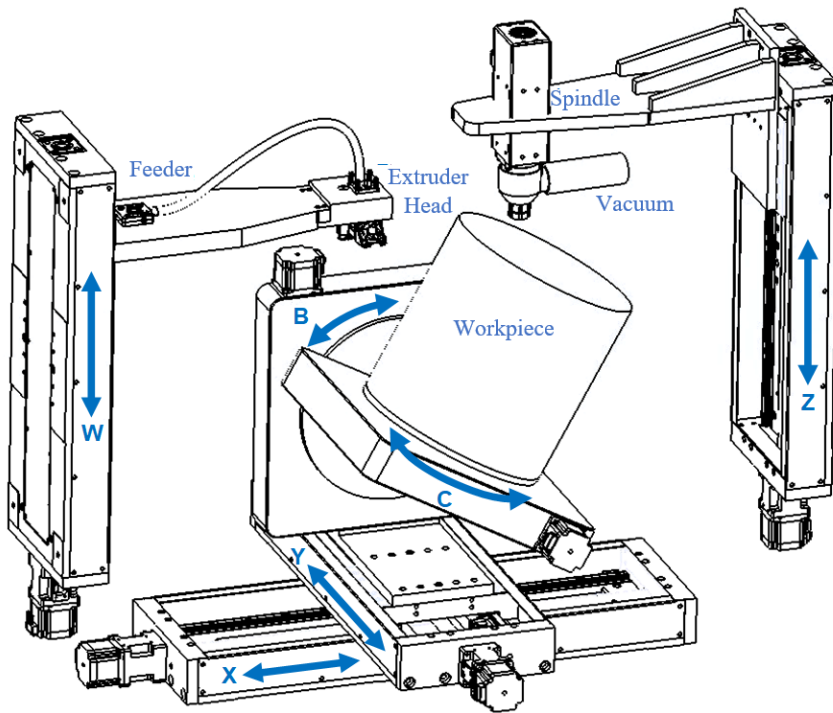


Figure 3.3. Final design

3.3. Dimensional Analysis

In Excel environment, dimensional analysis for manufacturing 300 [mm] diameter and 300 [mm] length workpiece has been done. Based on this analysis, stroke values and overall dimensions of the X-, Y- and Z axis are shown in Table 3.2.

Table 3.2. *Dimensions of hybrid manufacturing system*

	X	Y	Z/W
Axis Stroke [mm]	422	312	312
Working Volume [mm]	1100	1110	980.2
Structure Length [mm]	1370	1200	1115.2

3.3.1. Dimensional Analysis along X Direction

For the analysis of X axis, 2 different cases were considered. On the left side of Figure3.2 it is shown that workpiece is 90° rotated. In this case, workpiece can be machined completely and additional 11 [mm] allowance is left for the motion of 20 [mm] cutting tool to move around the workpiece. On the left side of Figure 3.4 it can be seen that more than half of the workpiece can be machined. Other half of the workpiece can be machined by rotating workpiece 180 degree with the C axis.

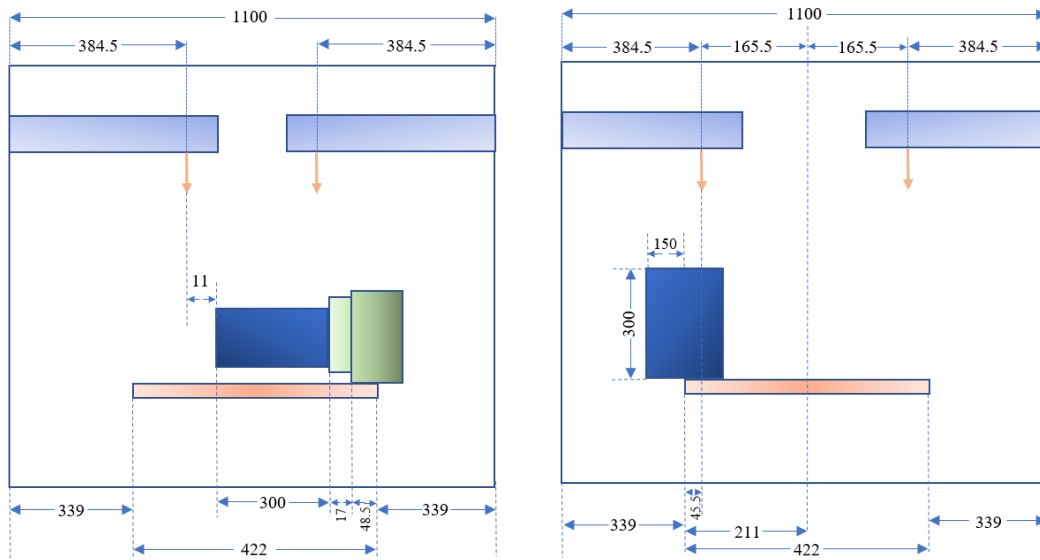


Figure 3.4. X direction dimensional analysis

3.3.2. Dimensional Analysis along Y Direction

For the Y direction, stroke of the Y axis is adjusted to 312 [mm]. For most of the cases, such as when the workpiece diameter is less than 290 [mm], workpiece can be produced/milled without need for C axis. However, in case of 300 [mm] workpiece and 20 [mm] cutting tool, C axis should be used. Figure 3.5 shows the details.

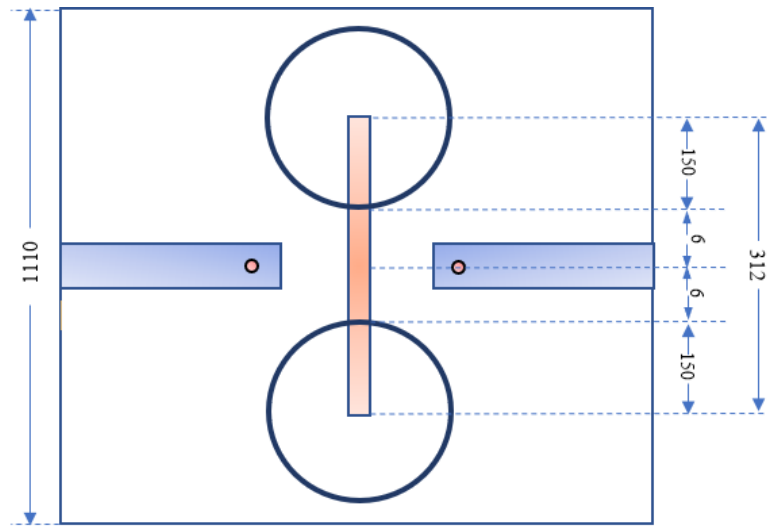


Figure 3.5. Y direction dimensional analysis

3.3.3. Dimensional Analysis along Z Direction

Similar to X axis, 90 [degree] rotated and non-rotated workpiece are examined for the dimensional analysis for the Z direction. It is observed that in order to manufacture a 300 [mm] length workpiece for both of the cases, nozzle or spindle should be shifted 53.1 [mm] in Z direction. Figure 3.6 shows the details for the Z direction.

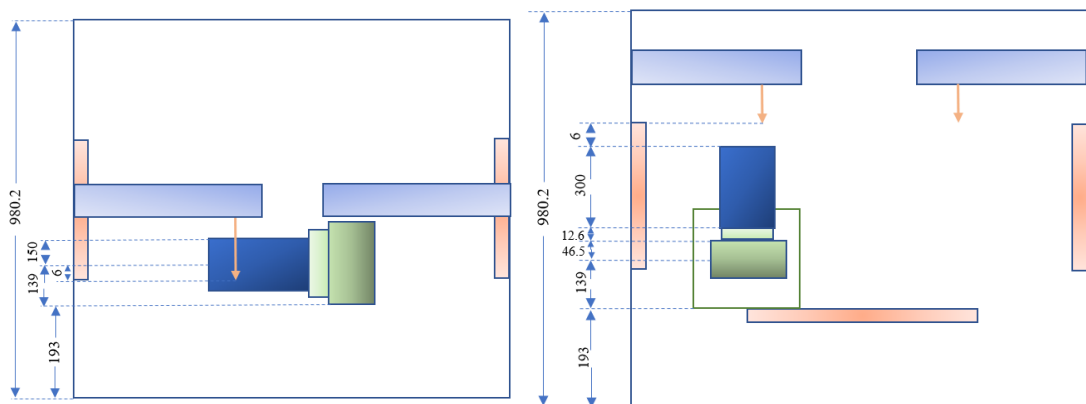


Figure 3.6. Z direction dimensional analysis

3.4. Kinematic Analysis and Error Budget

In this section, the kinematic analysis of the hybrid manufacturing machine is elaborated. Figure 3.7a indicates the main components of the hybrid manufacturing systems and Figure 3.7b indicates the coordinate system of each of these components. The following equations are based on Figure 3.7b.

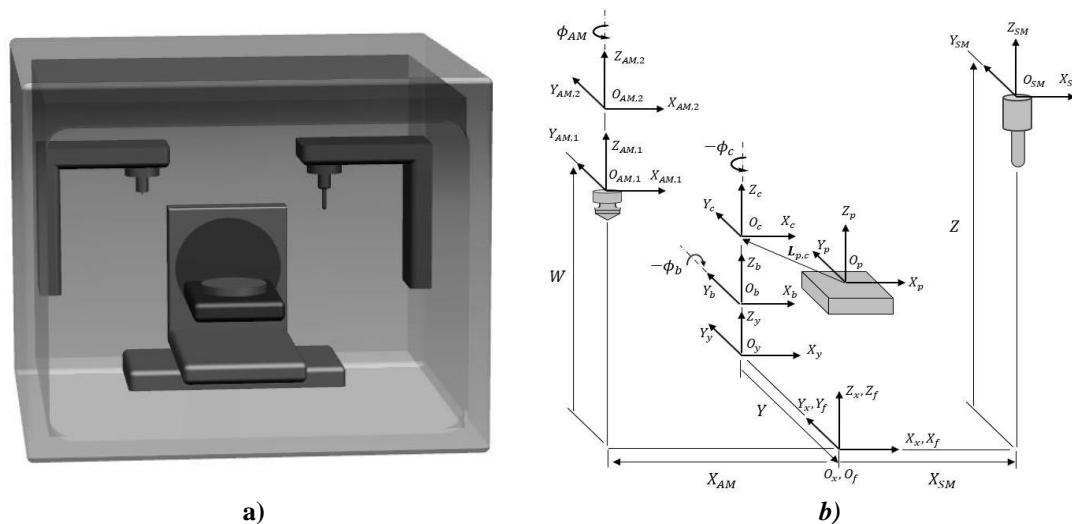


Figure 3.7. a) Solid view of hybrid manufacturing system. b) Coordinate frames of hybrid manufacturing system.

Table 3.3 shows the coordinate frames used in Figure 3.7. p subscript is used for workpiece, whereas c , b , x and y subscripts are used for rotary- and linear stages. SM subscript is used for subtractive manufacturing and AM subscript is used for additive manufacturing.

Table 3.3. Representation of coordinate frame shown in Figure 3.7

Representation	Related Coordinate Frame
$O_p X_p Y_p Z_p$	Workpiece coordinate frame
$O_c X_c Y_c Z_c$	C Rotary Table Coordinate Frame
$O_b X_b Y_b Z_b$	B Rotary Table Coordinate Frame
$O_x X_x Y_x Z_x$	X Linear Table Coordinate Frame
$O_y X_y Y_y Z_y$	Y Linear Table Coordinate Frame
$O_{SM} X_{SM} Y_{SM} Z_{SM}$	Subtractive Manufacturing Coordinate Frame
$O_{AM,1} X_{AM,1} Y_{AM,1} Z_{AM,1}$	Additive Manufacturing Coordinate Frame
$O_{AM,2} X_{AM,2} Y_{AM,2} Z_{AM,2}$	Additive Manufacturing Nozzle Coordinate Frame

Table 3.4 shows the joint variables used in kinematic analysis. Symbol ϕ is used for rotation, whereas symbols X , Y , Z and W are used for translation.

Table 3.4. Joint variables

Transformation	Joint Variable
C axis Rotation	ϕ_c
B axis Rotation	ϕ_b
Y axis Translation	Y
X axis Translation	X_{AM}, X_{SM}
W axis Translation	W
Z axis Translation	Z
C axis Rotation (nozzle)	ϕ_{AM}

General kinematic model of hybrid manufacturing machine is presented in the following equations. The tool contact point can be written as

$${}^f P_p = {}^f_x T(X_{SM}) {}^x_y T(Y) {}^y_b T(\phi_b) {}^b_c T(\phi_c) {}^c P_p \quad (3.1)$$

Here, ${}^f\mathbf{P}_p$ is the position vector of point P in the coordinate frame f and ${}^f_x\mathbf{T}$ is the homogenous transformation matrices (HTM) from the t coordinate frame to the x coordinate frame. Tool contact point can also be calculated over the Z axis as

$${}^f\mathbf{P}_p(Z) = {}^f_z\mathbf{T}(Z) {}^z\mathbf{P}_p \quad (3.2)$$

HTM included in Eqns. (3.1) and (3.2) is indicated as

$${}^f_x\mathbf{T}(X_{SM}) = \begin{bmatrix} 1 & -\varepsilon_{z1} & \varepsilon_{y1} & X_{SM} + \delta_{x1} \\ \varepsilon_{z1} & 1 & -\varepsilon_{x1} & \delta_{y1} \\ \varepsilon_{y1} & \varepsilon_{x1} & 1 & 76 + \delta_{z1} \\ 0 & 0 & 0 & 1 \end{bmatrix} \quad (3.3)$$

$${}^x_y\mathbf{T}(Y) = \begin{bmatrix} 1 & -\varepsilon_{z2} & \varepsilon_{y2} & \delta_{x2} \\ \varepsilon_{z2} & 1 & -\varepsilon_{x2} & Y + 178.5 + \delta_{y2} \\ \varepsilon_{y2} & \varepsilon_{x2} & 1 & 241 + \delta_{z2} \\ 0 & 0 & 0 & 1 \end{bmatrix} \quad (3.4)$$

$${}^y_b\mathbf{T}(\theta_y) = \begin{bmatrix} c\theta_y & -c\theta_y\varepsilon_{z3} & s\theta_y & \delta_{x3} \\ \varepsilon_{x3}s\theta_y + \varepsilon_{z3} & 1 & -\varepsilon_{x3}c\theta_y & -178.5 + \delta_{y3} \\ -s\theta_y & s\theta_y\varepsilon_{z3} + \varepsilon_{x3} & c\theta_y & 46.5 + \delta_{z3} \\ 0 & 0 & 0 & 1 \end{bmatrix} \quad (3.5)$$

$${}^b_c\mathbf{T}(\theta_z) = \begin{bmatrix} c\theta_z & -s\theta_z & \varepsilon_{y4} & \delta_{x4} \\ s\theta_z & c\theta_z & -\varepsilon_{x4} & \delta_{y4} \\ -\varepsilon_{y4}c\theta_z + \varepsilon_{x4}s\theta_z & \varepsilon_{y4}s\theta_z + \varepsilon_{x4}c\theta_z & 1 & 19 + \delta_{z4} \\ 0 & 0 & 0 & 1 \end{bmatrix} \quad (3.6)$$

Relative position of the spindle contact point with respect to the workpiece (${}^c\mathbf{P}_p$) can be written as

$${}^c\mathbf{P}_p(X_{SM}, Y, \theta_y, \theta_z, Z) = {}^c_f\mathbf{T}(X_{SM}) {}^f_z\mathbf{T}(Z) {}^z\mathbf{P}_p \quad (3.7)$$

By setting all error terms as 0, ideal position of the tool contact point (${}^{c*}\mathbf{P}_p$) can be calculated. Finally, error vector (\mathbf{E}) can be calculated as

$$\mathbf{E} = {}^c\mathbf{P}_p - {}^{c*}\mathbf{P}_p \quad (3.8)$$

Components of error vectors are

$$\mathbf{E} = [\Delta x \ \Delta y \ \Delta z]^T \quad (3.9)$$

where Δx , Δy and Δz are total errors in X-, Y- and Z directions respectively. Position error metric (ε) can be calculated as

$$\varepsilon = \sqrt{\Delta x^2 + \Delta y^2 + \Delta z^2} \quad (3.10)$$

3.4.1. Error Budget

In this section, boundaries for the angular and displacement errors are calculated by using Monte Carlo simulation. Algorithm for the error budget calculation is shown as

Algorithm 3.4.1 Monte Carlo Simulation for Error Budgeting

1. Set the accuracy of the machine.
 2. Set the angular and displacement error boundaries for each axis.
 3. Randomly generate angular and displacement errors for each axis.
 4. Construct kinematic model of the machine which includes angular and displacement errors, Eqns. (3.1) – (3.6).
 5. Calculate the tool position (spindle, or nozzle) with respect to workpiece from kinematic model (tool contact position) Eqn. (3.7).
 6. Calculate the ideal tool contact position by setting all error terms the zero.
 7. Subtract normal tool contact position from ideal tool contact position, Eqn. (3.8).
 8. Calculate the total error of the machine.
 9. Run the code from 1-8 100000 times
 10. Take the standard deviation of total error and multiply by 2
 11. If the calculated value is less than predetermined accuracy of the machine, increase the angular and displacement error boundaries or if the calculated value is more than predetermined accuracy of the machine, decrease the angular and displacement error boundaries.
-

Error boundaries can be set as

$$-25 \text{ arc sec} \leq \varepsilon_x, \varepsilon_y, \varepsilon_z \leq 25 \text{ arc sec} \quad (3.11)$$

$$-25 \mu\text{m} \leq \delta_x, \delta_y, \delta_z \leq 25 \mu\text{m} \quad (3.12)$$

Solving Eqns. (3.1) – (3.10) 100 000 times the following histogram plot is obtained, which is shown in Figure 3.8.

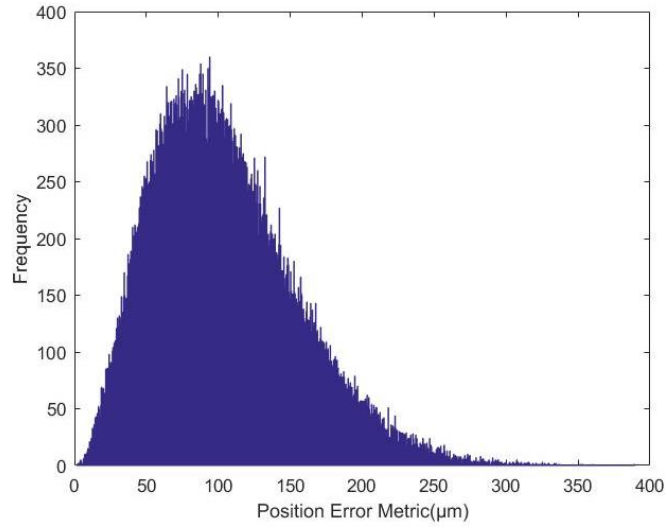


Figure 3.8. The results of Monte Carlo simulation.

Accuracy of the machine (A) can be calculated as

$$A = 2 \cdot \sigma = 2 \cdot \sqrt{\frac{1}{n-1} \sum_{j=1}^n (x_j - \bar{x})^2} \quad (3.13)$$

where σ is standard deviation. As a result of Eqn. (3.13), accuracy of the machine is found as ≈ 100 [μm].

Table 3.5. Results of error budget analysis

	δ_x [μm]	δ_y [μm]	δ_z [μm]	ϵ_x [arcsec]	ϵ_y [arcsec]	ϵ_z [arcsec]
X axis	25	25	25	25	25	25
Y axis	25	25	25	25	25	25
Z axis	25	25	25	25	25	25
B axis	25	25	25	25	25	25
C axis	25	25	25	25	25	25

3.5. Structures

Structures are the components of the machine tool that are dedicated to locating the other components geometrically and carry every load induced from each component. Any deflection on the structure will cause undesired displacement of other geometrical components. Therefore, structure of the machine tool should be rigid. Rigidity of the machine depends on both material and geometry of the component. Closed profiles such as rectangular tube or circular tubes have much higher stiffness in all directions compared to a rectangle which has the same amount of material.

Residual stress induced during manufacturing causes creep and dimensional instability. In order to keep the material dimensionally stable the ratio of residual stress to yield strength of the material should be minimized. Hardened or heat treated materials are subjected to high amount of residual stress. Therefore, they are more likely to be dimensionally instable. Apart from manufacturing, assembly process is important for dimensional stability. Thus, assembly process should be done at low stress levels.

Wolff [68] described dimensional stability as a function of compliance (S) in [1/MPa], coefficient of thermal expansion (α) in [1/K], coefficient of moisture expansion (β), coefficient of temporal expansion (η) in [1/s] and coefficient of radiation expansion (ψ) in [W/(m²K)]. This is described as

$$\varepsilon = S\Delta\sigma + \alpha\Delta T + \beta\Delta M + \eta\Delta t + \psi\Delta Q + \dots \quad (3.14)$$

where ε represents the linear strains, σ applied stress in [MPa], T temperature [K], M absorbed moisture, t time in [s] and Q radiation in [m²K/W]. According to Eqn. (3.14), materials which have the minimum coefficients explained above would have good dimensional stability.

Some properties of dimensionally stable structural materials can be found in [4]. Among the given materials, aluminium oxide has the highest stiffness with modulus of elasticity being 386 [GPa]. On the other hand, granite has the lowest modulus of elasticity which is 19 [GPa]. Higher the stiffness, less deformation under a certain

load. Thermal conductivity is another important parameter to consider in machinery. Materials with high thermal conductivity can be used to remove the heat from the desired location. For example, materials like copper have very high thermal conductivity. Moreover, thermal diffusivity is also important for precision machinery, because it is a measure of how fast heat moves from a hot end to the cold end. The coefficient of thermal expansion is also another important parameter. Materials like invar, Super invar and zerodur have very low coefficient of thermal expansion. Even if they are subjected to very high temperatures, they are dimensionally stable.

Al-6061-T6 is used as a structural material for entire machinery because of its good dimensional stability, low density, good enough stiffness, good thermal conductivity, good thermal diffusivity and low cost. Moreover, Al-6061-T6 is easily machinable.

Different structural members, which are also explained in Section 2.2, have been considered when deciding on which structure to use. By considering price, structural strength and ease of assembly, sigma profiles have been chosen as structural members. Sigma profiles are connected to each other by bolts and glue. Glue between sigma profiles increases the shear strength of the connection and the damping properties. Bolted connections are durable for tension and compression. Moreover, micro slips during dynamic motion of the structure dissipate the vibration of the system. At the same time, the combination of glued and bolted members makes superior tension, compression and shear strength as good damping properties.

3.5.1. Static- and Modal Analysis

Static- and vibration analysis of the structure are carried out to observe the static and dynamic properties of the system.

For the static structural analysis, material and contact properties are defined. Contact regions between the structure and the ground are fixed. 150 [N] force was applied on spindle and 350 [N] force was applied on C axis. 0.068 [mm] maximum deflection has been determined under these boundary and force conditions. Details are shown in Figure 3.9.

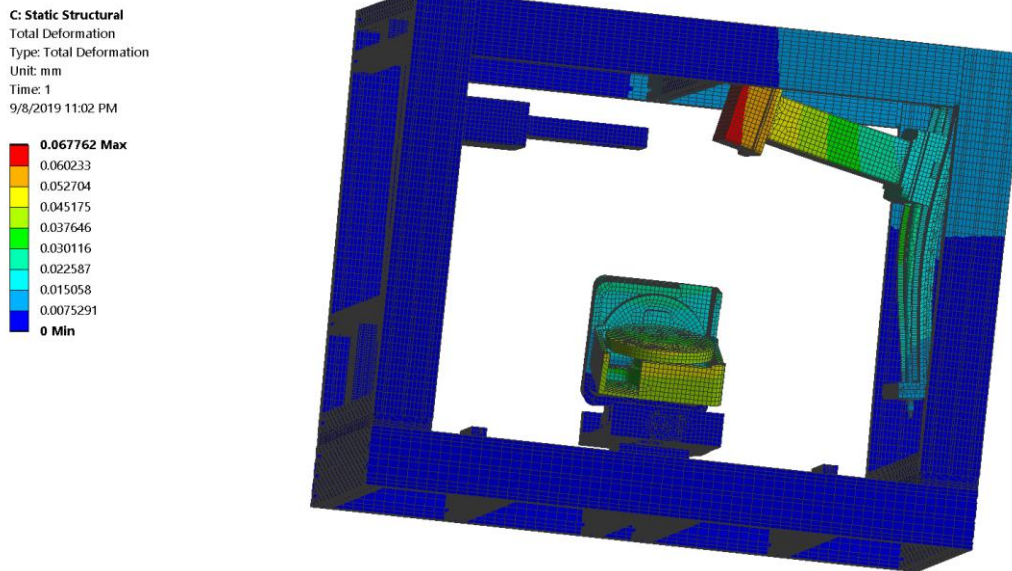
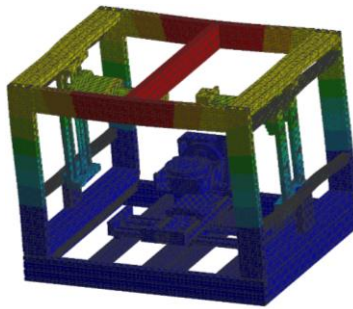
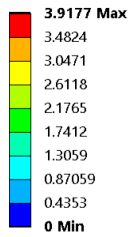


Figure 3.9. The result of static structural analysis

For the modal analysis, material and contact properties are defined. Contact region between the structure and the ground are fixed. Figures 3.10 – 3.12 indicate the first 15 mode shapes and total deformation of the structure for the natural frequencies of the machine.

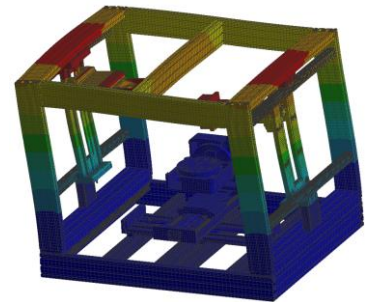
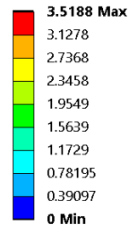
First natural frequency obtained from the analysis is 49 [Hz]. For 2 teeth cutter, the spindle speed should not come closer to 1470 [RPM] ($=49 \text{ [rev/s]} \times 60 \text{ [s/min]} \div 2 \text{ [teeth]}$) such that the structure is not subjected to such excitation frequencies that are closer to its natural ones.

B: Modal
 Total Deformation
 Type: Total Deformation
 Frequency: 48.981 Hz
 Unit: mm
 9/8/2019 10:36 AM



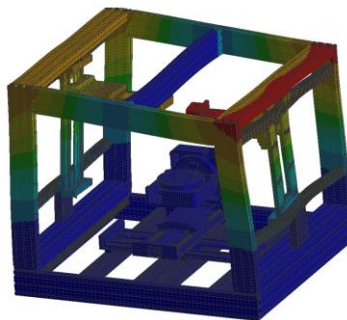
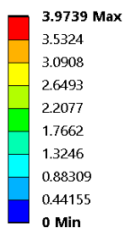
a) 1st mode

B: Modal
 Total Deformation 2
 Type: Total Deformation
 Frequency: 56.234 Hz
 Unit: mm
 9/8/2019 10:37 AM



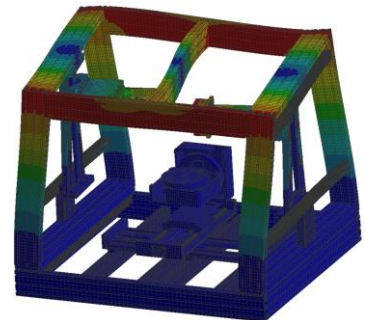
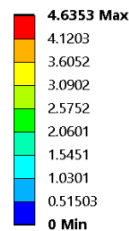
b) 2nd mode

B: Modal
 Total Deformation 3
 Type: Total Deformation
 Frequency: 65.057 Hz
 Unit: mm
 9/8/2019 10:37 AM



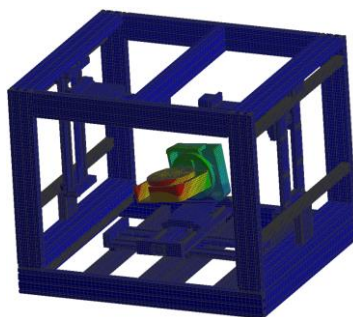
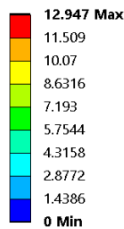
c) 3rd mode

B: Modal
 Total Deformation 4
 Type: Total Deformation
 Frequency: 94.547 Hz
 Unit: mm
 9/8/2019 10:38 AM



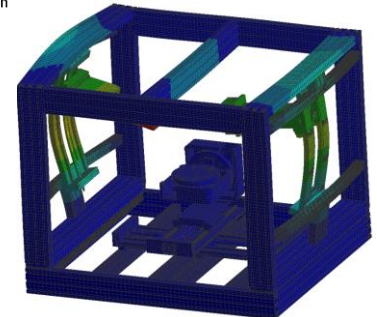
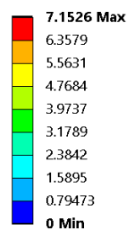
d) 4th mode

B: Modal
 Total Deformation 5
 Type: Total Deformation
 Frequency: 95.373 Hz
 Unit: mm
 9/8/2019 10:39 AM



e) 5th mode

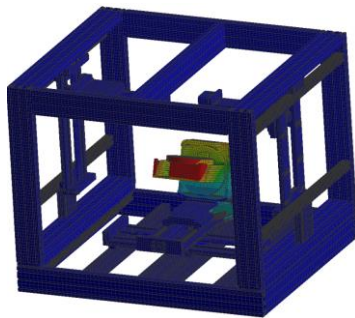
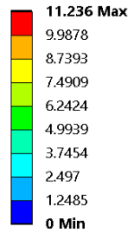
B: Modal
 Total Deformation 6
 Type: Total Deformation
 Frequency: 98.384 Hz
 Unit: mm
 9/8/2019 10:40 AM



f) 6th mode

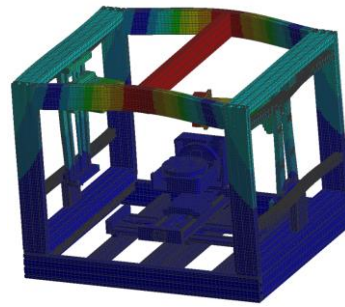
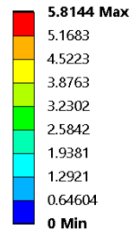
Figure 3.10. Natural frequencies and deflections from 1st to 6th mode.

B: Modal
 Total Deformation 7
 Type: Total Deformation
 Frequency: 107.21 Hz
 Unit: mm
 9/8/2019 10:41 AM



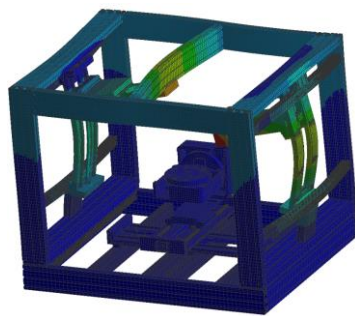
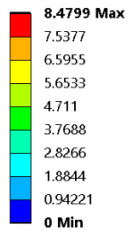
a) 7th mode

B: Modal
 Total Deformation 8
 Type: Total Deformation
 Frequency: 108.91 Hz
 Unit: mm
 9/8/2019 10:41 AM



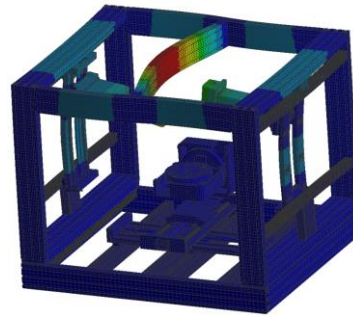
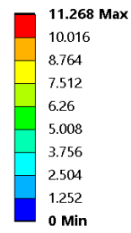
b) 8th mode

B: Modal
 Total Deformation 9
 Type: Total Deformation
 Frequency: 112.57 Hz
 Unit: mm
 9/8/2019 10:42 AM



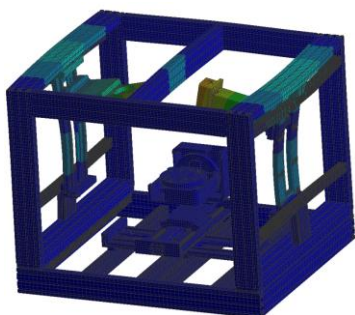
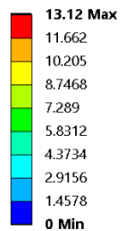
c) 9th mode

B: Modal
 Total Deformation 10
 Type: Total Deformation
 Frequency: 140.39 Hz
 Unit: mm
 9/8/2019 10:43 AM



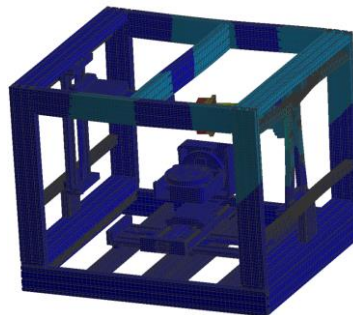
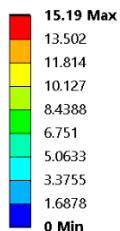
d) 10th mode

B: Modal
 Total Deformation 11
 Type: Total Deformation
 Frequency: 149.97 Hz
 Unit: mm
 9/8/2019 10:44 AM



e) 11th mode

B: Modal
 Total Deformation 12
 Type: Total Deformation
 Frequency: 160.64 Hz
 Unit: mm
 9/8/2019 10:45 AM



f) 12th mode

Figure 3.11. Natural frequencies and deflections from 7th to 12th mode.

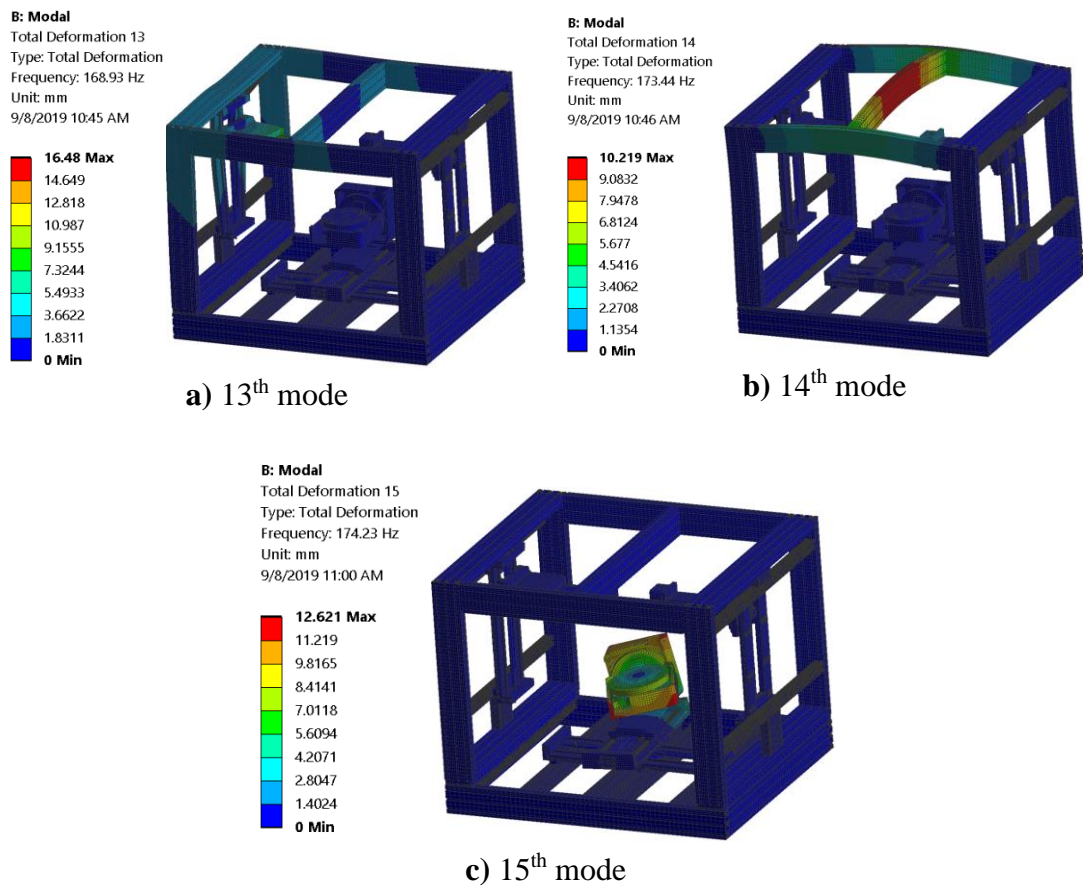


Figure 3.12. Natural frequencies and deflections from 13th to 15th mode.

Table 3.6 indicates the tabular results of the modal analysis. f represents the frequency in [Hz]. and δ represents the deflection in [mm].

Table 3.6. Results of modal analysis

No	f [Hz]	δ [mm]	No	f [Hz]	δ [mm]	No	f [Hz]	δ [mm]
1	49.0	3.9	6	98.4	7.2	11	150.0	11.3
2	56.2	3.5	7	107.2	11.2	12	160.6	15.2
3	65.1	4.0	8	108.9	5.8	13	168.9	16.5
4	94.6	4.6	9	112.6	8.5	14	173.4	10.2
5	95.4	12.9	10	140.4	11.3	15	174.2	12.6

3.6. Linear Stages

There are different ways to obtain linear motion. Structure, linear bearings, actuation and transmission system and sensor affect the overall performance of the system.

3.6.1. Structures

Al-6063-T5 is chosen for the construction of the linear axis. Having good material stability properties of Al-6063-T5 keeps the structure unchanged over time. Furthermore, good machinability properties of the Al-6000 series enable machining with low cutting forces. Therefore, residual stress occurring during machining of Al is lower compared to machining of steel. Moreover, Al is light and has enough strength properties for the application.

3.6.2. Actuation and Transmission

For the transmission system, all the systems which are discussed in Section 2.3.2 are considered. Although linear actuators provide superior accuracy and precision properties they are not chosen because of their high cost. Furthermore, friction drives are accurate and have zero backlash. However, they require closed loop system which makes the overall system expensive. Timing belts have no slippage problem and have good precision values. However, load carrying capacity of belts is limited. Furthermore, low stiffness of belts makes the system's accuracy lower under metal cutting forces. Moreover, Rack and Pinion system has some amount of backlash. This backlash can be prevented by double pinion design. However, it increases the price of the system. Finally, ball screw lead screw and planetary roller screw transmission systems are considered. Compactness, lower cost and ease to access are the reasons for choosing lead screw and ball screw mechanisms. Although lead screw transmission systems have lower precision, self-locking property of lead screw eliminates the requirement of having a brake system in vertical axis. Therefore, for the vertical axes the lead screw mechanism was chosen, whereas for the horizontal axes ball screw mechanism was chosen.

During ball screw selection process operation conditions should be considered. Based on commercial products (Ultimaker-2 Go) and machining catalogues, operation conditions are listed as

Table 3.7. *Speed and force requirements for different operations*

	Rapid Motion	Printing Operation	Milling Operation	Z- and W axis motion
Speed [mm/sec]	100-150	50-100	2-20	0-20
Required Force [N]	≈ 0	≈ 0	≤100	Weight calculation

Firstly, the speed requirements should be satisfied. Relation between axial speed of the axis and motor speed is given in Eqn. (3.15), where n is the rotational speed, v_a stands for axial speed and h represents the pitch in [mm].

$$n = V_a 60/h \quad (3.15)$$

Relation between required motor torque and axial force is given in Eqn. (3.16), where T is the torque and F_a is axial force.

$$T = F_a h/(2\pi \mu) \quad (3.16)$$

Based on Eqns. (3.15) and (3.16) Table 3.8 is constructed. h_1 represents pitch of the ball screw and h_2 stands for pitch of the lead screw, both in [mm].

Table 3.8. *Torque and force requirements for different operations*

	Rapid Motion	Printing Operation	Milling Operation	Z- and W axis motion
Speed [min⁻¹]	6000/h ₁ - 9000/h ₁	3000/h ₁ - 6000/h ₁	120/ h ₁ - 1200/h ₁	0-1200/h ₂
Required Torque [Nm]	≈ 0	≈ 0	≤0.0177· h ₁	Weight calculation

Hardest conditions to be satisfied for ball screw are $9000/h_1$ speed and near zero torque during rapid motion and $1200/h_1$ speed and $0.0177 \cdot h_1$ torque during milling operation. For the vertical axis the hardest condition is when the axial speed is $1200/h_2$. In this speed, torque should be calculated by considering weight of the components on the vertical axis. Unit of h_1 and h_2 is [mm]. Conditions to be satisfied are listed as

Table 3.9. *Speed and force requirements for different conditions in terms of feed*

	Speed [RPM]	Torque [Nm]
Operating point 1	$9000/h_1$	≈ 0
Operating point 2	$1200/h_1$	$0.0177 \cdot h_1$
Operating point 3	$1200/h_2$	Weight calculation

By examining Operating point 1 and setting the maximum speed of the motor as 450 [RPM], h_1 can be found as 20 [mm]. For lead screw it is required to have lower speed and higher torque values. This is only possible with relatively lower pitch values. Therefore, h_2 is chosen as 4 [mm]. Table 3.10 indicates pitch of the screw mechanisms.

Table 3.10. *Pitch of the feed screws*

	h_1 (for X- and Y axis)	h_2 (for X- and Y axis)
Pitch [mm]	20	4

After obtaining pitch of the ball screw (h_1) and pitch of the lead screw (h_2), conditions to be satisfied are listed in Table 3.11.

Table 3.11. *Speed and torque requirements for different conditions*

	Speed [RPM]	Torque [Nm]
Operating point 1	450	≈ 0
Operating point 2	60	0.35
Operating point 3	300	Weight calculation

Servo motors can satisfy the precision, torque and speed requirements. However, due to their lower cost, good enough precision and ability to be used in an open loop system the stepper motors are chosen for actuation system. Speed and torque relation of the chosen motor for X axis is shown in Figure 3.13.

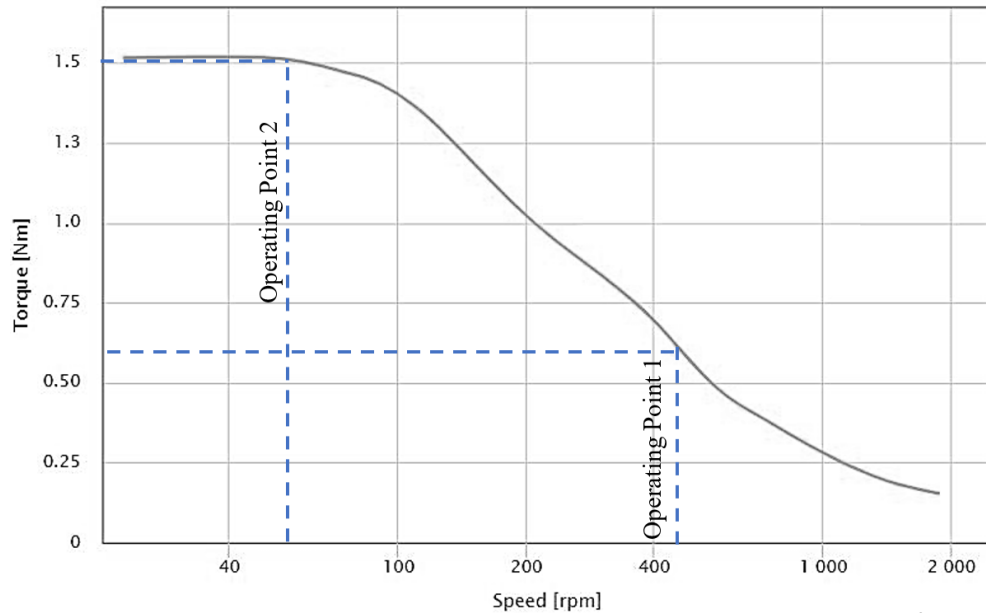


Figure 3.13. Torque/output power and speed of X axis [69]

Based on Figure 3.13 and Table 3.11 the required torque and motor torque for the given speeds are shown as

Table 3.12. Torque requirements and motor torque comparison

	Speed [RPM]	Required Torque [Nm]	Motor Torque [Nm]
Operating point 1	450	≈ 0	0.5
Operating point 2	60	0.35	2.8

As it can be seen from Table 3.12, for the given speed, motor torque is at least 8 times higher than required.

For the Operating point 3, weight of the system on the vertical axis is measured from the design as 122 [N]. Efficiency of the linear lead screw is taken as 0.4 [70]. From Eqn. (3.16) the required torque is calculated as 0.2 [Nm]. For the Y-, Z- and W axis bigger size motor is chosen. Speed and torque relation of the motor which is used in Y-, Z- and W axis is shown in Figure 3.14.

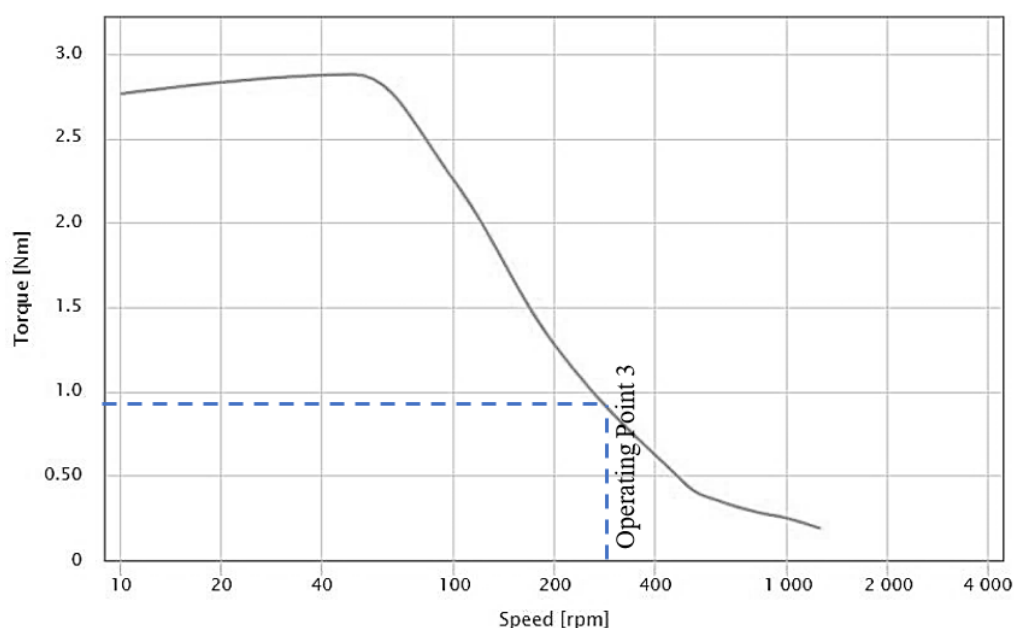


Figure 3.14. Torque/output power and speed of Y, Z and W axes [69]

Table 3.13 indicates that for Operating point 3 motor torque is 4 times higher than the required torque.

Table 3.13. Required torque and motor torque comparison for vertical axis

	Speed [RPM]	Required Torque [Nm]	Motor Torque [Nm]
Operating point 3	300	0.2	0.8

3.6.2.1. Feed Screw Bearing System

After selection of ball- and lead screws it is important to determine which configuration is the most appropriate for the operation. Figure 3.15 indicates four possible bearing configurations for feed screw mechanism.

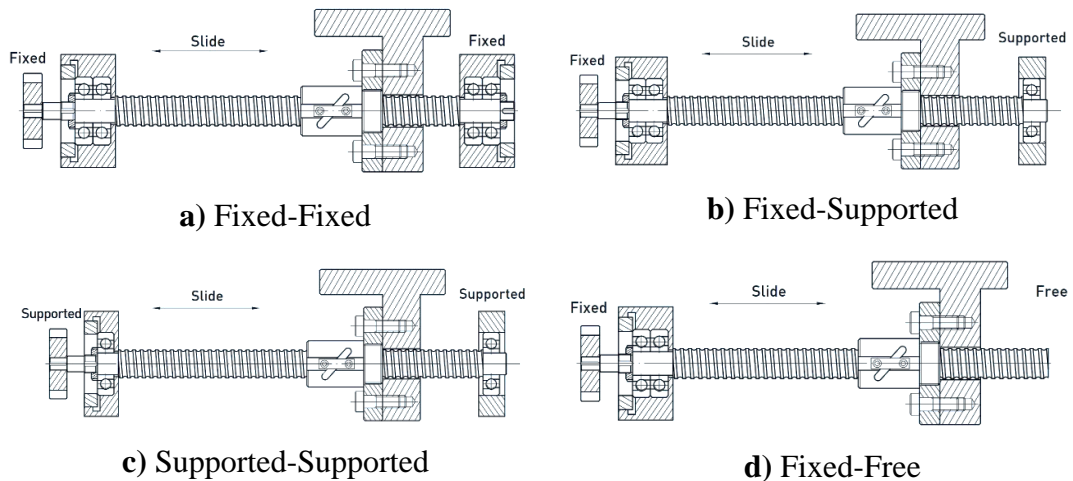


Figure 3.15. Feed screw bearing configurations [71]

Fixed-fixed configuration is one of the possibilities that can be used for mounting the feed screw. Both ends of the feed screw being fixed makes the system weak against thermal stress. In order to prevent this, feed screw should be pulled towards bearings with a certain preload. Making both sides of the feed screw supported causes undesired linear motion of the feed screw. Making one side fixed and another side free is a cost effective solution. But still, the vibration on free end is undemanding. Finally choosing one end as fixed and another end as supported disables unwanted linear motion by the fixed side. Moreover, leaving the other end free prevents thermo-elastic stresses. However, towards the support direction thermal expansion cause uncertainty in motion direction. By considering the discussion above the fixed-free configuration is chosen for mounting ball screw.

3.6.3. Linear Bearing System

There are various ways to guide the linear motion, some of which have already been explained in Section 2.4. Hydrodynamic and aerodynamic bearings are not applicable for linear motion. With aerostatic bearings smooth motion can be obtained. However, aerostatic bearings have very limited load carrying capacity. Hydrostatic bearings have quite good stiffness and precision properties. However, they are very expensive and require other hydraulic equipment to be in the system, which makes the system complicated. Similarly, magnetic bearings are costly and require more space than hydrostatic bearings to obtain the same carrying capacity. Finally, linear roller bearings are chosen which are inexpensive and at the same time have high stiffness and precision properties.

3.6.3.1. Accuracy of the Linear Bearings

Accuracy of the linear bearings determines the overall precision of the linear axis. Commercial companies have different precision grades for the linear roller bearings. Similarly, “Hiwin” has normal, high, super and ultra-precision options [71]. Figure 3.16 indicate the dimensional tolerances of linear guides and datum surfaces.

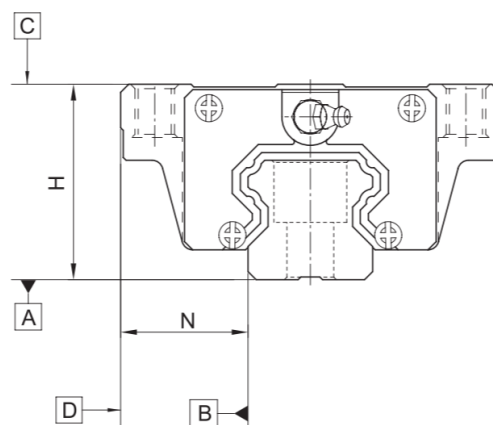


Figure 3.16. Linear bearings datum and dimensions [71]

In Hiwin catalogue [71], dimensional tolerances of HG-15 for each precision grade are indicated. As the precision grade increases, tighter tolerances are provided.

The running parallelisms of block surface C to surface A and surface D to surface B vary as the rail length changes. Accuracy of running parallelism with respect to the rail length is shown in Table 3.14.

Table 3.14. *Running accuracy for HG [71]*

Rail Length [mm]	Accuracy [μm]				
	Normal	High	Precision	Super Precision	Ultra Precision
0 ~ 100	12	7	3	2	2
100 ~ 200	14	9	4	2	2
200 ~ 300	15	10	5	3	2
300 ~ 500	17	12	6	3	2
500 ~ 700	20	13	7	4	2
700 ~ 900	22	15	8	5	3
900 ~ 1100	24	16	9	6	3
1100 ~ 1500	26	18	11	7	4
1500 ~ 1900	28	20	13	8	4
1900 ~ 2500	31	22	15	10	5
2500 ~ 3100	33	25	18	11	6
3100 ~ 3600	36	27	20	14	7
3600 ~ 4000	37	28	21	15	7

At this point, one should decide on the accuracy level of rail linear bearings and mounting surface accuracy tolerance. In Section 3.4, for each linear axis, amount of maximum axial error is set as 25 [μm] and angular errors were set as 25 [arcsec]. In this part of the thesis, it was decided on geometric tolerances of the mounting surface and running accuracy of the rails. Figure 3.17 indicates mounting block which has deviations at the bearing contact points and these deviations are bounded with parallelism and flatness geometric tolerances.

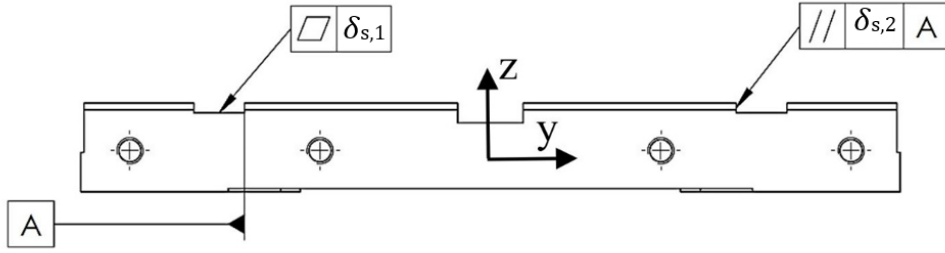


Figure 3.17. Geometric tolerances on mounting plate

$\delta_{P,1}$ is total deviation in Z direction can be calculated by summing running parallelisms of block surface C to surface A ($\delta_{r,1}$) and flatness of the mounting block ($\delta_{s,1}$).

$$\delta_{P,1} = \delta_{r,1} + \delta_{s,1} \quad (3.17)$$

Similarly, $\delta_{P,2}$ is total deviation in Z direction can be calculated by summing running parallelisms of block surface D to surface B ($\delta_{r,2}$) and flatness of the mounting block ($\delta_{s,2}$).

$$\delta_{P,2} = \delta_{r,2} + \delta_{s,2} \quad (3.18)$$

Firstly, four contact points (A, B, C, and D in Figure 3.18) on the bearing surfaces were analysed. As the tolerance boundary of the mounting surface increases, possibility of having high axial error on the contact points increases. Similarly, as the running accuracy of the linear bearing decreases, possibility of having high axial error on the contact points increases. Therefore, both running parallelism errors and geometric tolerances influence the angular and axial errors of the moving platform. In order to obtain angular and axial errors some simplifications were done, such as assuming guideway and moving platform to be rigid. Moreover, the table is moving in X direction and linear bearings provide stiffness in Y- and Z directions for each analysed point.

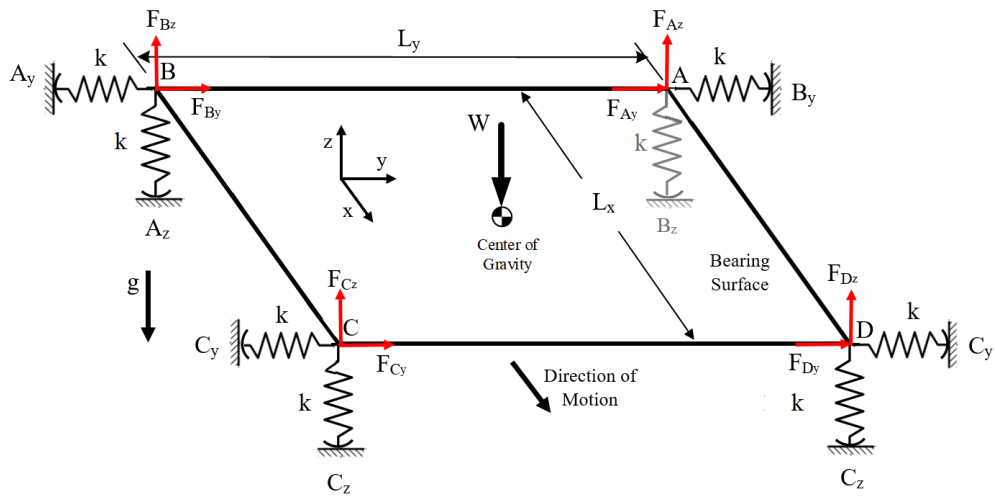


Figure 3.18. Force balance on the linear guide

Figure 3.19 indicates the force system of contact points in X-, Y- and Z directions.

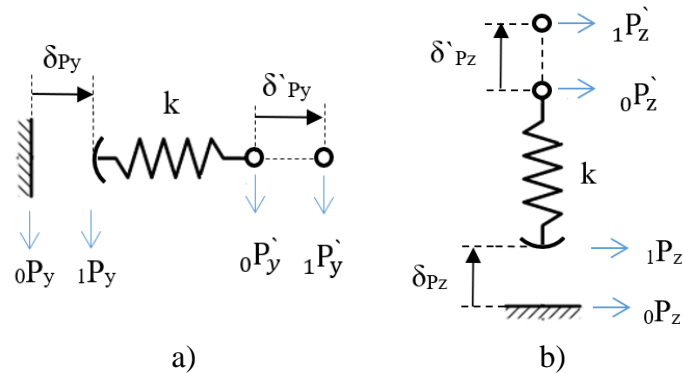


Figure 3.19. Force system of contact points in a) Y direction, b) Z direction.

In Figure 3.19, the subscript on the right side of the label indicates the direction of spring in the coordinate system. $1P'$ is the actual position of a point on the table, $0P'$ represents the ideal position of a point on the table, $1P$ is the actual position of a bearing surface, $0P$ the ideal position of a bearing surface, δ_p stands for the deviation of a point on the table, δ_P for the deviation of a bearing surface and k represents the stiffness of bearings. Since there is compression on the springs in all directions, force on the table (F) can be calculated as

$$\mathbf{F} = k \cdot \Delta\boldsymbol{\delta} \quad (3.19)$$

where $\Delta\boldsymbol{\delta}$ is

$$\Delta\boldsymbol{\delta} = [0 \quad (\delta_{Py} - \delta'_{Py}) \quad (\delta_{Pz} - \delta'_{Pz})]^T \quad (3.20)$$

For the selected bearings stiffness k is 500 [GPa]. The actual positions of the contact points A, B, C, and D (${}^1\mathbf{P}_n$) can be calculated as

$${}^1\mathbf{P}_n = {}^1\mathbf{T} \cdot {}^0\mathbf{P}_n \quad (3.21)$$

where ${}^0\mathbf{P}_n$ are the ideal positions of the contact points A, B, C, D and ${}^1\mathbf{T}$ is the homogenous transformation matrix. The homogenous transformation matrix having axial and angular errors can be shown as

$${}^1\mathbf{T} = \begin{bmatrix} 1 & 0 & \varepsilon_y & \delta_x \\ 0 & 1 & -\varepsilon_x & \delta_y \\ \varepsilon_y & \varepsilon_x & 1 & \delta_z \\ 0 & 0 & 0 & 1 \end{bmatrix} \quad (3.22)$$

Locations of the contact points are

$${}^0\mathbf{P}_A = [L_x/2 \quad L_y/2 \quad 0 \quad 1]^T \quad (3.23a)$$

$${}^0\mathbf{P}_B = [-L_x/2 \quad L_y/2 \quad 0 \quad 1]^T \quad (3.23b)$$

$${}^0\mathbf{P}_C = [-L_x/2 \quad -L_y/2 \quad 0 \quad 1]^T \quad (3.23c)$$

$${}^0\mathbf{P}_D = [L_x/2 \quad -L_y/2 \quad 0 \quad 1]^T \quad (3.23d)$$

where L_x is the distance between linear bearings in the direction of motion and L_y is the distance between linear bearings in Y direction.

Angular- ($\varepsilon_x, \varepsilon_y$) and axial errors ($\delta_x, \delta_y, \delta_z$) can be obtained by solving the equation of force balance and moment balance with respect to a point, which is in the centre of bearings. The equation for force equilibrium (\mathbf{F}) is shown as

$$\mathbf{F} = \mathbf{F}_A + \mathbf{F}_B + \mathbf{F}_C + \mathbf{F}_D + \mathbf{W} = \mathbf{0} \quad (3.24)$$

where each of \mathbf{F} is vector that has x-, y- and z components, \mathbf{W} indicates weight vector which has only z component towards gravity and A, B, C, D indicate the corresponding points. The equation for moment equilibrium with respect to O (\mathbf{M}_O) is shown as

$$\mathbf{M}_O = (\mathbf{r}_A \times \mathbf{F}_A) + (\mathbf{r}_B \times \mathbf{F}_B) + (\mathbf{r}_C \times \mathbf{F}_C) + (\mathbf{r}_D \times \mathbf{F}_D) = 0 \quad (3.25)$$

where

$$\mathbf{r}_* = [x_* \quad y_* \quad z_*] \quad (3.26)$$

$$\mathbf{F}_* = [F_{x*} \quad F_{y*} \quad F_{z*}] \quad (3.27)$$

In Eqns. (3.26) and (3.27) * is a place-holder for letters A, B, C and D. \mathbf{r}_* indicates the position vector and \mathbf{F}_* indicates reaction force vectors. Combining Eqns. (3.24) – (3.27) yields

$$\mathbf{A} \cdot \boldsymbol{\delta}_i = [a_{ij}] \boldsymbol{\delta}_i = \mathbf{F}_i \quad (3.28)$$

where \mathbf{A} is 5x5 constant matrix, and $\boldsymbol{\delta}_i$ and \mathbf{F}_i are as

$$\boldsymbol{\delta}_i = [\delta_y \quad \delta_z \quad \varepsilon_x \quad \varepsilon_y \quad \varepsilon_z]^T \quad (3.29)$$

$$\mathbf{F}_i = [F_y \quad F_z \quad M_x \quad M_y \quad M_z]^T \quad (3.30)$$

In order to find constants a_{11} , a_{21} , a_{31} , a_{41} , a_{51} and a_{61} all error terms δ_z , ε_x , ε_y , ε_z except δ_y should be set to zero. After setting + and – terms for δ_y , Eqn. (3.28) is reduced to

$$a_{11} \cdot \delta_y^+ = F_y^+ \quad (3.31)$$

$$a_{11} \cdot \delta_y^- = F_y^- \quad (3.32)$$

a_{11} can be obtained by combining and solving the Eqns. (3.31) and (3.32) to obtain

$$a_{11} = (F_y^+ - F_y^-) / \delta_y^+ - \delta_y^- \quad (3.33a)$$

Similarly,

$$a_{21} = (F_z^+ - F_z^-) / (\delta_y^+ - \delta_y^-) \quad (3.33b)$$

$$a_{31} = (M_x^+ - M_x^-) / (\delta_y^+ - \delta_y^-) \quad (3.33c)$$

$$a_{41} = (M_y^+ - M_y^-) / (\delta_y^+ - \delta_y^-) \quad (3.33d)$$

$$a_{41} = (M_z^+ - M_z^-) / (\delta_y^+ - \delta_y^-) \quad (3.33d)$$

Other error terms can be obtained by setting all error terms except one to 0 and assigning the remaining ones + and - values.

Instead of setting δ_p to a constant, its value is randomly generated inside of a predetermined interval. By using Monte Carlo simulation, error terms are obtained.

Finally, when δ_p is chosen as 18 [μm], the desired accuracy is achieved. As it is seen from Eqns. (3.17) and (3.18), δ_p is the summation of the running accuracy and the surface tolerance. For 300-500 [mm] rail length, high precision bearing is selected, which has 12 [μm] running accuracy. The remaining 6 [μm] error is the maximum surface error for the mounting surface. After the analysis, geometric tolerances of the mounting surface can be shown as

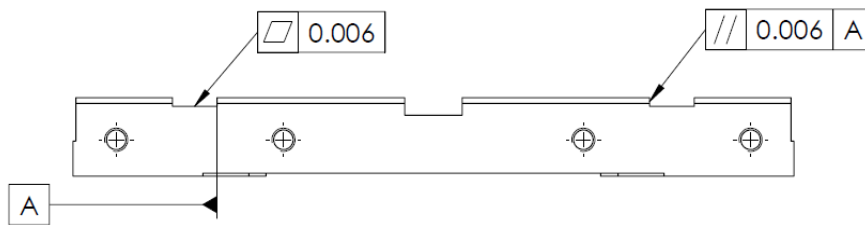
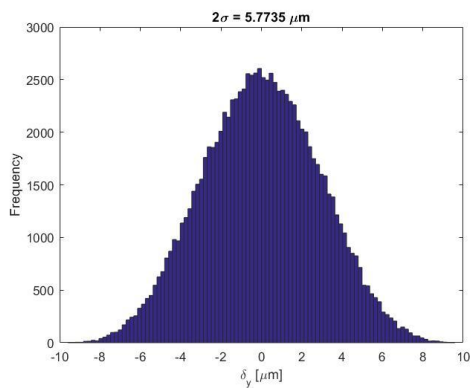
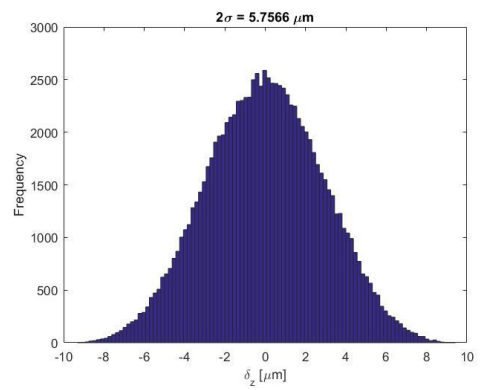


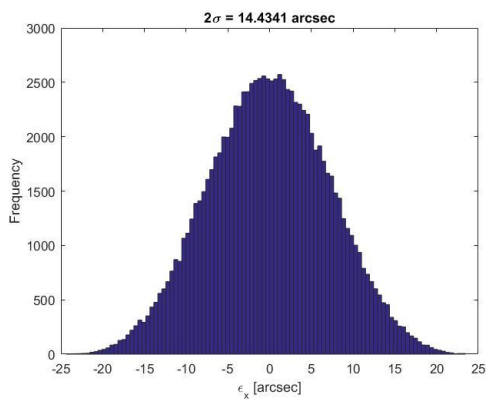
Figure 3.20. Geometric tolerances of the mounting surface after analysis



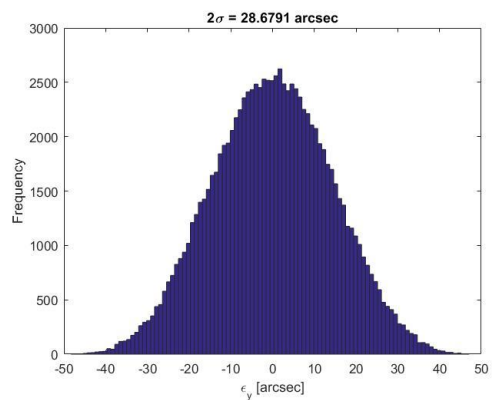
a)



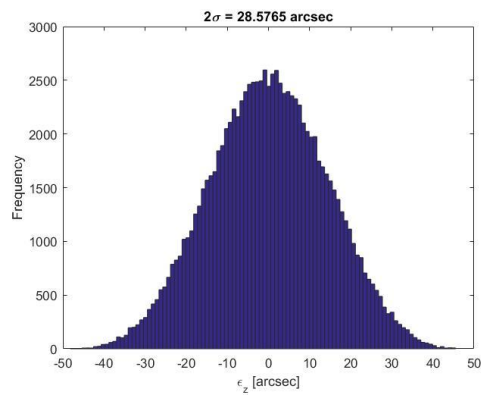
b)



c)



d)



e)

Figure 3.21. Axial- and radial errors generated by Monte Carlo simulation. a) axial error in Y direction, b) axial error in Z direction, c) angular error in X direction, d) angular error in Y direction, e) angular error in Z direction.

3.6.3.2. Force Analysis of Horizontal Linear Bearings

Firstly, forces should be obtained from the operation parameters. HGH-15 is chosen that is the most compact option for the linear roller bearings. For the horizontal axis, cutting force and weight are the external forces. These forces cause resultant force in four linear bearings. Details of forces for the horizontal axis is shown in Figure 3.22.

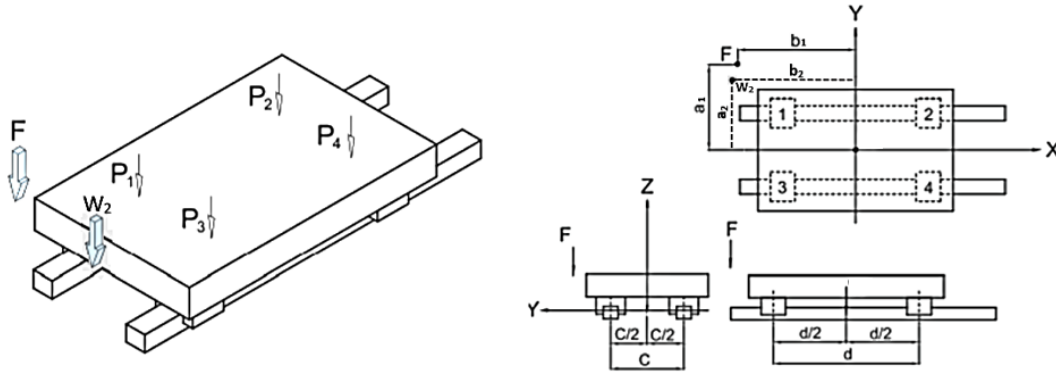


Figure 3.22. Force condition for horizontal axis [71]

Reaction forces for horizontal axis (\mathbf{P}_H) can be calculated as,

$$\mathbf{P}_H = \mathbf{C}_H \cdot \mathbf{F}_H \quad (3.34)$$

where

$$\mathbf{P}_H = [P_1 \ P_2 \ P_3 \ P_4]^T \quad (3.35)$$

$$\mathbf{F}_H = [W_1 \ W_2 \ F]^T \quad (3.36)$$

\mathbf{C}_H matrix is composed of dimensional constants. It is shown as

$$\mathbf{C}_h = 1/4 \begin{bmatrix} 1 & (1 + 2a_2/c + 2b_2/d) & (1 + 2a_1/c + 2b_1/d) \\ 1 & (1 + 2a_2/c - 2b_2/d) & (1 + 2a_1/c - 2b_1/d) \\ 1 & (1 - 2a_2/c + 2b_2/d) & (1 - 2a_1/c + 2b_1/d) \\ 1 & (1 - 2a_2/c - 2b_2/d) & (1 - 2a_1/c - 2b_1/d) \end{bmatrix} \quad (3.37)$$

W_1 is the weight of the horizontal axis itself and it is located at the geometric center of the bearings. W_2 is weight of the components on the horizontal axis and F is external force (cutting force)

where a_1 , b_1 , a_2 , b_2 , c and d are geometric parameters shown in Figure 3.22, W_1 represents weight of the horizontal axis itself and it is located at the geometric centre of the bearings. W_2 is weight on the horizontal axis and F stands for the external force (cutting force) applied on horizontal axis. Geometric dimensions used in Eqn. (3.34) are listed in Table 3.15.

Table 3.15. Geometric parameters for linear bearings of horizontal axis

a₁ [mm]	b₁ [mm]	a₂ [mm]	b₂ [mm]	c [mm]	d [mm]
0	300	0	150	165	83.4

External forces, cutting force and weight are shown in Table 3.16.

Table 3.16. External forces for linear bearings of horizontal axis

F [N]	W₁ [N]	W₂ [N]
100	120	564

By solving Eqn. (3.34), reaction forces are calculated for the horizontal axis and results are listed as

Table 3.17. Reaction forces for linear bearings of horizontal axis

P₁ [N]	P₂ [N]	P₃ [N]	P₄ [N]
543.3	-151.3	543.3	-151.3

Based on the calculated forces and high-level accuracy expectation and compactness, HGH15 linear guide has been selected for all the horizontal axis. Basic dynamic and static load rating values of HGH15 is compared with the maximum force in the horizontal axis in Table 3.18.

Table 3.18. Comparison of reaction forces and load capacities

P_m [kN]	${}_L C$ [kN]	${}_L C_0$ [kN]
0.54	14.7	23.47

In Table 3.18 P_m represents the maximum horizontal reaction force, ${}_L C$ stands for the basic dynamic load capacity for linear bearing and ${}_L C_0$ stands for the static load capacity for linear bearing. The maximum horizontal reaction force is well below load capacity of the linear bearings.

3.6.3.3. Force Analysis of Vertical Linear Bearings

Vertical axis linear guides should be analysed separately. Location of the external forces, weight and reaction forces for the vertical axis are shown in Figure 3.23.

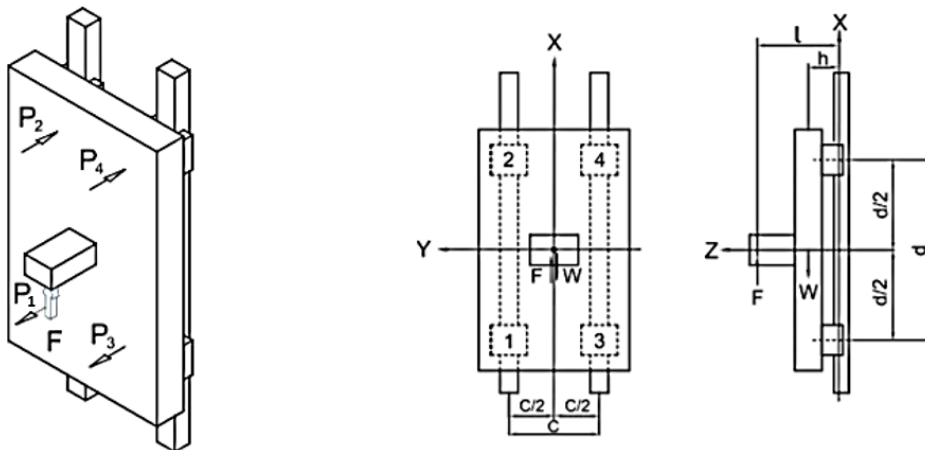


Figure 3.23. Force condition for vertical axis [71]

Reaction forces for the vertical axis (P_V) can be calculated as

$$P_V = C_V \cdot F_V \quad (3.38)$$

P_V , C_V , and F_V can be written as

$$\mathbf{P}_V = [P_1 \quad P_2 \quad P_3 \quad P_4]^T \quad (3.39a)$$

$$\mathbf{C}_V = \begin{bmatrix} h/2d & -h/2d & h/2d & -h/2d \\ -l/2d & l/2d & -l/2d & l/2d \end{bmatrix}^T \quad (3.39b)$$

$$\mathbf{F}_V = [W \quad F]^T \quad (3.39c)$$

where h , l and d are the geometric parameters shown in Figure 3.21, W is the weight of the components on vertical axis and F is the external force applied on vertical axis. Geometric parameters used in Eqns. (3.38) and (3.39) are indicated in Table 3.19.

Table 3.19. *Geometric parameters for linear bearings of Z axis*

h [mm]	l [mm]	d [mm]
150	165	83.4

Weight of the system above linear bearings (W) and cutting force (F) are listed in Table 3.20.

Table 3.20. *External forces for linear bearings of Z axis*

W [N]	F [N]
122	100

After solving Eqns. (3.38) and (3.39) the reaction forces are calculated for the horizontal axis and the results are listed in Table 3.21.

Table 3.21. *Reaction forces for linear bearings of horizontal axis*

P₁ [N]	P₂ [N]	P₃ [N]	P₄ [N]
-107.4	107.4	-107.4	107.4

Based on the calculated forces and high-level accuracy expectation and compactness, HGH-15 linear guide has been selected for all the vertical axis. Basic dynamic and static load rating values of HGH-15 is compared with the maximum force in the vertical axis in Table 3.22, where P_m stands for the maximum vertical reaction force.

Table 3.22. Comparison of reaction forces and load capacities

P_m [kN]	L_C [kN]	L_{C0} [kN]
0.11	14.7	23.47

Results show that maximum vertical reaction force is well below load capacity of the linear bearings.

3.6.3.4. Life of the Linear Bearings

After obtaining maximum forces on the linear guides, life of the linear guides (L) can be estimated by using Eqns. (3.40) – (3.41).

$$L(km) = 50km (f_h f_t L_C) / (f_w L P_c) \quad (3.40)$$

$$L_h = L 10^3 / (V_a 60) \quad (3.41)$$

In Eqn. (3.40) and (3.41), f_h is the hardness factor, f_t is the temperature factor, v_a stands for the axial speed, f_w for the load factor and L_h represents the life of linear guides in terms of hours.

Since the hardness of the HGH-15 is between HRC 58 and HRC 62 the hardness factor is taken as 1. Moreover, since the system works below 100 [°C] the temperature factor is taken as 1 as well. The speed is 9 [m/min] for horizontal axis and 1.8 [m/min] for vertical axis. For such speeds in no impact and no vibration case, the load factor is taken as 1.2.

Table 3.23. Life of the linear bearings for horizontal and vertical axis

	Horizontal Axis	Vertical Axis
L [km]	1134.3	4772.7
L_h [hour]	2100.5	66287.5

To accomplish the given service life the rails and blocks should be mounted properly. Figure 3.24 indicates how to mount rails and blocks.

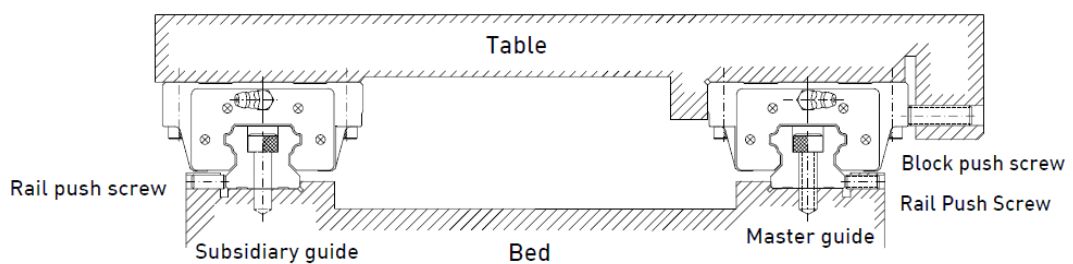


Figure 3.24. Mounting rails and block [71]

3.6.4. Final Design

Finally, based on all considerations explained in previous sections, linear axis are designed and their final forms are indicated in Figure 3.25.

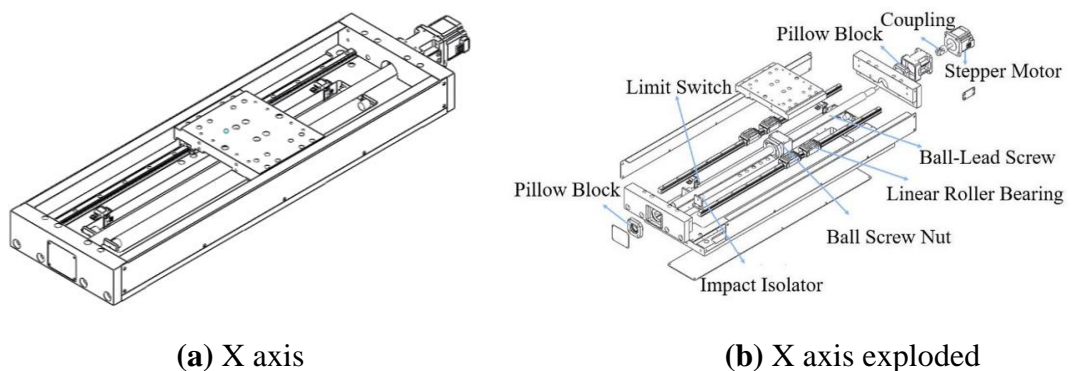


Figure 3.25. X axis normal and exploded view

3.7. Rotary Stages

Hybrid manufacturing system has rotary stages that provide rotation for workpiece around B- and C axis. Two rotary stages are identical except for the interface of their platforms. Rotary stage is composed of four main components which are indicated in Table 3.24.

Table 3.24. *Components of the rotary stage*

Structural material	Al-6061-T6
Bearing system	Face to face arrangement of angular contact bearings
Actuation and transmission	Stepper motor and worm gear
Sensor	Optical position encoder

3.7.1. Structures

Al-6061-T6 is used for the structural components of the rotary axis because of the reasons explained in previous sections.

3.7.2. Actuation and Transmission

Worm gear and stepper motor pair is used to actuate the system. Speed and torque required for the system shown in Table 3.25.

Table 3.25. *Speed and torque values of rotary platform*

Speed [RPM]	Torque [Nm]
3.6	31.75

For 0.1% coefficient of dynamic friction and 100 reduction ratio motor parameters should be as in Table 3.26.

Table 3.26. *Speed and torque values of stepper motor*

Speed [RPM]	Torque [Nm]	Required Torque [Nm]
360	0.76	0.32

Figure 3.26 indicates the motor performance. As can be seen, for 360 [RPM], 0.76 [Nm] torque can be generated, which is more than twice the required torque.

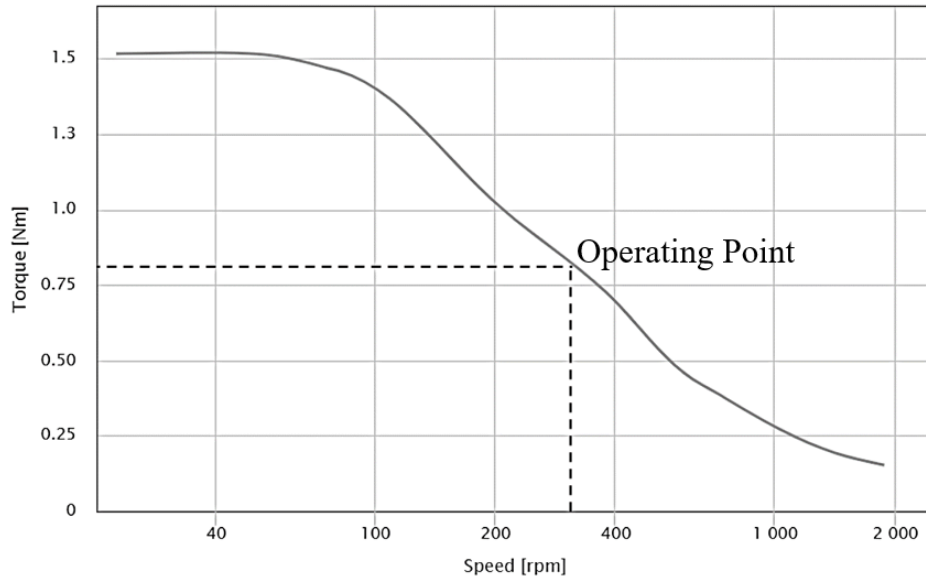


Figure 3.26. Speed vs torque plot for rotary stages [69]

3.7.2.1. Force Analysis of Actuation and Transmission System

Figure 3.27 indicates the forces on worm gear and worm wheel. Table 3.27 indicates the formulas for the worm gear forces

Table 3.27. Formulas for worm gear forces

Types of gears	F_p : Tangential force [N]	F_a : Axial force [N]	F_n : Radial force [N]
Worm (Driver)	$\frac{2000 T_1}{d_1}$	$F_{p1} \frac{\cos \alpha_n \cos \gamma - \mu \sin \gamma}{\cos \alpha_n \sin \gamma + \mu \cos \gamma}$	$\frac{\sin \alpha_n}{\cos \alpha_n \sin \gamma + \mu \cos \gamma}$
Worm Wheel (Driven)	$F_{p1} \frac{\cos \alpha_n \cos \gamma - \mu \sin \gamma}{\cos \alpha_n \sin \gamma + \mu \cos \gamma}$	F_{p1}	

Properties of the worm gear is shown in Table 3.28. Dynamic friction coefficient between aluminium bronze and ground steel is taken as 0.1.

Table 3.28. Properties of worm gear

Pressure angle (α_n)	Lead angle (γ)	Coefficient of friction (μ)
20°	3.43°	0.1

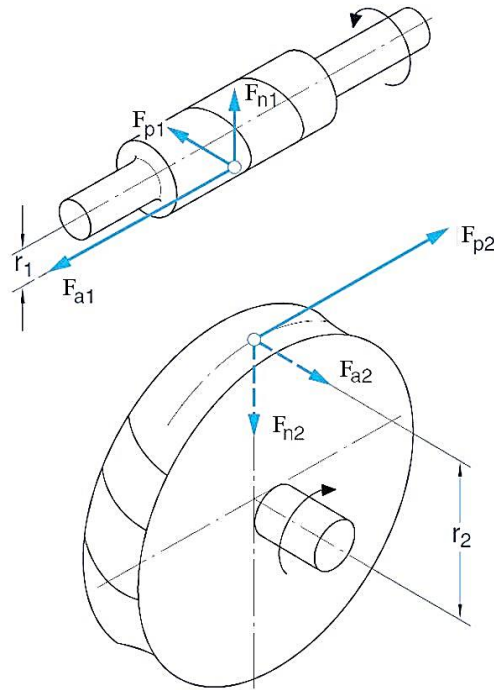


Figure 3.27. Forces on worm gear and worm wheel [72]

By using formulas shown in table 3.27 and geometric properties of the worm gear, force analysis is done. Results of worm gear force analysis is shown as

Table 3.29. Results of worm gear force analysis

Types of gears	F_p : Tangential force [N]	F_a : Axial force [N]	F_n : Radial force [N]
Worm (Driver)	$F_{p1} = 60.8$	$F_{a1} = 362.8$	$F_n = 133.1$
Worm Wheel (Driven)	$F_{p2} = 362.8$	$F_{a2} = 60.8$	

3.7.3. Rotary Bearing System

Two angular contact bearings that are arranged in face to face configurations are carrying the axial and radial forces in the system. Bearing arrangement is identical in both of the rotary axis. However, external forces applied on the bearings are different because of the position of the B- and C axis.

3.7.3.1. Accuracy of the Rotary Bearings

In this section, run outs for bearing seats and precision class of the bearing is determined. Run out on the shaft, run out on the bearing seat and the deviation on the bearing surfaces have the combined effect for the accuracy of the rotary stage. Figure 3.28 indicates the run out geometric tolerances on bearing seats and shaft.

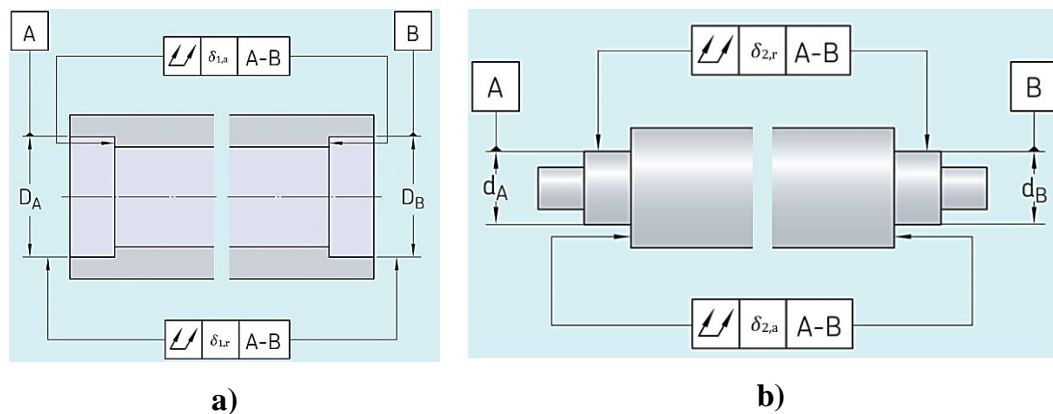


Figure 3.28. Geometric tolerances for bearing seat and shaft [72]

Manufacturer provides different quality angular contact bearings. For 30 [mm] bore diameter, accuracy grade of the angular contact bearings is shown in Table 3.30.

Table 3.30. Accuracy grades of angular contact bearing [72]

Quality	Normal	P6-P5	P4	P2
Accuracy [μm]	13	8	4	2

Total deviation in radial direction (δ_R) can be calculated by summing radial run out error of bearing seat ($\delta_{1,r}$), radial run out error of shaft ($\delta_{2,r}$) and radial run out error of bearing ($\delta_{3,r}$).

$$\delta_R = \delta_{1,r} + \delta_{2,r} + \delta_{3,r} \quad (3.42)$$

Similarly, Total deviation in axial direction (δ_A) can be calculated by summing axial run out error of bearing seat ($\delta_{1,a}$), axial run out error of shaft ($\delta_{2,r}$) and axial run out error of bearing ($\delta_{3,r}$).

$$\delta_A = \delta_{1,a} + \delta_{2,a} + \delta_{3,a} \quad (3.43)$$

Combination of these deviations and external forces applied on the shaft make the axis of the motion move out from the ideal rotation axis. Moment and force balance in three principle directions results in five equations to obtain axial- and angular errors of the rotation axis in X-, Y- and Z directions. Angular error around Z direction is not calculated, because it is in the direction of motion.

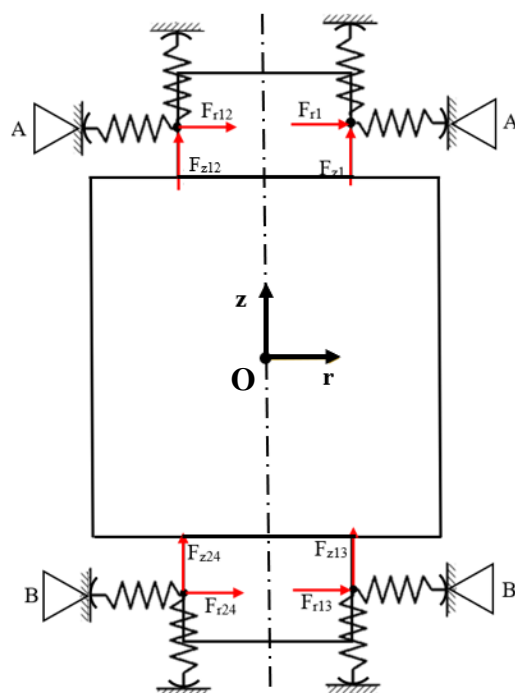


Figure 3.29. Forces on the bearing surface for rotary axes

In Figure 3.29, F_{r1} through F_{r12} represent 12 radial forces on bearing A and F_{z1} through F_{z12} represent 12 axial forces on bearing A. Similarly, F_{r13} through F_{r24} represent 12 radial forces on bearing B and F_{z13} through F_{z24} represent 12 axial forces on bearing B. Each contacting elements which also happens to be modelled as a spring element are equally spaced and the angle between each contacting element is represented as θ . For 12 contacting elements, it is $2\pi/12=\pi/6$. The spring system for radial and axial directions for each contact point is presented in Figure 3.30. The subscript on the right side of the label indicates the direction of spring in the coordinate system.

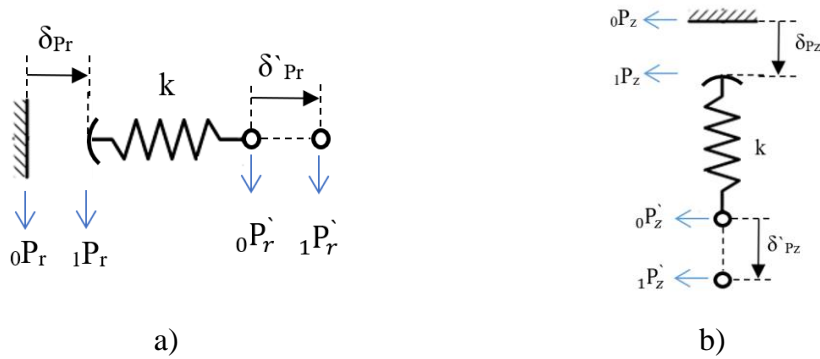


Figure 3.30. Force system of contact points in a) radial direction, b) Z direction

Because of the force directions shown in Figure 3.30, force on the table (\mathbf{F}) can be calculated as

$$\mathbf{F} = k\Delta\boldsymbol{\delta} \quad (3.44)$$

where $\Delta\boldsymbol{\delta}$ is

$$\Delta\boldsymbol{\delta}(n) = [(\delta_{Pr} - \delta'_{Pr}) \cdot \cos n\theta \quad (\delta_{Pr} - \delta'_{Pr}) \cdot \sin \theta \quad (\delta_{Pz} - \delta'_{Pz})] \quad (3.45)$$

where n is the index for bearing contact point and varies in between 1 and 12. The actual positions of the contact points A_1 through A_{12} and B_1 through B_{12} (${}^1\mathbf{P}_n$) can be calculated as

$${}^1\mathbf{P}_n = {}^1\mathbf{T} \quad {}^0\mathbf{P}_n \quad (3.46)$$

where ${}^0\mathbf{P}_n$ are the ideal positions of the contact points A₁ through A₁₂ and B₁ through B₁₂ and ${}^1_0\mathbf{T}$ is the homogenous transformation matrix. The homogenous transformation matrix having axial and angular errors can be shown as

$${}^1_0\mathbf{T} = \begin{bmatrix} 1 & 0 & \varepsilon_y & \delta_x \\ 0 & 1 & -\varepsilon_x & \delta_y \\ \varepsilon_y & \varepsilon_x & 1 & \delta_z \\ 0 & 0 & 0 & 1 \end{bmatrix} \quad (3.47)$$

Locations of the contact points can be described as.

$${}_{A_n}^0\mathbf{P} = [r \cos n\theta \quad r \sin n\theta \quad L_z/2 \quad 1]^T \quad (3.48a)$$

$${}_{B_n}^0\mathbf{P} = [r \cos n\theta \quad r \sin n\theta \quad -L_z/2 \quad 1]^T \quad (3.48b)$$

where L_z is the distance between linear bearings in Z direction, r is the bore radius. Angular ($\varepsilon_x, \varepsilon_y, \varepsilon_z$) and axial errors ($\delta_x, \delta_y, \delta_z$) can be obtained by solving the equation of force and moment balance with respect to a point, which is in the centre of bearings. The equation for force balance (\mathbf{F}) is shown as

$$\mathbf{F} = \sum_{n=1}^{12} \mathbf{F}_{A,n} + \sum_{n=1}^{12} \mathbf{F}_{B,n} = \mathbf{0} \quad (3.49)$$

where A and B indicate the bearings and n represents location of the contact point. The equation for moment balance with respect to O (\mathbf{M}_O) is shown as

$$\mathbf{M}_O = \sum_{n=1}^{12} \mathbf{r}_{A,n} \times \mathbf{F}_{A,n} + \sum_{n=1}^{12} \mathbf{r}_{B,n} \times \mathbf{F}_{B,n} = \mathbf{0} \quad (3.50)$$

In Eqn. (3.50), $\mathbf{r}_{A,n}$ and $\mathbf{r}_{B,n}$ indicate the positions of points A₁ through A₁₂ and B₁ through B₁₂, $\mathbf{F}_{A,n}$ and $\mathbf{F}_{B,n}$ indicate the forces on each contact point and \times represents the cross product. Finally, when δ_p is chosen as 6 [μm], the desired accuracy is achieved. As it is seen from Eqns. (3.42) and (3.43), δ_p is the summation of the runout errors of the bearing seat, shaft and bearing. 0.02 axial and radial runout tolerances

are determined for bearing seat and shaft. Furthermore, P2 accuracy grade angular contact bearings are chosen to satisfy accuracy requirement of the rotary stage.

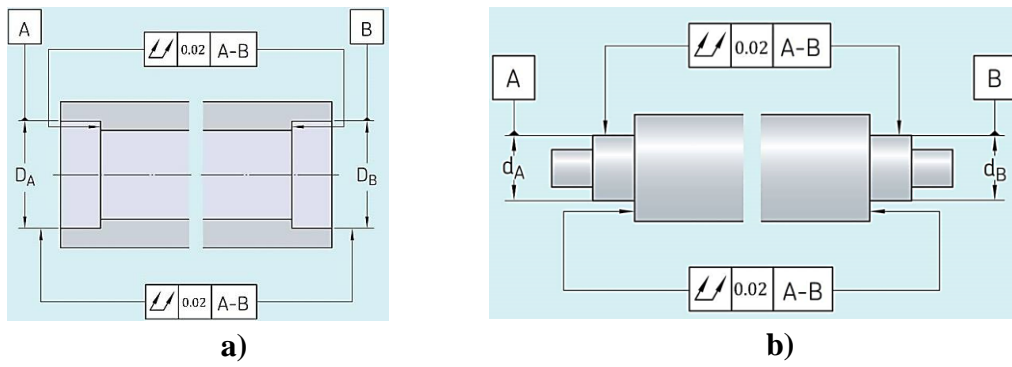
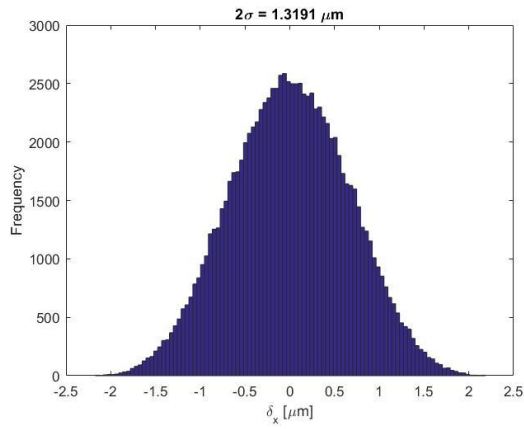
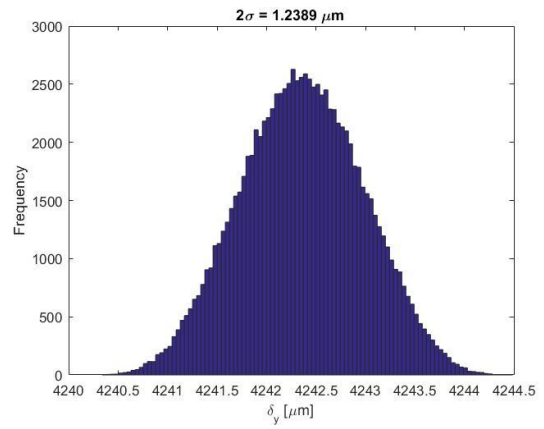


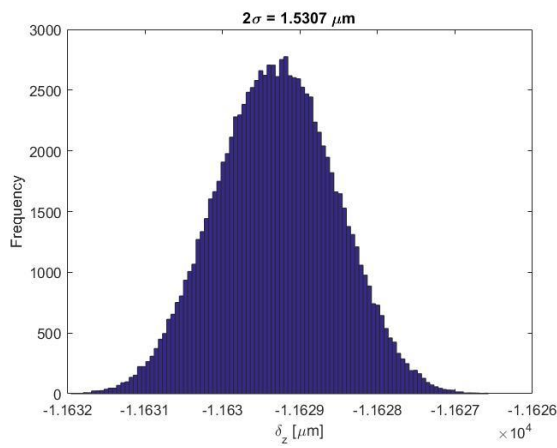
Figure 3.31. Geometric tolerances for bearing seat and shaft after analysis [72]



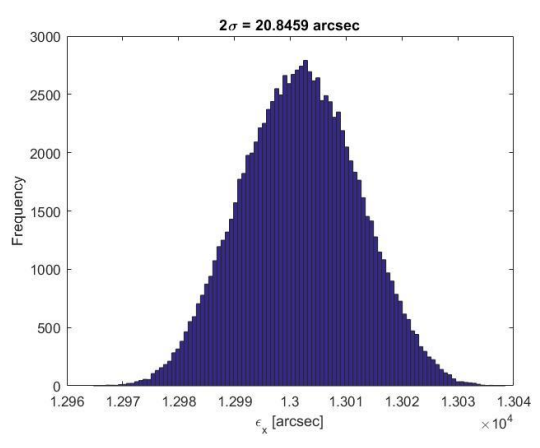
a)



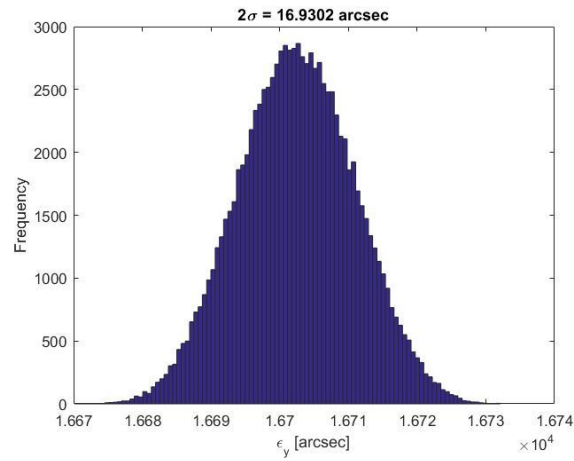
b)



c)



d)



e)

Figure 3.32. Axial and radial errors generated by Monte Carlo simulation. a) axial error in X direction, b) axial error in Y direction, c) axial error in Z direction, d) angular error in X direction, e) angular error in Y direction

3.7.3.2. Force analysis of C axis

Cutting force and weight are the external forces effecting reaction forces induced in angular contact bearings. Forces on the bearing systems are shown in Figure 3.33. F_x , F_y and F_z represent external forces applied on C axis towards X-, Y- and Z directions respectively. W stands for the weight on the C axis and O for the geometric centre of bearings in C axis. F_{n2} , F_{p2} and F_{a2} are the transmission forces explained in Section 3.7.2.1. Based on Figure 3.33, moments induced in the centre of the bearings (M_O) can be calculated as

$$\mathbf{M}_O = \mathbf{r}_t \times \mathbf{F}_t + \mathbf{r}_F \times \mathbf{F}_F + \mathbf{r}_W \times \mathbf{F}_W \quad (3.51)$$

where \mathbf{r}_t , \mathbf{r}_F and \mathbf{r}_W are position vectors of transmission point, external force point and location of weight point respectively. \mathbf{F}_t , \mathbf{F}_F and \mathbf{F}_W are transmission force vector, external force vector and weight vector respectively. Symbol \times stands for cross product. The magnitudes of the external forces are shown in Table 3.31.

Table 3.31. Magnitudes of the external forces for C axis

F_x [N]	F_y [N]	F_z [N]	W [N]
100	100	100	500

Moment around X axis is 56153 [N·mm], moment around Y axis is -35373 [N·mm], and moment around Z axis is -16745 [N·mm]. M_z component is negative, which indicates that transmission system produces enough torque to rotate against cutting forces.

Moments in X- and Y direction result in reaction forces on angular bearings. Figure 3.34 indicates forces on the bearings and how moment causes reaction forces in X- and Y direction. It is assumed that the reaction forces are applied from the middle of the bearing surfaces. A stand for angular contact bearing above and B stands for angular contact bearing which is located below. Details are seen in Figure 3.34

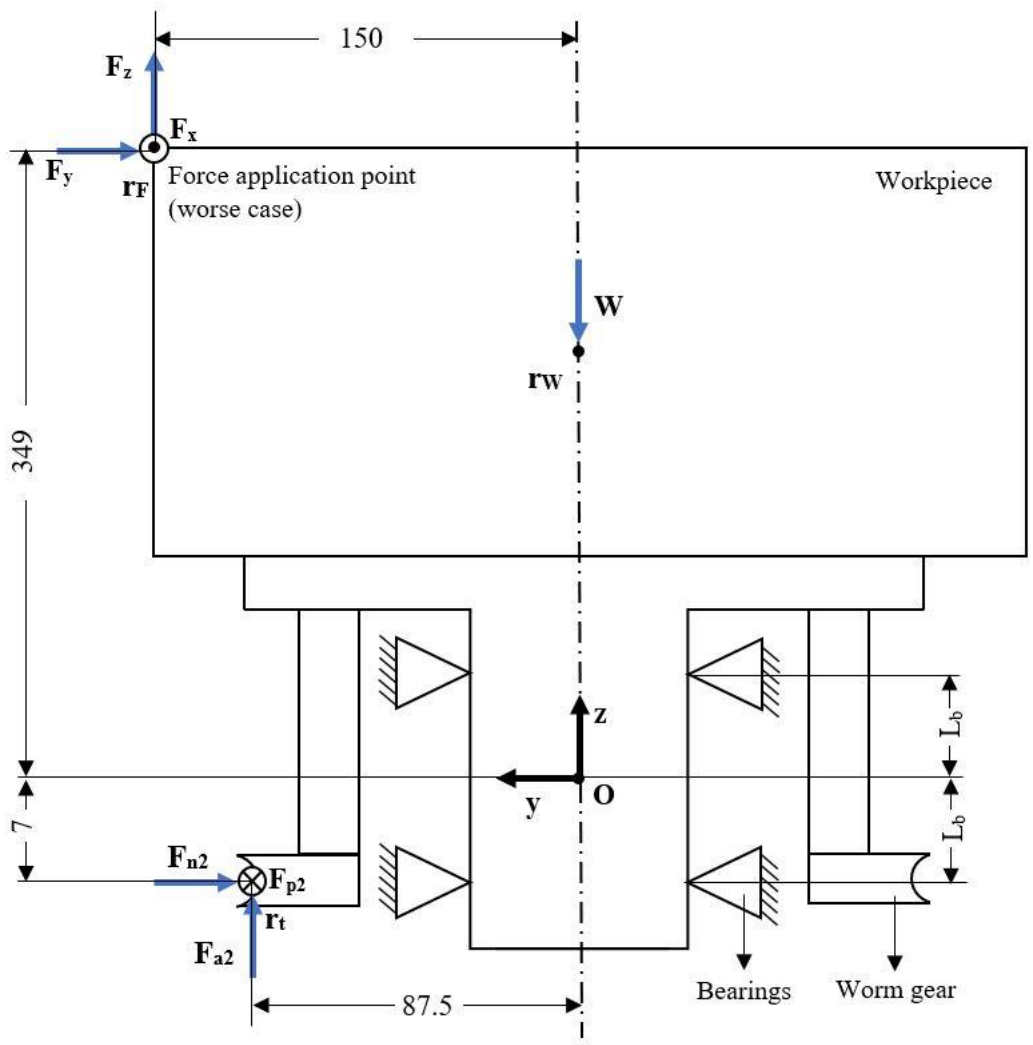


Figure 3.33. Force condition for C axis

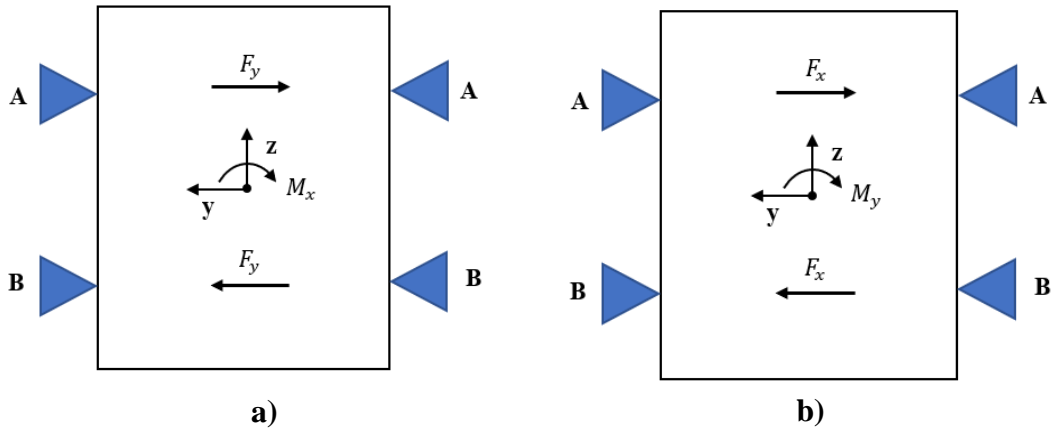


Figure 3.34. Moments affecting bearings for C axis. a) Effect of M_x on bearings b) Effect of M_y on bearings. A stands for the upper bearing and B for the lower bearing.

External forces contribute to the reaction forces on the bearing. Reaction force vector (\mathbf{P}) can be calculated as

$$\mathbf{P} = \begin{bmatrix} P_{Ax} \\ P_{Ay} \\ P_{Bx} \\ P_{By} \end{bmatrix} = 1/(2L_b) \begin{bmatrix} M_y + L_b F_{p2} - L_b F_x \\ -M_x - L_b F_{n2} - L_b F_y \\ -M_y + L_b F_{p2} - L_b F_x \\ M_x - L_b F_{n2} - L_b F_y \end{bmatrix} \quad (3.52)$$

In Eqn. 3.52, P_{Ax} and P_{Ay} represent x- and y components of the reaction forces of bearing A and P_{Bx} and P_{By} represent x- and y components of the reaction forces of bearing B. $2L_B$ is the distance between bearing centres. Reaction forces in X- and Y directions are shown in Table 3.32.

Table 3.32. Reaction forces in X- and Y directions for C axis

\mathbf{P}_{Ax} [N]	\mathbf{P}_{Ay} [N]	\mathbf{P}_{Bx} [N]	\mathbf{P}_{By} [N]
-2208.6	-3422.1	2471.4	3305.4

Radial force vector (\mathbf{P}_r) for bearings A and B can be calculated as

$$\mathbf{P}_r = \begin{bmatrix} P_{rA} \\ P_{rB} \end{bmatrix} = \begin{bmatrix} \sqrt{P_{Ax}^2 + P_{Ay}^2} \\ \sqrt{P_{Bx}^2 + P_{By}^2} \end{bmatrix} \quad (3.53)$$

Using Eqn. (3.53), the radial reaction forces acting on the C axis are calculated in Table 3.33.

Table 3.33. Radial reaction forces for C axis

\mathbf{P}_{rA} [N]	\mathbf{P}_{rB} [N]
4072.9	4127.2

Radial forces in bearing system cause axial load. Since $P_{rA} < P_{rB}$ and weight is downward, the axial reaction force vector (\mathbf{P}_a) for bearings A and B can be calculated as

$$\mathbf{P}_a = \begin{bmatrix} P_{aA} \\ P_{aB} \end{bmatrix} = \begin{bmatrix} P_{aB} + K_a \\ R \cdot P_{rB} \end{bmatrix} \quad (3.54)$$

where K_a is the load in Z direction. R is the bearing parameter that depends on the contact angle. The chosen bearing has 40° contact angle, for which R has the value of 0.88. By using Eqn. (3.54), axial reaction forces for C axis can be listed as in Table 3.34.

Table 3.34. Axial reaction forces for C axis

\mathbf{P}_{aA} [N]	\mathbf{P}_{aB} [N]
4231.9	3631.3

Table 3.35 indicates calculation parameters for the selected bearing.

Table 3.35. Bearing calculation parameters and load rating (C)

e	\mathbf{Y}_1	C [kN]
1.14	0.55	24

Ratio of axial to radial forces is important for calculation of equivalent dynamic force. Since the ratio of axial to radial force is for both bearings lower than e , equivalent reaction force vector (\mathbf{P}) for bearings A and B can be calculated as

$$\mathbf{P} = \begin{bmatrix} P_A \\ P_B \end{bmatrix} = \begin{bmatrix} P_{rA} + Y_1 P_{aA} \\ P_{rB} + Y_1 P_{aB} \end{bmatrix} \quad (3.55)$$

Reaction forces obtained from Eqn. (3.55) are shown in Table 3.36.

Table 3.36. Reaction forces for C axis

\mathbf{P}_A [N]	\mathbf{P}_B [N]
6400.4	6124.4

3.7.3.2.1. Life of the Angular Contact Bearings

After obtaining equivalent dynamic forces for both bearings in C axis, life of the bearings can be calculated by using Eqn. (3.56). L_{10} represents the basic rating life, C is the basic dynamic load rating for rotary bearing, P is the equivalent dynamic bearing load and p is a constant equal to 3 for ball bearings.

$$L_{10} = (C/P)^p \quad (3.56)$$

Based on Eqn. (3.56) the basic rating lives of bearings A and B are 52.7 and 60.2 [millions of revolutions] respectively.

3.7.3.3. Force Analysis of B axis

C axis and other connection components are connected with B axis. Figure 3.35 indicates forces on B axis. F_x , F_y and F_z are the x-, y- and z components of external forces applied on B axis. O represents the geometric centre of bearing in B axis and W represent the weight on the B axis.

Based on Figure 3.35, the moments induced in the centre of bearings (M_o) can be calculated by using Eqn. (3.51). The magnitudes of the external forces are shown in Table 3.37.

Table 3.37. Magnitudes of the external forces for B axis

F_x [N]	F_y [N]	F_z [N]	W [N]
92.1	100	100	600

Moment around X axis is 157940 [N·mm], moment around Y axis is 7522.2 [N·mm], and moment around Z axis is 7.34 [N·mm]. M_z component is positive, which indicates that transmission system produces enough torque to rotate against cutting forces.

External forces contribute to the reaction forces on the bearings. Reaction forces vector (\mathbf{P}) can be calculated with the following equations.

$$\mathbf{P} = \begin{bmatrix} P_{Ax} \\ P_{Ay} \\ P_{Bx} \\ P_{By} \end{bmatrix} = (2L_B)^{-1} \begin{bmatrix} M_y - L_B F_{p2} + L_B F_x + L_B W_B \\ -M_x + L_B F_{n2} - L_B F_y \\ -M_y - L_B F_{p2} + L_B F_x + L_B W_B \\ M_x + L_B F_{n2} - L_B F_y \end{bmatrix} \quad (3.57)$$

In Eqn. (3.57) P_{Ax} and P_{Ay} represent x- and y components of the reaction forces of bearing A and P_{Bx} and P_{By} represent x- and y components of the reaction forces of bearing B. $2L_B$ is the distance between bearing centres. The reaction forces in X- and Y directions are shown in Table 3.38.

Table 3.38. Reaction forces in X- and Y directions for B axis

P_{Ax} [N]	P_{Ay} [N]	P_{Bx} [N]	P_{By} [N]
670.7	-9854.7	-269.5	9954.4

By using Eqn. (3.53) radial reaction forces for B axis can be calculated and they are listed in Table 3.39.

Table 3.39. *Radial reaction forces for B axis*

P_{rA} [N]	P_{rB} [N]
9877.5	9958

By using Eqn. (3.54) axial reaction forces for B axis can be calculated and they are listed in Table 3.40.

Table 3.40. *Axial reaction forces for B axis*

P_{aA} [N]	P_{aB} [N]
8323.8	8323.8

Ratio of axial to radial forces is important for calculation of equivalent dynamic force. Since the ratio of axial to radial force is for both bearings lower than e , equivalent reaction forces (P) for bearings A and B can be calculated by using Eqn. (3.55). Reaction forces obtained are shown in Table 3.41.

Table 3.41. *Reaction forces for B axis*

P_A [N]	P_B [N]
14455.6	14536.1

3.7.3.4. Life of the Rotary Bearings

After obtaining equivalent dynamic forces for both bearings in C axis, life of the bearings can be calculated by using Eqn. (3.56). Based on Eqn. (3.56) basic rating lives of bearings A and B are 4.6 and 4.5 [millions of revolution] respectively.

3.7.4. Sensors

Direct measurement is implemented in rotary stages. Code wheel is engaged with the end of the shaft and rotates together with the platform. Code wheel which has optical pattern on it rotates in between detector and emitter. Encoder converts rotation of the shaft into two square waves in quadrature and index pulse. 5000 [CPR] resolution can be obtained with the AEDC-5xxx series encoder.

Table 3.42. Encoder and stepper motor parameters

	S [steps/rev]	P [pulse/step]	z
Sensor	5000	4	1
Stepper Motor	200	16	100

$$R = 360^\circ / (S \cdot P \cdot z) \quad (3.58)$$

For the motor, resolution is 4.05 [arcsec/pulse], whereas for the encoder resolution is 64.8 [arcsec/pulse]. From Eqn. (3.58), motor resolution is obtained as 4.05 [arcsec/pulse]. However, transmission system has backlash. Therefore, sensor with resolution lower than 4.05 [arcsec/pulse] can be chosen. When considering the cost, sensor with resolution of 64.8 [arcsec/pulse] is chosen.

3.7.5. Final Design

The rotary stage is composed of driver worm gear and driven gear. The driver worm gear is connected to the stepper motor and supported by bearings. Figure 3.36 indicates the exploded view of actuation system of the rotary stage.

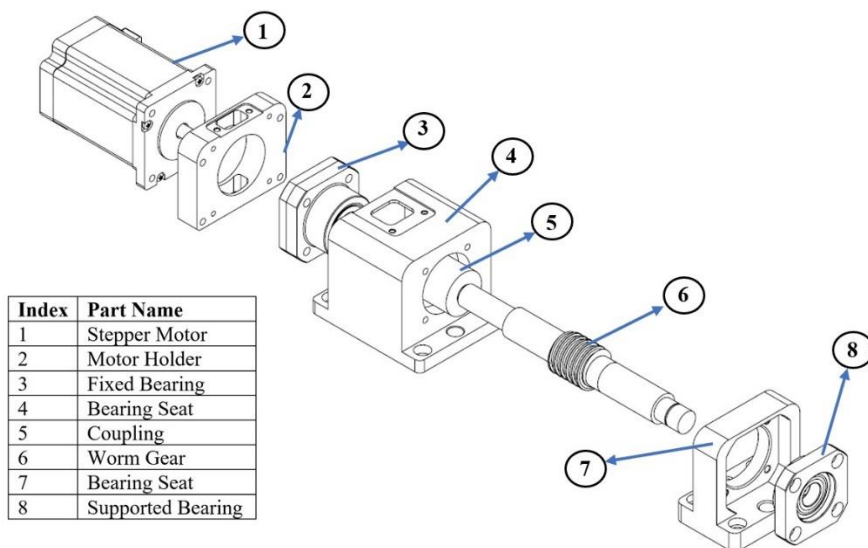


Figure 3.36. Exploded view of actuation system of the rotary stage

Driven gear side is connected to platform and supported by angular contact bearings. Optical encoder under the shaft registers the position of the platform directly, as indicated in Figure 3.37.

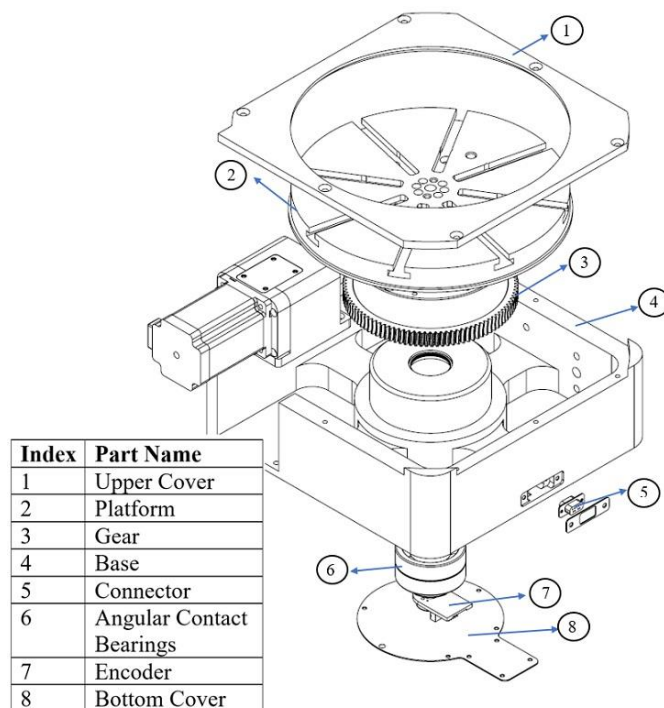


Figure 3.37. Exploded view of the rotary stage

3.8. Spindle Design

Main task of a spindle is to support the tool and/or workpiece with sufficient accuracy under the action of external forces (e.g. cutting force). The accuracy and surface quality of machined workpieces and the feasible cutting performance of a machine tool depend directly on static-, dynamic- and thermal behaviour of the spindle-bearing system. Thus, the design of bearing arrangement is very significant [73].

Figure 3.38 indicates the typical spindle construction with roller bearings. Based on the selected bearings, axial-, bending- and radial stiffness of the spindle change. Typically, 18° to 25° contact angled angular contact bearings are used for high speed applications. Higher the contact angle, more axial load the bearing can carry. On the tool side, bearing's outer surface should be compressed slightly (10 – 30 [μm]) with the outer cap. Flatness and parallelism of the outer cap affect the precision of the spindle. To increase rigidity on the tool side of the spindle, bearing spacers can be mounted in between the bearings. Clamping nut spacer is used to ensure that clamping nut presses on the inner ring of the bearing. On the tool side angular contact bearings are fixed and on the rear side angular contact bearings are floating. Therefore, on the rear side bearings and shaft should have clearance fit. Shaft on the rear side can be connected with coupling, belt or other transmission systems [74].

On the other hand, it is possible to have a spindle which has a motor inside. This kind of structure eliminates transmission error. However, having motor inside of the spindle causes heat generation. Therefore, spindle design should have a cooling system that can dissipate the heat from the spindle.

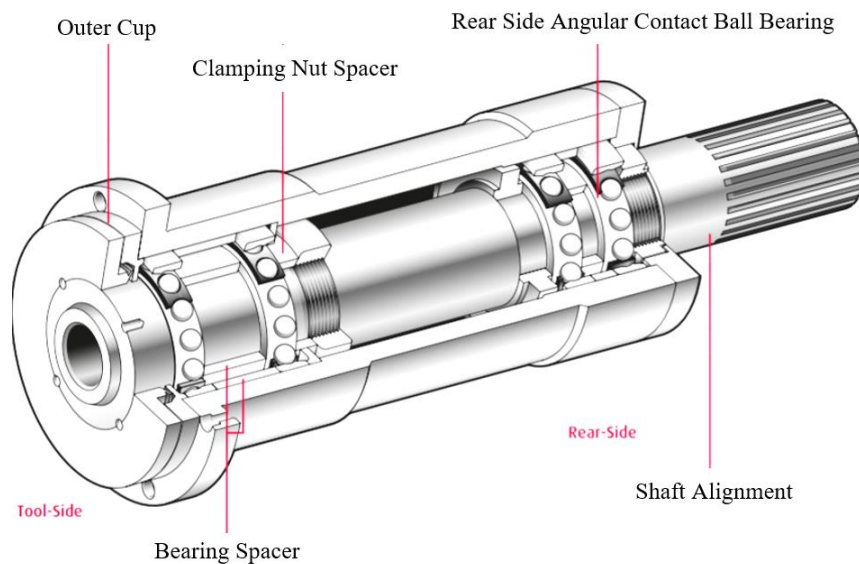


Figure 3.38. Spindle structure [74]

In order to drive spindle shaft, which does not incorporate a built-in motor, it is necessary to use additional servo motor, which has high torque and speed. Commercial company Pocket NC used for their 5-axis machining centre NSK-NRR 2651 spindle, which has 50000 [RPM] nominal speed and 1 [μ m] accuracy. Its price is around 1000 [USD] and the price of typical servo motor along with its driver is approximately 1000 [USD]. Therefore, total cost of the spindle is around 2000 [USD]. Higher cost of this concept led to the evaluation of different alternatives. Bosh GBM 10 RE drilling machine has 20 [Nm] nominal torque and 1676 [RPM] nominal speed. Internal components of the drilling machine (power drill) are indicated in Figure 3.39.

Run out errors of the driller are very high due to clearance fit used in bearings on the tool side. Moreover, having plastic surface around the bearings causes lack of accuracy. Therefore, it is decided to change the housing of the bearings with machined aluminium. Furthermore, plastic structure around the motor inhibits the dissipation of heat generated by the motor. To provide better heat transfer, fin structure aluminium is used. Furthermore, for easier assembly, necessary bolt and pin holes are included in the base structure.

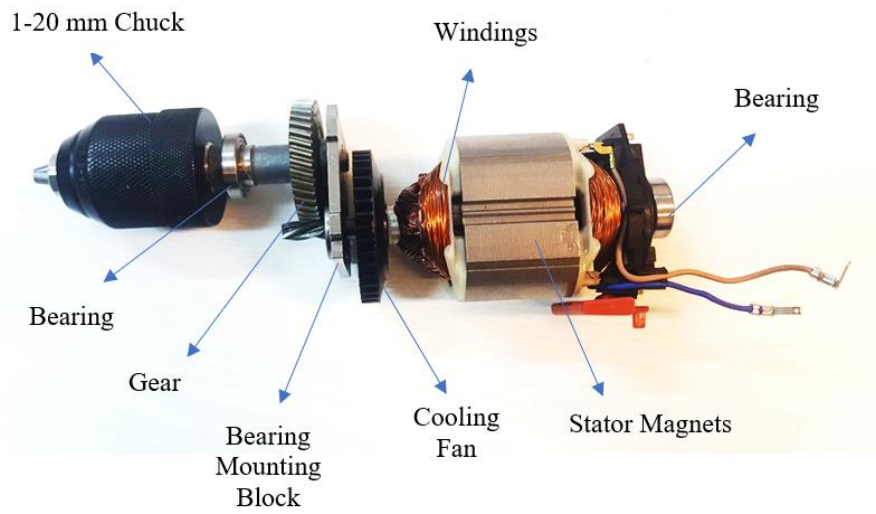


Figure 3.39. Internal components of the drilling machine

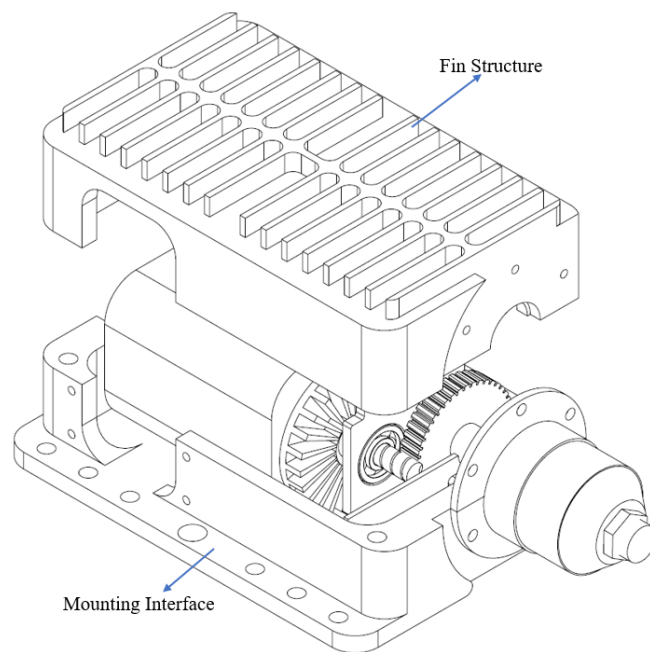


Figure 3.40. Fin structure aluminum base

Furthermore, in order to control the speed of the driller, CNY-70 (Reflective Optical Sensor with Transistor Output) is mounted on the top of the rotating shaft between bearing and gear. Figure 3.41 indicates the location of CNY-70.

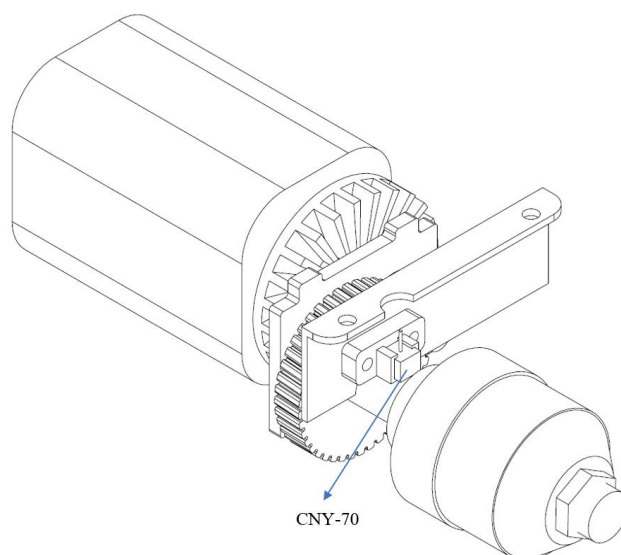


Figure 3.41. Location of rotary sensor in the spindle

3.9. Extruder Head Design

Extruder head has special design. By changing the cross-sectional area of the nozzle dynamically by the “intelligent” control system, both the amount of plastic flow and the cross-sectional geometry can be adjusted automatically according to the geometric properties of the part to be printed during production. Thus, it will be possible to print complex geometric shapes on the printed object quickly and with high fidelity. Figure 3.42 indicates how the system works. Right side of the figure indicates bottom view of the rectangular cross section nozzle. When the nozzle position is as in upper part of the Figure 3.42, maximum bead width is obtained. When the nozzle position is as in bottom part of the Figure 3.42, minimum bead width is attained. By adjusting nozzle angle variable bead width can be obtained.

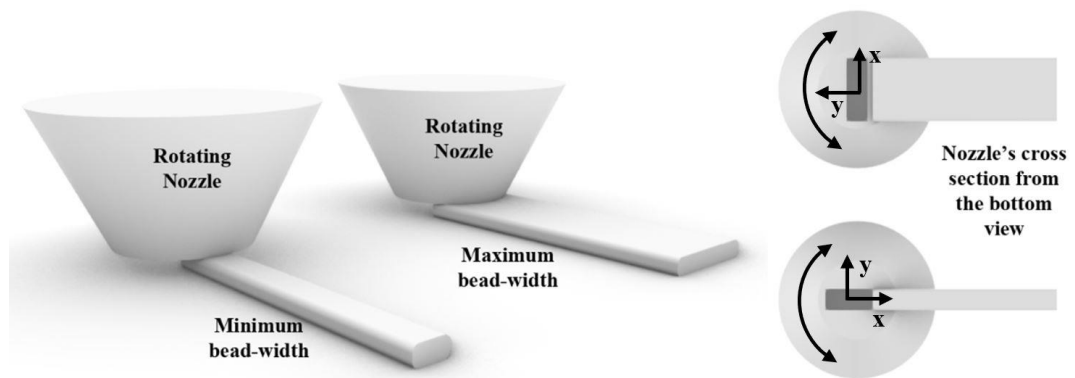


Figure 3.42. Variable bead width [75]

It is thought to have 2 different extruder nozzles in the system. One is a rectangular cross-section and the other is a conventional fixed cross-section. For the rectangular cross-section to be easily changed by the control system of the cross-sectional area, a concentric gear to the rectangular cross-section is controlled by another gear which is actuated by the stepper motor. Details of the design are shown in Figure 3.43.

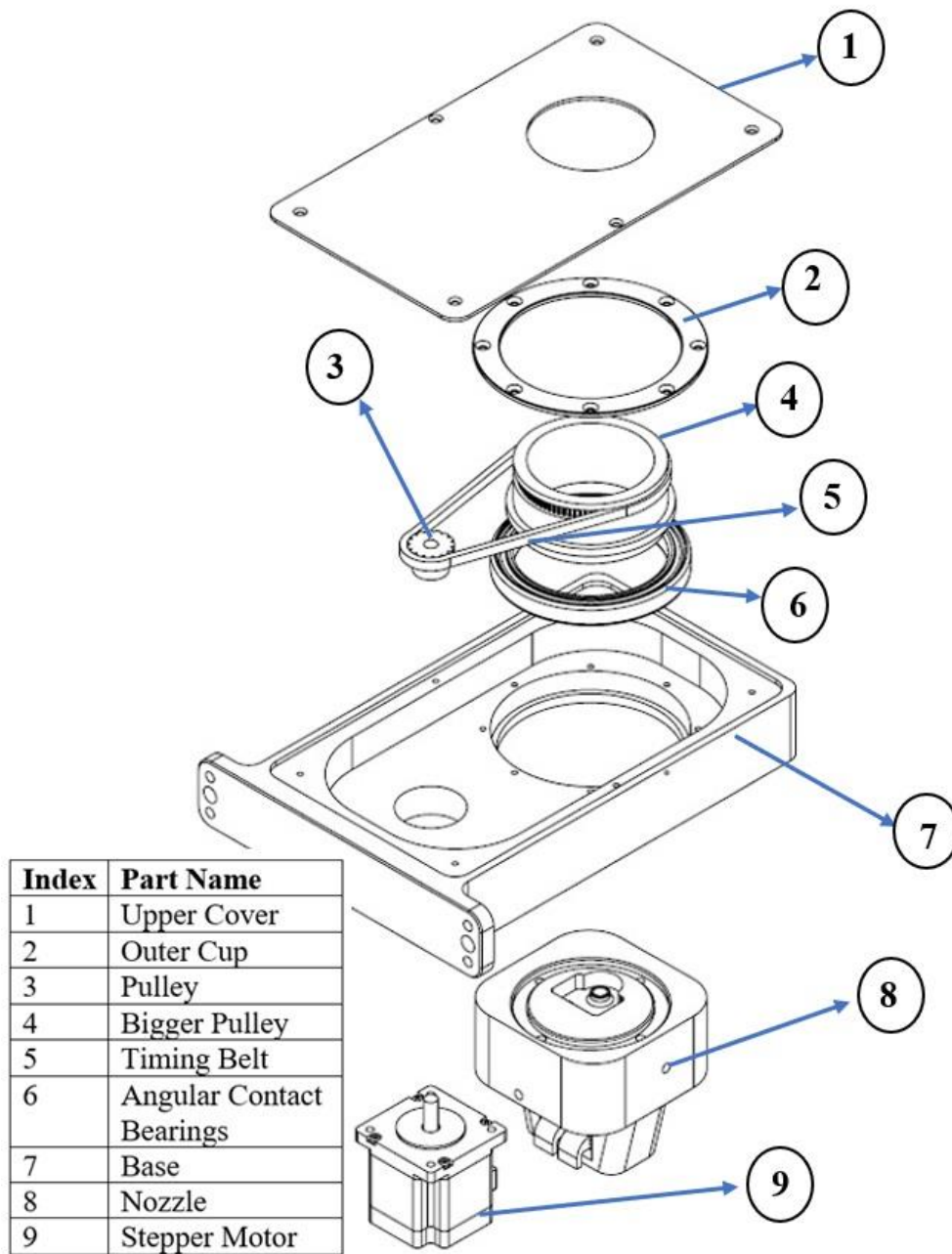


Figure 3.43. Exploded view of the extruder

Left side of Figure 3.44 illustrates the bottom view of the extruder head. Closer view of the detailed nozzle is shown in the right side of Figure 3.44. The center of rotation is the center of nozzle which has rectangular cross section.

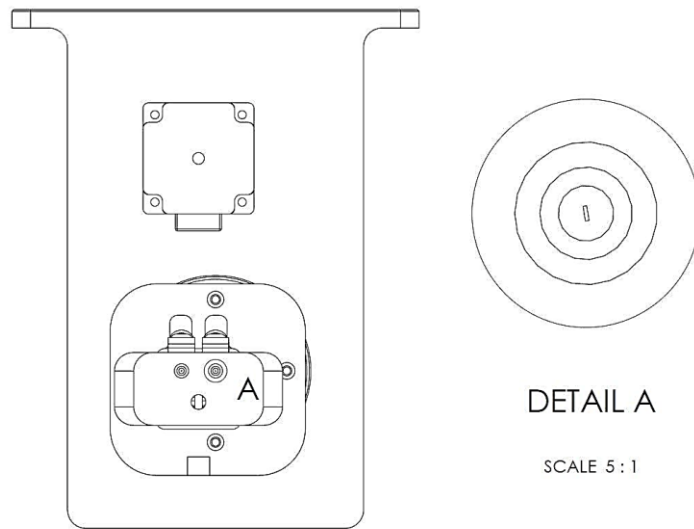


Figure 3.44. Left side shows the bottom view of the extruder and the right side indicates the detailed view of the region within the detail A

Figure 3.45 indicates the top view of the extruder.

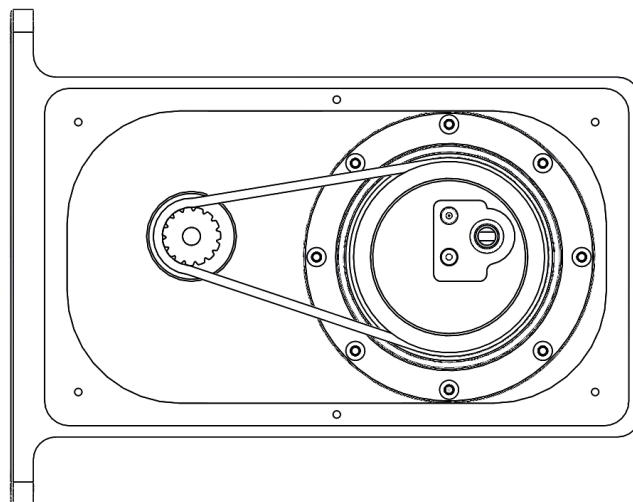
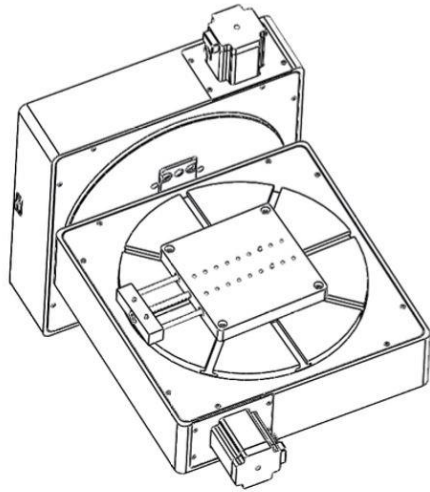


Figure 3.45. Top view of the extruder

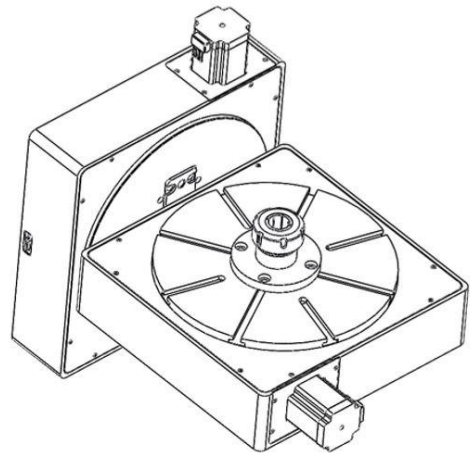
3.10. Workpiece Holding

Material mounting is one of the most important factors for FDM process and CNC milling. In commercial 3-axis FDM machines, most of the time it is enough to hold workpiece with the adhesion of first layer to the platform. However, for the 5-axis FDM processes position of the workpiece and platform is not always aligned with the gravity. Moreover, for the milling process the cutting forces will cause separation of workpiece from the platform. Therefore, fixture to hold the workpiece is required. Fixture should prevent any motion during manufacturing process, for which the rigid connection is vital.

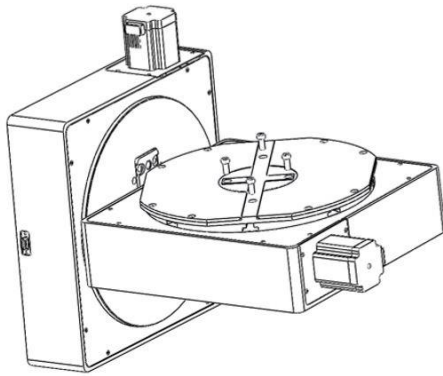
Fixture should be adopted to wide variety of shapes and sizes. Nevertheless, it is impossible to hold all kinds of shapes with one specific fixture. Therefore, different fixtures are designed for different shapes materials. Multi-purpose tables mounted on B- and C axes are shown in Figure 3.46a – 3.46c. By using a clamp, workpieces of different sizes can be fixed to the system. Collet-type fixing refers to fixing the cylindrical parts rigidly to the system. With the fixation system in the form of dovetail, the bonding between the filament and fixture will be ensured. Details are shown in Figure 3.46d.



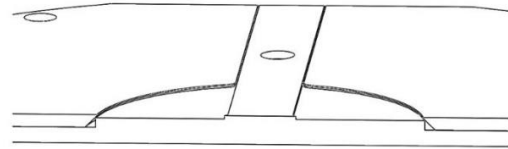
a)



b)



c)



d)

Figure 3.46. Work holders on B/C axis a) universal type, b) collet type, c) dove tail, d) details of the dove tail

3.11. Closure

The structure, linear axis, rotary axis, spindle, extruder head and work holder are designed modularly. In previous sections details of these designs are described. The overall view of the system is shown in Figure 3.47.

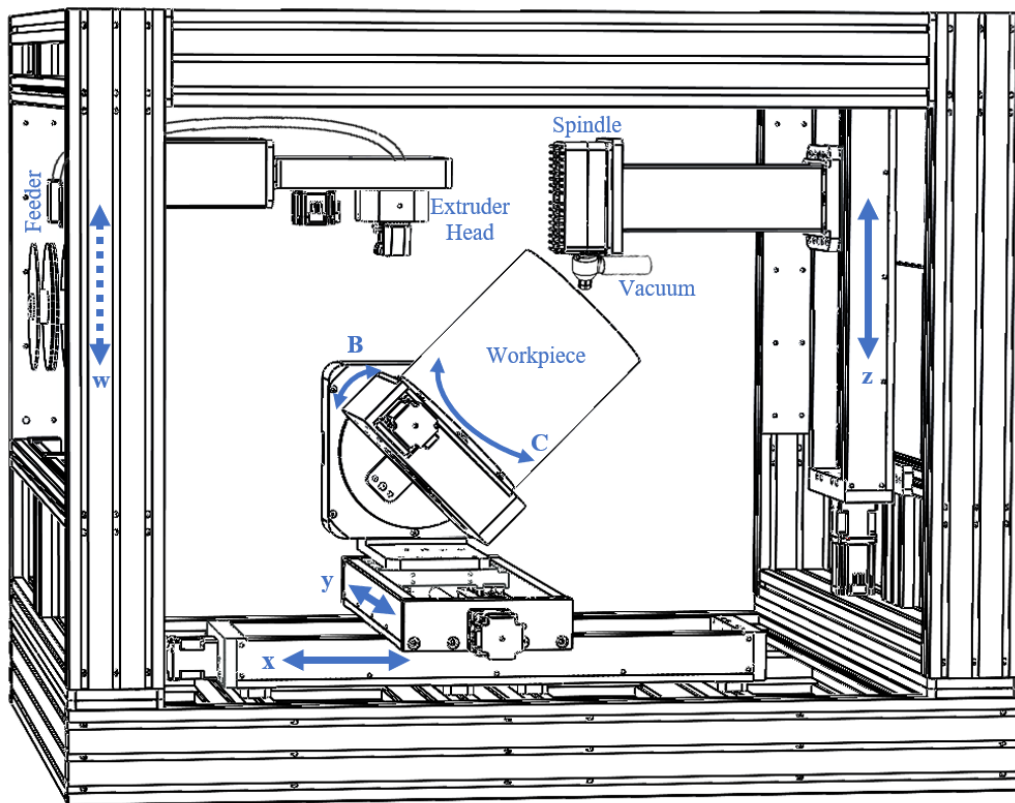


Figure 3.47. Final design

CHAPTER 4

PRODUCTION OF HYBRID MANUFACTURING SYSTEM

4.1. Production

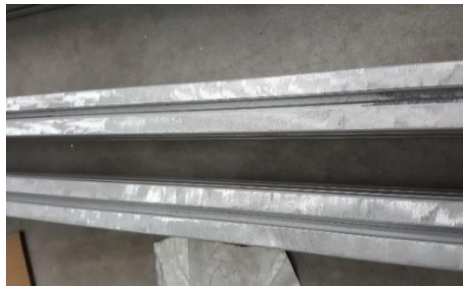
During manufacturing, CNC milling and turning machines were used for production of components. Since Al-6000 series material was used, additional grinding could not be applied for the reference surfaces. Squareness of the CNC machines is the factor that affects precision of the parts. During manufacturing of the precision components there were distortions. In order to avoid them, the workpiece was removed from the clamp and waited for a while to relax just before the final surface finish. Then, the workpiece was clamped less tightly and supported evenly for the final machining.

Structures, linear stages and rotary stages have modular design. Firstly, each of them was assembled separately, their functionality was controlled and, finally, combined together.

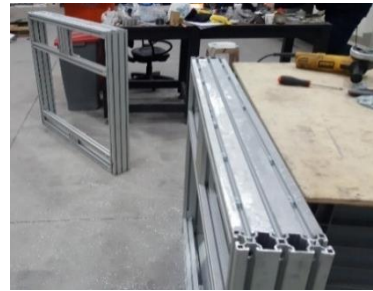
4.2. Production of the Structure

First, the basic structures, columns and lower body that forms the carcass structure were mounted modularly. During the assembly it was foreseen that the hollow structure of the bolt connections that was used as the primary fastening element of the sigma profiles would move during the production and over time. Therefore, the connections were reinforced with industrial epoxy in addition to the bolt connections. In order to provide good penetration of industrial epoxy into surfaces, the connection surfaces were ground and cleaned. Then, industrial epoxy was applied to both contact surfaces and fixed with the help of a gripper and the adhesive was let to cure.

Reference surfaces of the columns and lower body were milled with Bohrwerk machine with a single clamping operation. The components of the frame structure (processed separately at Bohrwerk benches) were removed from the metal chips, masked and sent for painting. In order to prevent distortion during and after painting, the components of the frame structure were painted with wet paint without being subjected to any heat treatment. After painting, the components were assembled with pins and bolts. Assembly and production stage of carcass structure is shown in Figure 4.1.



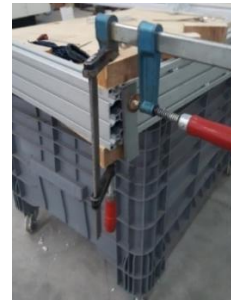
a)



b)



c)



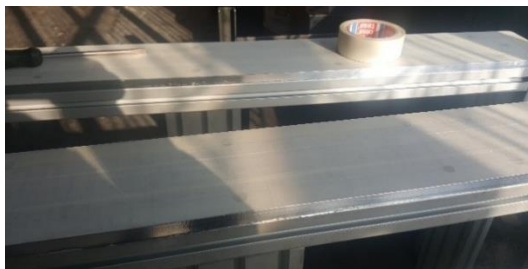
d)



e)



f)



g)



h)

Figure 4.1. Production and assembly stages of the system: a) Sigma profile contact surfaces after grinding, b) columns after grinding, c) epoxy on ground surfaces, d) connection of sigma profiles, e) assembled bottom structure, f) bottom and columns assembled before Bohrwerk operation, g) masking before painting, h) assembly of overall structure.

4.3. Production of Linear Stages

Components of linear stages were manufactured in 5-axis and 3-axis CNC milling machines. Ball screw ends were manufactured with the 5-axis lathe. Figure 4.2 indicates the components of the linear stages.

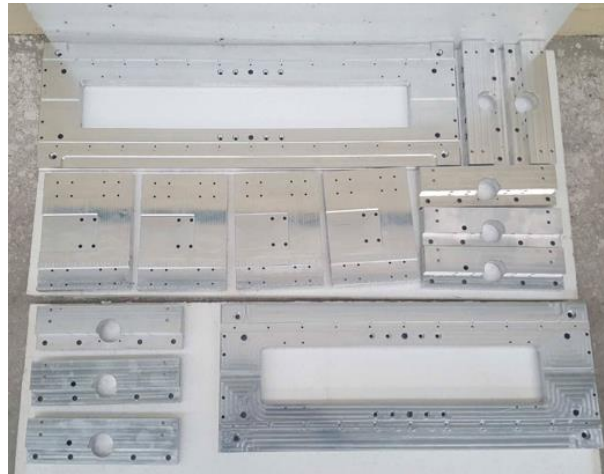


Figure 4.2. Components of the linear stages

After production of the components of the linear stages, assembly process was carried out. To ensure parallelism between the rails in the axes, the carriages were preloaded with the aid of clamping device. First, the preloaded carriages were brought to the middle. The position of the rail was then determined with the help of setscrews under the carriages. The carriages were then pulled slightly to one side and the rails were bolted to the body. This process was repeated by moving the carriages to the right and left one by one, until the whole rail was fixed to the body. To ensure parallelism, the distance in-between the reference surfaces of the carriages was measured with a caliper. All bolts were then inserted into the carriage holes and some clearance was removed. With the preload, the upper table reference surface and the reference surfaces of the carriages were kept in contact and the bolts were tightened in the sequence shown in Figure 4.3. Then, space was taken with a setscrew. After the linear bearings were connected to the carriage, the screw shaft nut and the carriage were bolted in accordance with the principle described above.

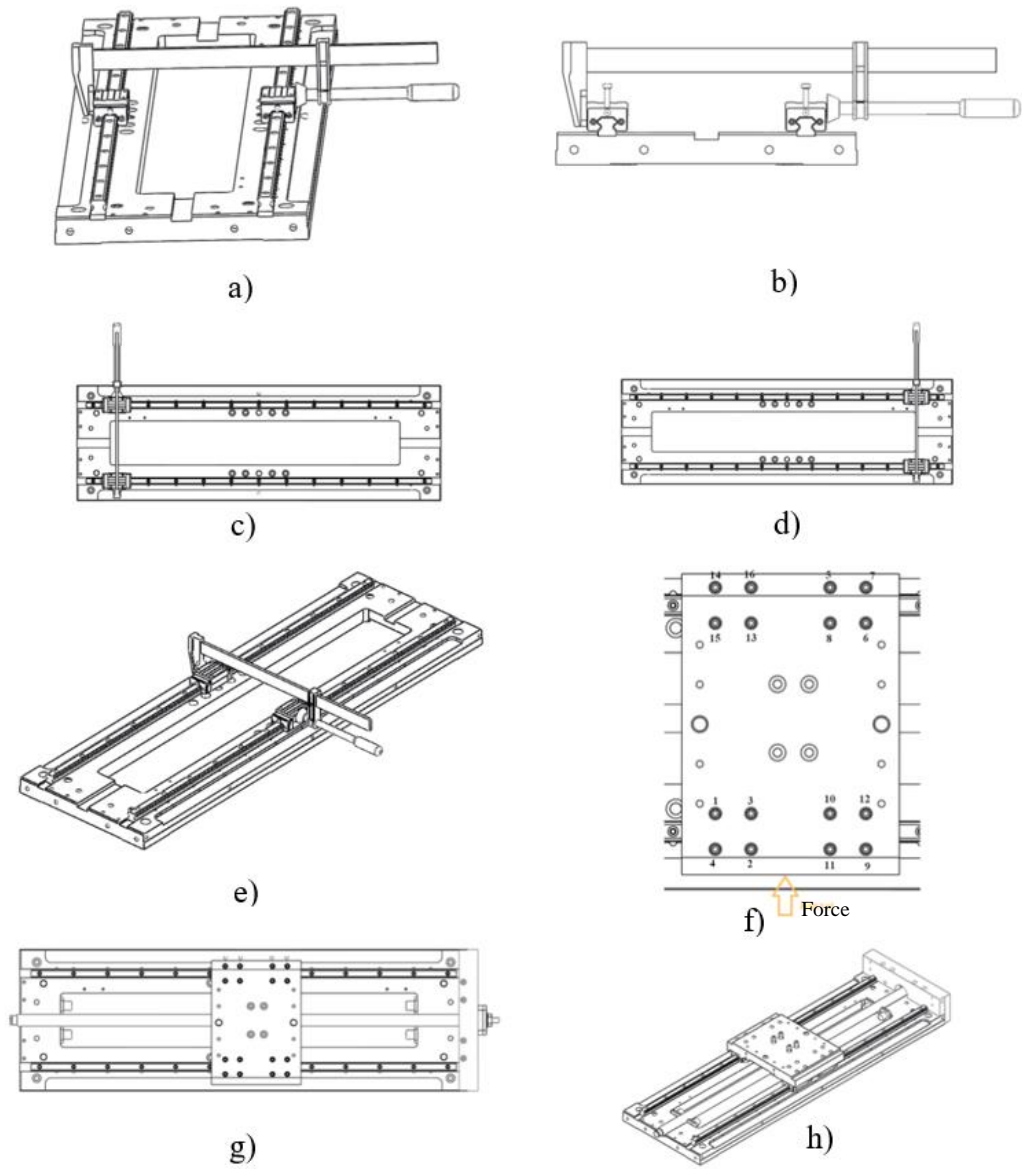


Figure 4.3. Assembly stages of the axes: a) preloading linear bearings and removing the empty space with set screw, b) tightened bolts, c) pushing the bearings left, d) pushing the bearings right, e) isometric view, f) applying nested force and tightening bolts with the given order, g) taking empty space with a setscrew, h) tightening bolts to connect carriage and feed screw nut

4.4. Production of Rotary Stages

Main components of rotary stages were produced by 3-axis and 5-axis CNC milling machines. None of the components required specifically 5-axis machining. However, using 5-axis milling decreases the number of clamping operations. Therefore, overall manufacturing time decreases. Since the material used was Al6061, components could be machined with relatively high speeds. For the circular components, turning operation was used. However, for some of the components secondary milling operation was required because of the noncircular patterns involved on the components.

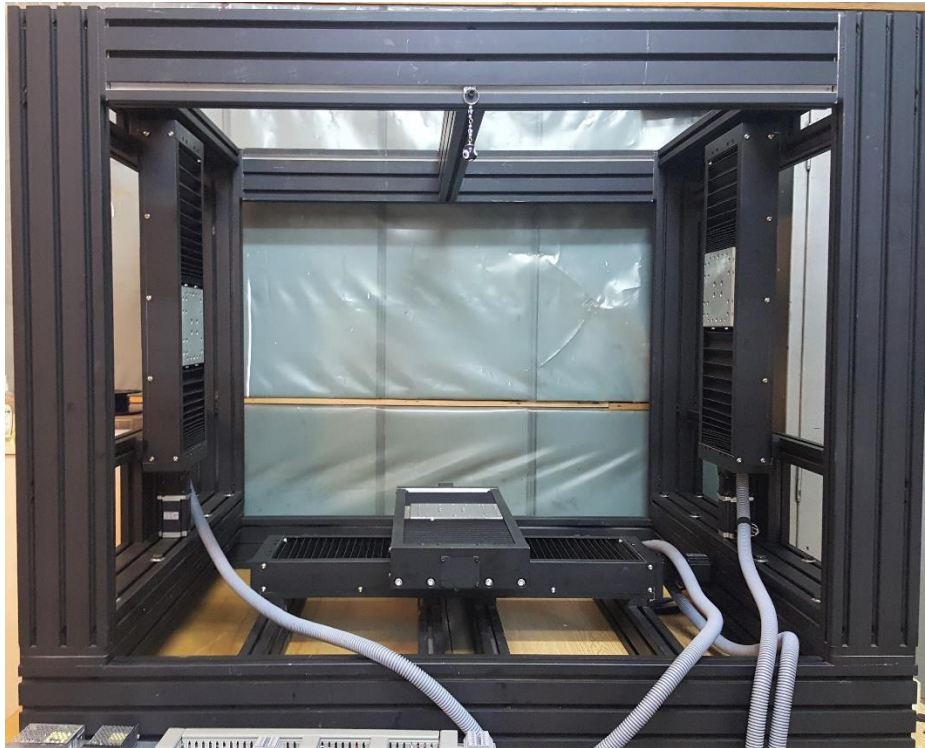
Worm gear pairs are manufactured in 3 stages. Firstly, turning operations were used to bring the geometry of the gear in desired dimensions. Then, gear teeth were machined. Finally, steel driver worm gears were sent to heat treatment for hardening.



Figure 4.4. Assembly of rotary stage a) C axis b) B axis

4.5. Final Assembly

Structures, linear- and rotary stages were assembled with each other by locating pins and bolts. The final assembly is shown in Figure 4.5.



*Figure 4.5.*The final assembly

4.6. Closure

Manufacturing of the system can be divided into 4 groups: machining, tapping, surface treatment and assembly. Important observations about the manufacturing are explained as

- For each component, special arrangement in the CNC milling machine is done. Keeping the components of the X-, Y-, Z- and W axis identical and producing 4 of them one after another reduces the production time. Similarly, most of the components of the B- and C axis except platform were identical.
- As the amount of metal removal increases, residual stress induced in the components increases. Reference surface of the components of the X-, Y-, Z-, and W axis were produced with 1 [μm] flatness. After 1 week, when the components were measured again, shape of the overall system was changed, and flatness of the reference surface was measured as 15 [μm]. Therefore, additional machining was required. For this machining process, components were clamped on the CNC milling machine with very light clamping force and very little amount of material is removed in each pass.
- Tapping is not feasible for the deep holes and making holes too shallow causes problems during assembly.
- For the connections which have to be very stiff and durable, helicoil can be used. However, hole diameter required for the same size tap is higher in helicoil.
- For the eloxal coating, component should be sunk into liquid bath. Therefore, special interface to hold the component should be involved in the system.
- Using epoxy for the connections increased the damping properties of the system.

CHAPTER 5

CONCLUSIONS AND FUTURE WORK

5.1. Conclusion

In this thesis, design and manufacturing of hybrid manufacturing system are done. In the first chapter, significance of high-quality printing is explained. Moreover, related literature about increasing product quality in printing is delivered. In the second chapter, components of precision machine systems and hybrid printer systems are reviewed from recent studies and projects. In the beginning of Chapter 3, requirements of hybrid manufacturing systems are expressed. After that, the related conceptual designs for the hybrid manufacturing system are indicated and the reason, why the specific design was chosen, is justified. In the next section, dimensional analysis for the chosen concept is done and necessary dimensions for the structures and modular axis are obtained. In Section 3.4, kinematic analysis of the machine with the error parameters is carried out. After that, the axial- and angular error boundaries for each axis are calculated by Monte Carlo simulation. In the next section, material and shape selection of the structure is explained and the results of static structural and modal analysis are indicated. In Section 3.6, structure, transmission and actuation and bearing components of the linear stages are explained. Similarly, in Section 3.7, structure, transmission and actuation and bearing components of the rotary stages are explained. Furthermore, in Sections 3.6 and 3.7, component selection process is explained by considering precision and strength. For the precision analysis, linear and roller bearings are modelled with springs and effects of geometric errors and external forces on the overall accuracy are observed. In the next sections, design of spindle, nozzle and work holding devices are examined. In Chapter 4, manufacturing of the structure, linear stages and rotary stages is explained.

5.2. Future Works

During design and manufacturing, due to cost and feasibility, many components that could make the system better could not be chosen. In this section, future work about the hybrid manufacturing system will be explained.

Al-6061-T6 sigma profiles are used as a structural material. During FEA, it is observed that for the chosen spindle, structure has enough dynamic properties. However, if higher speed spindle was used, machine structure would be prone to natural frequencies. To reduce unwanted vibration, sandwich type shear dampers can be used. By putting visco-elastic layer on sigma profiles and sheet metal on the visco-elastic layer, the sandwich type shear-damper is constructed layer by layer. During dynamic motion of the machine structure, relative motion between sigma profiles and constructing layer will cause heat dissipation. Therefore, unwanted vibration is going to be dissipated by heat. Furthermore, filling up sigma profiles with sands also provides similar effect. At the same time, movement of the structure makes sands inside of the sigma profiles move as well. Therefore, friction in between sands would dissipate the energy used for vibration.

Actuation of the linear stages is with the stepper motor connected to the coupling. Having such a structure decreases the effective stroke of the linear stage to the total length of linear stage. Instead of coupling, belt can be used as an additional transmission element and motor can be mounted by the side of the linear stage. This change would decrease the size of the structure in X direction and enable spindle and nozzle to be closer to Z- and W axis. Moreover, having more compact structures would improve the dynamic properties of the system.

Furthermore, linear stages are controlled with stepper motor in an open loop system. If the machining forces exceed the transmission force, stepper motor will miss the step and position control of the system will be impossible. Therefore, either rotary encoder should be put on the axis of feed screw or the linear scale should be fixed to the system.

Rotary stage has a complete aluminium structure. The bearings used are made of steel, while shafts and seats surrounding the bearings are made of aluminium. Because of the difference between thermal expansion coefficients of bearing, shaft and seat material, there will be thermal stresses in the inner rings of bearings and loose connection in the outer rings of bearings. In order to prevent this, shaft and seat material should be the same as the bearing material.

Lastly, the designs of spindle, nozzle and work holding are completed and will be produced in near future.

REFERENCES

- [1] M. Taufik and P. Jain, “A Study of Build Edge Profile for Prediction of Surface Roughness in Fused Deposition Modeling”, *Journal of Manufacturing Science and Engineering*, vol. 138, no. 6, 2016.
- [2] I. Gajdoš, E. Spišák, L. Kaščák and V. Krasinskyi, “Surface Finish Techniques for FDM Parts”, *Materials Science Forum*, vol. 818, pp.45-48, 2015.
- [3] H. C. Möhring, C. Brecher, E. Abele, J. Fleischer and F. Bleicher, “Materials in machine tool structures”, *CIRP Ann. - Manuf. Technol.*, vol. 64, no. 2, pp. 725–748, 2015.
- [4] A. Slocum, *Precision machine design*. Englewood Cliffs, N.J: Prentice Hall, 1992.
- [5] W. J. Wills-Moren, H. Modjarrad, R. F. J. Read and P. A. McKeown, “Some Aspects of the Design and Development of a Large High Precision CNC Diamond Turning Machine”, *CIRP Ann. - Manuf. Technol.*, vol. 31, no. 1, pp. 409–414, 1982.
- [6] M. Munirathnam, "Einfluss masseoptimierter Kragarmstrukturen auf die dynamische Bahngenauigkeit von HSC-Fräsmaschinen", *Doctoral Dissertation*, TU Darmstadt, 2008.
- [7] Y. Ito, *Modular design for machine tools*. New York: McGraw-Hill, 2008.
- [8] I. Zaman, A. Khalid, B. Manshoor, S. Araby and M. I. Ghazali, “The effects of bolted joints on dynamic response of structures”, *IOP Conf. Ser. Mater. Sci. Eng.*, vol. 50, no. 1, 2013.
- [9] R.D. Adams, “The Damping Characteristics of Certain Metals Steels, Cast”, *Journal of Sound and Vibration*, vol. 23, no. 2, pp. 199–216, 1972.

- [10] M. Dölen, "Design of Precision Machinery". ME 551 – Lecture Notes.
- [11] P. Scheelekens et al., "Design for Precision: Current Status and Trends", *Annals of the CIRP*, vol. 47, no. 2, pp.557-586, 1998.
- [12] A. Grotz, "Natürliches Hartgestein als Basis für hochdynamische Positionier-und Bewegungssysteme, Maschinengestelle heute—Werkstoffe Konzepte Innovationen", *Proceedings Wangener Maschinen Tage, Wangen, Germany*, 115–134, 2012.
- [13] S. Z. Abdin, R. K. Shenoy and M. E. Visveswaran, "Investigation on Granite as a Material for Metrology Aids", *Annals of the CIRP*, vol. 27, no. 1, pp.377–381, 1978.
- [14] W. deBruin, "Dimensional Stability of Materials for Metrological and Structural Applications", *Annals of the CIRP*, vol. 31, no. 2, pp.553–560, 1982.
- [15] R. Bedi, R. Chandra and S. P. Singh, "Mechanical Properties of Polymer Concrete", *J. of Composites*, 2013.
- [16] H. Haddad and M. Al Kobaisi, "Optimization of the polymer concrete used for manufacturing bases for precision tool machines", *Compos. Part B Eng.*, vol. 43, no. 8, pp. 3061–3068, 2012.
- [17] J. Do Suh and D. G. Lee, "Design and manufacture of hybrid polymer concrete bed for high-speed CNC milling machine", *Int. J. Mech. Mater. Des.*, vol. 4, no. 2, pp. 113–121, 2008.
- [18] S. Gordon and M. T. Hillery, "Development of a high-speed CNC cutting machine using linear motors", *J. of Material Processing Tech.*, vol. 166, no.3, pp.321-329, 2005.

- [19] A. Harnoy, Bearing design in machinery. New York: Marcel Dekker, 2003.
- [20] Schaeffler.com, 2015. [Online]. Available: https://www.schaeffler.com/remotemedien/media/_shared_media/08_media_library/01_publications/schaeffler_2/tpi/downloads_8/tpi_149_en_en.pdf. [Accessed: 11- May- 2019].
- [21] B. W. Rowe, Hydrostatic, aerostatic and hybrid bearing design. Waltham, US: Butterworth-Heinemann LTD, 2012.
- [22] Physikinstrumente.com, 2009. [Online]. Available: <https://www.physikinstrumente.com/en/products/linear-stages/stages-with-pimag-magnetic-direct-drive-linear-motor/a-110-piglidge-lc-linear-stage-with-air-bearings-900711/>. [Accessed: 11- May- 2019].
- [23] S. K. Ro, S. Kim, Y. Kwak and C. H. Park, "A linear air bearing stage with active magnetic preloads for ultraprecise straight motion", *Precis. Eng.*, vol. 34, no. 1, pp. 186–194, 2010.
- [24] "THK General Catalogue", *Noc.ua*, 2010. [Online]. Available: <https://www.noc.ua/pdfs/thk-5001e-en.pdf>. [Accessed: 12- May- 2019].
- [25] E. Milić, Ž. Šitum and M. Essert, "Robust position control synthesis of an electro-hydraulic servo system", *ISA Transactions*, vol. 49, no. 4, pp. 535-542, 2010.
- [26] C. C. Wei and R. S. Lai, "Kinematical analyses and transmission efficiency of a preloaded ball screw operating at high rotational speeds", *Mech. Mach. Theory*, vol. 46, no. 7, pp. 880–898, 2011.
- [27] E. Kiliç, M. Dölen and A. B. Koku, "Analysis and estimation of motion transmission errors of a timing belt drive", *Turkish J. Electr. Eng. Comput. Sci.*, vol. 18, no. 5, pp. 883–897, 2010.

- [28] Skf.com, 2014. [Online]. Available: <https://www.skf.com/binary/82-153959/14489-EN---Roller-screw-catalogue.pdf>. [Accessed:10- Jun- 2019].
- [29] V. Venkatesh and S. Izman, Precision engineering. Estados Unidos: McGraw-Hill Companies, Inc., 2008.
- [30] K. Spanner and B. Koc, "Piezoelectric Motors, an Overview," *Actuators*, vol. 5, no. 1, p. 6, 2016.
- [31] "Linear Encoders for Numerically Controlled Machine Tools Product Catalog", Heidenhain.de, 2017. [Online]. Available: https://www.heidenhain.de/fileadmin/pdb/media/img/571470-2B_Linear_Encoders_For_Numerically_Controlled_Machine_Tools.pdf. [Accessed:10- Jun- 2019].
- [32] Mtssensors.com, 2001. [Online]. Available: <http://www.mtssensors.com/fileadmin/media/pdfs/551019.pdf>. [Accessed 8- Jun- 2019].
- [33] Broad.com, 2018. [Online]. Available: <https://docs.broadcom.com/docs/AV02-1132EN>. [Accessed 8- Jun- 2019].
- [34] G. M. J. Delhaes, A. V. Beek, R. A. V. Ostayen and R. H. M. Schmidt, "A High-Speed Air Bearing Spindle", Delft University of Technology, 2007.
- [35] Zollern.com, 2010. [Online]. Available <https://www.zollern.com/en/drive-technology/aerostatic-bearings.html>. [Accessed 17- May- 2019].
- [36] B. J. Stone, "The State of the Art in the Measurement of the Stiffness and Damping of Rolling Element Bearings", *CIRP Ann. - Manuf. Technol.*, vol. 31, no. 2, pp. 529–538, 1982.
- [37] Kollmorgen.com, 2011. [Online]. Available: <https://www.kollmorgen.com/en-us/products/motors/brush-dc/dc-torque-motor/dc-torque-motors/>. [Accessed 29-Apr- 2019].

- [38] “Planetary Gear Units Series Catalogue”, Wikov, 2018. [Online]. Available: <https://www.wikov.com/file/edee/prilohy/orbi-flex-catalogue-2018-20180511-130912.pdf?fbclid=IwAR09Jk4eO6deqmN9L9L-uNvBkbY1WkfNWxnfDKI5A865VjvKsBt4008-N-Y>. [Accessed 15- Jun- 2019].
- [39] Tec-Science.com, 2018. [Online]. Available: <https://www.tec-science.com/mechanical-power-transmission/planetary-gear/epicyclic-planetary-gear/>. [Accessed 15- Jun- 2019].
- [40] R. Budynas, J. Nisbett and J. Shigley, Shigley's mechanical engineering design. New York: McGraw-Hills., 2010.
- [41] Harmonic Drive AG - Strain wave gear principle, 2011. [Video] Available: https://www.youtube.com/watch?v=bzRh672peNk&fbclid=IwAR237X_rhfhuCLAIH9ZHASdQoNwzDBNhp9zcTSC5opSOihsx8xW70DOZniQ. [Accessed 8-May- 2019].
- [42] “Speed Reducers for Precision Motion Control Catalogue”, Harmonic Drive, 2018. [Online]. Available: https://www.harmonicdrive.net/_hd/content/documents/CSF-Mini_GearUnits.pdf?fbclid=IwAR1ubAp62t7hAOjbbgeJSBUMjREebwmsrCXeJzQjYEZic_XMIVbt5HBh9UY. [Accessed 7- May- 2019].
- [43] P. Sandin, Robot mechanisms and mechanical devices illustrated. New York: McGraw-Hill, 2003.
- [44] Pascaleng.com, 2018. [Online]. Available: <https://www.pascaleng.co.jp/us/>. [Accessed 19- May- 2019].
- [45] PCBMotor.com, 2012. [Online]. Available: https://pcbmotor.com/?fbclid=IwAR0GD_wjXJiPgSHccGXp0NUbFDUnMtLXoyOvuzJXuPvXdmlzK4NuFqaO6c. [Accessed 9- Jul- 2019].

- [46] S. Sanda and K. Hayakawa, K. “Traction Drive System and its Characteristic as Power Transmission”, R&D Review of Toyota CRDL, vol. 40, no. 3, pp. 30-39, 2005.
- [47] Rmidrive.com, 2019. [Online]. Available: <https://rmidrive.com/index.php/specs/>. [Accessed 27- May- 2019].
- [48] "Spindle Solutions Product Catalog", Siemens AG, 2007. [Online]. Available: <http://literature.puertoricosupplier.com/017/TM17232.pdf>. [Accessed 29- May- 2019].
- [49] E. Abele, Y. Altintas and C. Brecher, “Machine tool spindle units”, CIRP Annals, vol. 59, no. 2, pp. 781-802, 2010.
- [50] H. Yoshioka, S. Matsumara, H. Hashizume and H. Shinno, “Minimizing Thermal Deformation of Aerostatic Spindle System by Temperature Control of Supply Air”, JSME International Journal Series C Mechanical Systems Machine Elements and Manufacturing, vol. 49, no. 2, pp. 606–611, 2006.
- [51] F. Jakob and H. Sykora, “Special Tool Clamping Requirements in the Field of High Speed Spindles”, 7th International Conference on High Speed Machining, Darmstadt, 28–29 May 2008.
- [52] E. Rivin, “Tooling Structure: Interface between Cutting Edge and Machine Tool”, CIRP Annals Manufacturing Technology, vol. 49, no. 2, pp. 591–634, 2000.
- [53] E. Marsh, Precision spindle metrology. Lancaster, Pa.: DEStech Publications.
- [54] Hermle.de, 2017. [Online]. Available: https://www.hermle.de/en/machining_centres/models/c_400_machining_centre. [Accessed 6- Jun- 2019].
- [55] Cybmantech.co.uk, 2018. [Online]. Available: http://www.cybamantech.co.uk/en/products/milling_machines/cybaman_replicator. [Accessed 6- Jun- 2019].

- [56] Dmgmori.com, 2017. [Online]. Available: <https://en.dmgmori.com/products/machines/additive-manufacturing/powder-nozzle/lasertec-65-3d-hybrid>. [Accessed 7- Jun- 2019].
- [57] Hamuel.de, 2013. [Online]. Available: <https://www.hamuel.de/en/produkte/hstm/index.php>. [Accessed 6- Jun- 2019].
- [58] Mazakusa.com, 2014. [Online]. Available: <https://www.mazakusa.com/machines/integrex-i-400am/>. [Accessed 6- Jun- 2019].
- [59] Optomec.com, 2019. [Online]. Available: https://www.multistation.com/voy_content/uploads/2017/10/lens-3d-hybrid-20-open-atmosphere-system_web0817.pdf. [Accessed 6- Jun- 2019].
- [60] 3dhybridsolutions.com, 2018. [Online]. Available: <http://www.3dhybridsolutions.com/>. [Accessed 5- Jun- 2019].
- [61] Ctc.com, 2017. [Online]. Available: <https://www.ctc.com/public/solutions/techan-dinnovation/additive-manufacturing-hybrid.aspx>. [Accessed 6- Jun- 2019].
- [62] Ibarria.com, 2015. [Online]. Available: <https://www.ibarria.com/en/today/ibarria-additive-manufacturing-multitasking>. [Accessed 6- Jun- 2019].
- [63] Solidscape. (2017). "Creating Family Heirlooms". [online] Available at: <https://www.solidscape.com/experiences/creating-family-heirlooms/>. [Accessed 7 June 2019].
- [64] Lumex-matsuura.com, 2018. [Online]. Available: <https://www.lumex-matsuura.com/english/contents/lumex25.html>. [Accessed 7- Jun- 2019].
- [65] Sodick.org, 2016. [Online]. Available: <https://www.sodick.org/products/additive-manufacturing/opm350l.html>. [Accessed 6- Jun- 2019].

- [66] Concept-laser.de, 2016. [Online]. Available: <https://www.concept-laser.de/en/products/machines.html>. [Accessed 6- Jun- 2019].
- [67] Fabrisonic.com, 2013. [Online]. Available: <https://fabrisonic.com/soniclayer-4000/>. [Accessed 6- Jun- 2019].
- [68] E. G. Wolff, Introduction to the Dimensional Stability of Composite Materials. Pennsylvania: DEStech Publications, 2004.
- [69] Nanotec.com, 2019. [Online]. Available: <https://en.nanotec.com/>. [Accessed 19- Aug- 2019].
- [70] Pbcllinear.com, 2018. [Online]. Available: https://www.pbcllinear.com/Blog/2018/February/What-is-Lead-Screw-Efficiency-in-Linear-Motion?fbclid=IwAR0NdsOsdY30lhFWQthL4x_5GPi9d6zqOois-1eWBY1YDY4IL2Vx2ydbRhg. [Accessed 16- Aug- 2019].
- [71] "Linear Guideway Product Catalog", Hiwin, 2018. [Online]. Available: https://www.hiwin.com/pdf/linear_guideways.pdf. [Accessed 17- Aug- 2019].
- [72] "Rolling bearings in industrial gearboxes Catalog", SKF, 1997.
- [73] M. Weck and C. Brecher, Werkzeugmaschinen Konstruktion und Berechnung, Heidelberg: Springer, 2006.
- [74] "Standard Spindles Catalog", NSK, 2012. [Online]. Available: https://www.nsk.com/common/data/ctrGPdf/e2202a.pdf?fbclid=IwAR05nxOeXhzR2ZrjSeux-0W-6UdlIOXY2heCQZjB_Y7YI88KJ-2q3LXqBwOE. [Accessed 22- Aug- 2019].
- [75] U. M. Dilberoğlu, V. Haseltalab, U. Yaman and M. Dölen (FAIM2019). Simulator of an Additive and Subtractive type of hybrid manufacturing system. Manuscript submitted for publication.

APPENDICES

In this section, MATLAB codes are provided for Sections 3.4 (for A) 3.6.3.1 (for B, C and F) and 3.7.3.1 (for D, E and F).

A. Monte Carlo Simulation for Kinematic Analysis

```
1   t=100000;
2   radasec=pi/(180*3600);
3   Ps=[350;0;-71.2;1];
4   empty=zeros(4);
5   for i=1:t
6       % Range of angular errors
7       a0=-25;b0=25; %arcsec
8       a = a0*radasec;b = b0*radasec;r = (b-a).*rand(21,1) + a;
9       ex1=r(1);ex2=r(2);ex3=r(3);ex4=r(4);ex5=r(5);
10      ex6=r(6); eex1=r(19);
11      ey1=r(7);ey2=r(8);ey3=r(9);ey4=r(10);ey5=r(11);
12      ey6=r(12);eey1=r(20);
13      ez1=r(13);ez2=r(14);ez3=r(15);ez4=r(16);ez5=r(17);
14      ez6=r(18);eez1=r(21);
15      % Range of axial errors
16      a1 = -25/1000;b1 = 25/1000;r1 = (b1-a1).*rand(21,1) + a1;
17      dx1=r1(1);dx2=r1(2);dx3=r1(3);dx4=r1(4);dx5=r1(5);
18      dx6=r1(6);ddx1=r1(19);
19      dy1=r1(7);dy2=r1(8);dy3=r1(9);dy4=r1(10);dy5=r1(11);
20      dy6=r1(12);ddy1=r1(20);
21      dz1=r1(13);dz2=r1(14);dz3=r1(15);dz4=r1(16);dz5=r1(17);
22      dz6=r1(18);ddz1=r1(21);
23      % Range of angles
24      a2 =0.1;b2 = 2*pi-0.1;r2 = (b2-a2).*rand(3,1) + a2;
25      tetx=r2(1);tety=r2(2);tetz=r2(3);
26
27      %Range of x
```

```

28     a3 =-221;b3 =221;r3 = (b3-a3).*rand(1,1) + a2;
29     x=r3;
30     % Range of y
31     a4 =-312/2;b4 =312/2;r4 = (b4-a4).*rand(2,1) + a2;
32     y=r4(1);
33     % Range of z
34     z=155;
35
36     %x errors
37     Tr1e= [1 -ez1 ey1 dx1+x; ez1 1 -ex1 dy1; -ey1 ex1 1
76+dz1; 0 0 0 1];
38     %y errors
39     T12e = [1 -ez2 ey2 dx2;...
40             ez2 1 -ex2 dy2+y+178.5;...
41             -ey2 ex2 1 241+dz2;...
42             0 0 0 1];
43     %b rotary errors
44     T23e = [cosd(tety) -cosd(tety)*ez4 sind(tety) dx4;...
45             ex4*sind(tety)+ez4 1 -ex4*cosd(tety) -178.5+dy4;...
46             -sind(tety) sind(tety)*ez4+ex4 cosd(tety) 46.5+dz4;...
47             0 0 0 1];
48     %c rotary errors
49     T34e = [cosd(tetz) -sind(tetz) ey6 dx6;...
50             sind(tetz) cos(tetz) -ex6 dy6;...
51             -ey6*cosd(tetz)+ex6*sind(tetz)
52             ey6*sind(tetz)+ex6*cosd(tetz) 1 19+dz6;...
53             0 0 0 1];
53     %Tr4 calculation
54     Ttot=Tr1e*T12e*T23e*T34e;
55     empty(1:3,1:3)=Ttot(1:3,1:3)';
56     empty(1:3,4)=-Ttot(1:3,1:3) '*Ttot(1:3,4);
57     empty(4,4)=1;
58
59     iTtot=inv(Ttot);

```

```

60     Tr1ze= [1 -eez1 eey1 -515.5+ddx1;...
61           eez1 1 -eex1 ddy1;...
62           -eey1 eex1 1 598.7+ddz1+z;...
63           0 0 0 1];
64     Ps1=empty*Tr1ze*Ps;
65
66     ex1=0;ey1=0;ez1=0;dx1=0;dy1=0;dz1=0;
67     ex2=0;ey2=0;ez2=0;dx2=0;dy2=0;dz2=0;
68     ex3=0;ey3=0;ez3=0;dx3=0;dy3=0;dz3=0;
69     ex4=0;ey4=0;ez4=0;dx4=0;dy4=0;dz4=0;
70     ex5=0;ey5=0;ez5=0;dx5=0;dy5=0;dz5=0;
71     ex6=0;ey6=0;ez6=0;dx6=0;dy6=0;dz6=0;
72     eex1=0;eey1=0;eez1=0;ddx1=0;ddy1=0;ddz1=0;
73
74     %x errors
75     Tr1e= [1 -ez1 ey1 dx1+x; ez1 1 -ex1 dy1; -ey1 ex1 1
76           76+dz1; 0 0 0 1];
77     %y errors
78     T12e = [1 -ez2 ey2 dx2;...
79           ez2 1 -ex2 dy2+y+178.5;...
80           -ey2 ex2 1 241+dz2;...
81           0 0 0 1];
82     %b rotary errors
83     T23e = [cosd(tety) -cosd(tety)*ez4 sind(tety) dx4;...
84           ex4*sind(tety)+ez4 1 -ex4*cosd(tety) -178.5+dy4;...
85           -sind(tety) sind(tety)*ez4+ex4 cosd(tety) 46.5+dz4;...
86           0 0 0 1];
87     %c rotary errors
88     T34e = [cosd(tetz) -sind(tetz) ey6 dx6;...
89           sind(tetz) cos(tetz) -ex6 dy6;...
90           -ey6*cosd(tetz)+ex6*sind(tetz)
91           ey6*sind(tetz)+ex6*cosd(tetz) 1 19+dz6;...
92           0 0 0 1];
93     %Tr4 calculation

```

```

92     Ttot=Tr1e*T12e*T23e*T34e;
93     empty(1:3,1:3)=Ttot(1:3,1:3)';
94     empty(1:3,4)=-Ttot(1:3,1:3) '*Ttot(1:3,4);
95     empty(4,4)=1;
96     Tr1ze= [1 -eez1 eey1 -515.5+ddx1;...
97             eez1 1 -eex1 ddy1;...
98             -eey1 eex1 1 598.7+ddz1+z;...
99             0 0 0 1];
100    Ps2=empty*Tr1ze*Ps;
101    Err=Ps1-Ps2;
102    Er(i)=(Err(1)^2+Err(2)^2+Err(3)^2)^0.5*1000;
103
104    end
105    hist(Er,t/100)
106    disp(2*std(Er))
107    xlabel('Position Error Metric(?m)');
108    ylabel('Frequency');

```

B. Linear Bearings Accuracy Analysis Function

```

1    function [dy01,dz01,ex01,ey01,ez01] = linearbalance5(a0,b0)
2    %Unit Conversion
3    radasec=pi/(180*3600);
4    %Random Errors
5    a = -10/1000;b = 10/1000;r = (b-a).*rand(8,1) + a;
6    daz=r(1);day=r(2);dbz=r(3);dby=r(4);dcz=r(5);dcy=r(6);ddz=r(7);ddy=r(8);
7    k=5e8;
8    da=[0;day;daz;0];db=[0;dby;dbz;0];dc=[0;dcy;dcz;0];dd=[0;ddy;ddz;0];
9    Lx=83.4;Ly=165;
10   %External Forces
11   Fxt=100;Fyt=100;Fzt=100;Rx=150;Ry=150;Rz=150;Weight=350;

```

```

12  [Mxc,Myc,Mzc,Fxc,Fyc,Fzc]=CenterForces(Fxt,Fyt,Fzt,Rx,Ry,Rz,Weight);
13  %for numeric solution L=[dx1 dy1 dz1 ex1 ey1 ez1]
14  A1=zeros(5);
15  D=zeros(5);
16  L = [.001 .001 .00001 .00001 .00001];
17  for i=1:5 %[dy dz ex ey ez]
18      D(i,i)=L(i);
19  end
20  for j=1:5
21      dy1=D(1,j);dz1=D(2,j);ex1=D(3,j);
22      ey1=D(4,j);ez1=D(5,j);
23      T= [1 -ez1 ey1 0; ez1 1 -ex1 dy1; -ey1 ex1 1 dz1; 0 0 0 1];
24      PA=[-Lx/2;Ly/2;0;1];PB=[-Lx/2;-Ly/2;0;1];
25      PC=[Lx/2;-Ly/2;0;1];PD=[Lx/2;Ly/2;0;1];
26      POA=T*PA;POB=T*PB;POC=T*PC;POD=T*PD;
27      dda=PA-POA;ddb=PB-POB;ddc=PC-POC;ddd=PD-POD;
28      DA=dda+da;DB=ddb+db;DC=ddc+dc;DD=ddd+dd;
29      FA=k*DA;FB=k*DB;FC=k*DC;FD=k*DD;
30      FA(1)=0;FB(1)=0;FC(1)=0;FD(1)=0;
31      MA=cross(PA(1:3),FA(1:3));MB=cross(PB(1:3),FB(1:3));
32      MC=cross(PC(1:3),FC(1:3));MD=cross(PD(1:3),FD(1:3));
33      Mtot=MA+MB+MC+MD;
34      Mx=MA(1)+MB(1)+MC(1)+MD(1)+Mxc;
35      My=MA(2)+MB(2)+MC(2)+MD(2)+Myc;
36      Mz=MA(3)+MB(3)+MC(3)+MD(3)+Mzc;
37      Fy=FA(2)+FB(2)+FC(2)+FD(2)+Fyc;
38      Fz=FA(3)+FB(3)+FC(3)+FD(3)+Fzc;
39  %second part
40  dy1=-D(1,j);dz1=-D(2,j);ex1=-D(3,j);
41  ey1=-D(4,j);ez1=-D(5,j);
42  T= [1 -ez1 ey1 0; ez1 1 -ex1 dy1; -ey1 ex1 1 dz1; 0 0 0 1];
43  PA=[-Lx/2;Ly/2;0;1];PB=[-Lx/2;-Ly/2;0;1];
44  PC=[Lx/2;-Ly/2;0;1];PD=[Lx/2;Ly/2;0;1];

```

```

45     POA=T*PA;POB=T*PB;POC=T*PC;POD=T*PD;
46     dda=PA-POA;ddb=PB-POB;ddc=PC-POC;ddd=PD-POD;
47     DA=dda+da;DB=ddb+db;DC=ddc+dc;DD=ddd+dd;
48     FA=k*DA;FB=k*DB;FC=k*DC;FD=k*DD;
49     FA(1)=0;FB(1)=0;FC(1)=0;FD(1)=0;
50     MA=cross(PA(1:3),FA(1:3));MB=cross(PB(1:3),FB(1:3));
51     MC=cross(PC(1:3),FC(1:3));MD=cross(PD(1:3),FD(1:3));
52     Mtot=MA+MB+MC+MD;
53     MX=MA(1)+MB(1)+MC(1)+MD(1)+Mxc;
54     MY=MA(2)+MB(2)+MC(2)+MD(2)+Myc;
55     MZ=MA(3)+MB(3)+MC(3)+MD(3)+Mzc;
56     FY=FA(2)+FB(2)+FC(2)+FD(2)+Fyc;
57     FZ=FA(3)+FB(3)+FC(3)+FD(3)+Fzc;
58     div=L(j)*2;
59     A1(1,j)=(Mx-MX)/(div);A1(2,j)=(My-MY)/(div);A1(3,j)=(Mz-MZ)/(div);
60     A1(4,j)=(Fy-FY)/(div);A1(5,j)=(Fz-FZ)/(div);
61     end
62     dy1=0;dz1=0;ex1=0;ey1=0;ez1=0;
63     T= [1 -ez1 ey1 0; ez1 1 -ex1 dy1; -ey1 ex1 1 dz1; 0 0 0 1];
64     PA=[-Lx/2;Ly/2;0;1];PB=[-Lx/2;-Ly/2;0;1];
65     PC=[Lx/2;-Ly/2;0;1];PD=[Lx/2;Ly/2;0;1];
66     POA=T*PA;POB=T*PB;POC=T*PC;POD=T*PD;
67     dda=PA-POA;ddb=PB-POB;ddc=PC-POC;ddd=PD-POD;
68     DA=dda+da;DB=ddb+db;DC=ddc+dc;DD=ddd+dd;
69     FA=k*DA;FB=k*DB;FC=k*DC;FD=k*DD;
70     FA(1)=0;FB(1)=0;FC(1)=0;FD(1)=0;
71     MA=cross(PA(1:3),FA(1:3));MB=cross(PB(1:3),FB(1:3));
72     MC=cross(PC(1:3),FC(1:3));MD=cross(PD(1:3),FD(1:3));
73     Mtot=MA+MB+MC+MD;
74     MX=MA(1)+MB(1)+MC(1)+MD(1)+Mxc;
75     MY=MA(2)+MB(2)+MC(2)+MD(2)+Myc;
76     MZ=MA(3)+MB(3)+MC(3)+MD(3)+Mzc;
77     FY=FA(2)+FB(2)+FC(2)+FD(2)+Fyc;

```

```

78     FZ=FA(3)+FB(3)+FC(3)+FD(3)+Fzc;
79     b1=MX;b2=MY;b3=MZ;b4=FY;b5=FZ;
80     B=[b1;b2;b3;b4;b5];
81     C=A1\B;
82     C1=[C(1)*1000;C(2)*1000;C(3)/radasec;C(4)/radasec;C(5)/radasec];
83     dy01=C1(1);dz01=C1(2);ex01=C1(3);
84     ey01=C1(4);ez01=C1(5);
85     end

```

C. Monte Carlo Simulation for Linear Bearings Accuracy Analysis

```

1     a0=-8/1000;
2     b0=8/1000;
3     p=100000;
4     dy01=zeros(1,p);dz01=zeros(1,p);
5     ex01=zeros(1,p);ey01=zeros(1,p);ez01=zeros(1,p);
6     for r=1:p
7         [dy01(r),dz01(r),ex01(r),ey01(r),ez01(r)]=linearbalance5(a0,b0);
8     end
9     close all
10    figure(1)
11        hist(dy01,100)
12        xlabel('\delta_y [\mum]'); ylabel('Frequency')
13        title(['2\sigma = ' num2str(2*std(dy01)) ' \mum'])
14    figure(2)
15        hist(dz01,100)
16        xlabel('\delta_z [\mum]'); ylabel('Frequency')
17        title(['2\sigma = ' num2str(2*std(dz01)) ' \mum'])
18    figure(3)
19        hist(ex01,100)
20        xlabel('\epsilon_x [arcsec]'); ylabel('Frequency')

```

```

21     title(['2\sigma = ' num2str(2*std(ex01)) ' arcsec'])
22     figure(4)
23     hist(ey01,100)
24     xlabel('\epsilon_y [arcsec]'); ylabel('Frequency')
25     title(['2\sigma = ' num2str(2*std(ey01)) ' arcsec'])
26     figure(5)
27     hist(ez01,100)
28     xlabel('\epsilon_z [arcsec]'); ylabel('Frequency')
29     title(['2\sigma = ' num2str(2*std(ez01)) ' arcsec'])

```

D. Rotary Bearings Accuracy Analysis Function

```

1     function [dx10,dy10,dz10,ex10,ey10] = rotarybalance4(a0,b0)
2     %Unit Conversions
3     radasec=pi/(180*3600);
4     %Geometric Parameters
5     r=15;
6     zd=16;
7     %Number of Balls
8     c=12;
9     %Stiffness
10    k=5e8;
11    %External Forces
12    Fxt=100;Fyt=100;Fzt=100;Rx=150;Ry=150;Rz=150;Weight=350;
13    [Mxc,Myc,Mzc,Fxc,Fyc,Fzc]=CenterForces(Fxt,Fyt,Fzt,Rx,Ry,Rz,Weight);
14    %Generating Random Errors
15    a = a0;b = b0;
16    ra = (b-a).*rand(c,1) + a;
17    rb = (b-a).*rand(c,1) + a;
18    rz = (b-a).*rand(c*2,1) + a;
19    %for numeric solution L=[dx1 dy1 dz1 ex1 ey1]
20    L = [.0001 .0001 .0001 .00001 .00001];

```

```

21  for i=1:5
22      D(i,i)=L(i);
23  end
24  for j = 1:5
25      dx1=D(1,j);dy1=D(2,j);dz1=D(3,j);
26      ex1=D(4,j);ey1=D(5,j);
27      T= [1 0 ey1 dx1; 0 1 -ex1 dy1; -ey1 ex1 1 dz1; 0 0 0 1];
28      %Ideal locations
29      for i=1:12
30          PA(1,i)=r*cosd(i*30-30);
31          PA(2,i)=r*sind(i*30-30);
32          PA(3,i)=zd;
33          PA(4,i)=1;
34          PB(1,i)=r*cosd(i*30-30);
35          PB(2,i)=r*sind(i*30-30);
36          PB(3,i)=-zd;
37          PB(4,i)=1;
38      end
39      %Actual Positions
40      for i=1:12
41          POA(:,i)=T*PA(:,i);
42          POB(:,i)=T*PB(:,i);
43      end
44      for i=1:12
45          dA1(:,i)=PA(:,i)-POA(:,i);
46          dB1(:,i)=PB(:,i)-POB(:,i);
47      end
48      %Actual position of bearing a
49      for i=1:c
50          xa(i)=(r+ra(i))*cosd(i*360/c-360/c);
51          ya(i)=(r+ra(i))*sind(i*360/c-360/c);
52          za(i)=zd+rz(i);
53      end

```

```

54     %Actual position of bearing b
55     for i=1:c
56         xb(i)=(r+rb(i))*cosd(i*360/c-360/c);
57         yb(i)=(r+rb(i))*sind(i*360/c-360/c);
58         zb(i)=zd+rz(i+12);
59     end
60     %stiffness for a and b based on location
61     for i=1:c
62         k1(1,i)=k*cosd(i*360/c-360/c);
63         k1(2,i)=k*sind(i*360/c-360/c);
64         k1(3,i)=k;
65         k1(4,i)=0;
66     end
67     % actual position matrix for A and B
68     % |x1 x2 ... x12|
69     % |y1 y2 ... y12|
70     % |z1 z2 ... z12|
71     % |..... 0.....|
72     for i=1:c
73         A(1,i)=xa(i);B(1,i)=xb(i);
74         A(2,i)=ya(i);B(2,i)=yb(i);
75         A(3,i)=za(i);B(3,i)=zb(i);
76         A(4,i)=0;B(4,i)=0; %check
77     end
78     for i=1:c
79         A(1,i)=A(1,i)+dA1(1,i);B(1,i)=B(1,i)+dB1(1,i);
80         A(2,i)=A(2,i)+dA1(2,i);B(2,i)=B(1,i)+dB1(2,i);
81         A(3,i)=A(3,i)+dA1(3,i);B(3,i)=B(1,i)+dB1(3,i);
82         A(4,i)=0;B(4,i)=0; %check
83     end
84     A=A-PA; B=B-PB;
85     for i=1:12
86         FA1(1,i)=k1(1,i)*A(1,i);

```

```

87         FA1(2,i)=k1(2,i)*A(2,i);
88         FA1(3,i)=k1(3,i)*A(3,i);
89         FA1(4,i)=0;
90         FB1(1,i)=k1(1,i)*B(1,i);
91         FB1(2,i)=k1(2,i)*B(2,i);
92         FB1(3,i)=k1(3,i)*B(3,i);
93         FB1(4,i)=0;
94     end
95     %Total moments and forces in x y and z directions
96     Msum=0;Fx=0;Fy=0;Fz=0;
97     Msum=cross(PA(1:3,1)',FA1(1:3,1)')+cross(PA(1:3,2)',FA1(1:3,2)')...
98     +cross(PA(1:3,3)',FA1(1:3,3)')+cross(PB(1:3,1)',FB1(1:3,1)')...
99     +cross(PB(1:3,2)',FB1(1:3,2)')+cross(PB(1:3,3)',FB1(1:3,3)');
100     Mx=Msum(1)+Mxc;My=Msum(2)+Myc;
101     FC1=FA1+FB1;
102     Fx=FC1(1,1)+FC1(1,2)+FC1(1,3)+FC1(1,4)+Fxc;
103     Fy=FC1(2,1)+FC1(2,2)+FC1(2,3)+FC1(2,4)+Fyc;
104     Fz=FC1(3,1)+FC1(3,2)+FC1(3,3)+FC1(3,4)+Fzc;
105     %Second Part-----Second Part
106     %Second Part-----Second Part
107     %Second Part-----Second Part
108     dx1=-D(1,j);dyl=-D(2,j);dz1=-D(3,j);
109     ex1=-D(4,j);ey1=-D(5,j);
110     T= [1 0 ey1 dx1; 0 1 -ex1 dyl; -ey1 ex1 1 dz1; 0 0 0 1];
111     %Ideal locations
112     for i=1:12
113         PA(1,i)=r*cosd(i*30-30);
114         PA(2,i)=r*sind(i*30-30);
115         PA(3,i)=zd;
116         PA(4,i)=1;
117         PB(1,i)=r*cosd(i*30-30);
118         PB(2,i)=r*sind(i*30-30);

```

```

119         PB(3,i)=-zd;
120         PB(4,i)=1;
121     end
122     %Actual Positions
123     for i=1:12
124         POA(:,i)=T*PA(:,i);
125         POB(:,i)=T*PB(:,i);
126     end
127     for i=1:12
128         dA1(:,i)=PA(:,i)-POA(:,i);
129         dB1(:,i)=PB(:,i)-POB(:,i);
130     end
131     %Actual position of bearing a
132     for i=1:c
133         xa(i)=(r+ra(i))*cosd(i*360/c-360/c);
134         ya(i)=(r+ra(i))*sind(i*360/c-360/c);
135         za(i)=zd+rz(i);
136     end
137     %Actual position of bearing b
138     for i=1:c
139         xb(i)=(r+rb(i))*cosd(i*360/c-360/c);
140         yb(i)=(r+rb(i))*sind(i*360/c-360/c);
141         zb(i)=zd+rz(i+12);
142     end
143     %stiffness for a and b based on location
144     for i=1:c
145         k1(1,i)=k*cosd(i*360/c-360/c);
146         k1(2,i)=k*sind(i*360/c-360/c);
147         k1(3,i)=k;
148         k1(4,i)=0;
149     end
150     % actual position matrix for A and B
151     % |x1 x2 ... x12|

```

```

152     % |y1 y2 ... y12|
153     % |z1 z2 ... z12|
154     % |..... 0.....|
155     for i=1:c
156         A(1,i)=xa(i);B(1,i)=xb(i);
157         A(2,i)=ya(i);B(2,i)=yb(i);
158         A(3,i)=za(i);B(3,i)=zb(i);
159         A(4,i)=0;B(4,i)=0; %check
160     end
161     for i=1:c
162         A(1,i)=A(1,i)+dA1(1,i);B(1,i)=B(1,i)+dB1(1,i);
163         A(2,i)=A(2,i)+dA1(2,i);B(2,i)=B(1,i)+dB1(2,i);
164         A(3,i)=A(3,i)+dA1(3,i);B(3,i)=B(1,i)+dB1(3,i);
165         A(4,i)=0;B(4,i)=0; %check
166     end
167     A=A-PA; B=B-PB;
168     for i=1:12
169         FA1(1,i)=k1(1,i)*A(1,i);
170         FA1(2,i)=k1(2,i)*A(2,i);
171         FA1(3,i)=k1(3,i)*A(3,i);
172         FA1(4,i)=0;
173         FB1(1,i)=k1(1,i)*B(1,i);
174         FB1(2,i)=k1(2,i)*B(2,i);
175         FB1(3,i)=k1(3,i)*B(3,i);
176         FB1(4,i)=0;
177     end
178     %Total moments and forces in x y and z directions
179     Msum=0;FX=0;FY=0;FZ=0;
180     Msum=cross(PA(1:3,1)',FA1(1:3,1)')+cross(PA(1:3,2)',FA1(1:3,2)')...
181     +cross(PA(1:3,3)',FA1(1:3,3)')+cross(PB(1:3,1)',FB1(1:3,1)')...
182     +cross(PB(1:3,2)',FB1(1:3,2)')+cross(PB(1:3,3)',FB1(1:3,3)');
183     MX=Msum(1)+Mxc;MY=Msum(2)+Myc;

```

```

184     FC1=FA1+FB1;
185     FX=FC1(1,1)+FC1(1,2)+FC1(1,3)+FC1(1,4)+Fxc;
186     FY=FC1(2,1)+FC1(2,2)+FC1(2,3)+FC1(2,4)+Fyc;
187     FZ=FC1(3,1)+FC1(3,2)+FC1(3,3)+FC1(3,4)+Fzc;
188     %Finding component of A1
189     div=L(j)*2;
190     A1(1,j)=(Mx-MX)/(div);A1(2,j)=(My-MY)/(div);
191     A1(3,j)=(Fx-FX)/(div);A1(4,j)=(Fy-FY)/(div);A1(5,j)=(Fz-
FZ)/(div);
192 end
193
194 %For Final solution
195 dx1=0;dy1=0;dz1=0;
196 ex1=0;ey1=0;ez1=0;
197 T= [1 -ez1 ey1 dx1; ez1 1 -ex1 dy1; -ey1 ex1 1 dz1; 0 0 0 1];
198 %Ideal locations
199     for i=1:12
200         PA(1,i)=r*cosd(i*30-30);
201         PA(2,i)=r*sind(i*30-30);
202         PA(3,i)=zd;
203         PA(4,i)=1;
204         PB(1,i)=r*cosd(i*30-30);
205         PB(2,i)=r*sind(i*30-30);
206         PB(3,i)=-zd;
207         PB(4,i)=1;
208     end
209     %Actual Positions
210     for i=1:12
211         POA(:,i)=T*PA(:,i);
212         POB(:,i)=T*PB(:,i);
213     end
214     for i=1:12
215         dA1(:,i)=PA(:,i)-POA(:,i);
216         dB1(:,i)=PB(:,i)-POB(:,i);

```

```

217     end
218     %Actual position of bearing a
219     for i=1:c
220         xa(i)=(r+ra(i))*cosd(i*360/c-360/c);
221         ya(i)=(r+ra(i))*sind(i*360/c-360/c);
222         za(i)=zd+rz(i);
223     end
224     %Actual position of bearing b
225     for i=1:c
226         xb(i)=(r+rb(i))*cosd(i*360/c-360/c);
227         yb(i)=(r+rb(i))*sind(i*360/c-360/c);
228         zb(i)=zd+rz(i+12);
229     end
230     %stiffness for a and b based on location
231     for i=1:c
232         k1(1,i)=k*cosd(i*360/c-360/c);
233         k1(2,i)=k*sind(i*360/c-360/c);
234         k1(3,i)=k;
235         k1(4,i)=0;
236     end
237     % actual position matrix for A and B
238     % |x1 x2 ... x12|
239     % |y1 y2 ... y12|
240     % |z1 z2 ... z12|
241     % |..... 0.....|
242     for i=1:c
243         A(1,i)=xa(i);B(1,i)=xb(i);
244         A(2,i)=ya(i);B(2,i)=yb(i);
245         A(3,i)=za(i);B(3,i)=zb(i);
246         A(4,i)=0;B(4,i)=0; %check
247     end
248     for i=1:c
249         A(1,i)=A(1,i)+dA1(1,i);B(1,i)=B(1,i)+dB1(1,i);

```

```

250     A(2,i)=A(2,i)+dA1(2,i);B(2,i)=B(1,i)+dB1(2,i);
251     A(3,i)=A(3,i)+dA1(3,i);B(3,i)=B(1,i)+dB1(3,i);
252     A(4,i)=0;B(4,i)=0; %check
253     end
254     A=A-PA; B=B-PB;
255     for i=1:12
256         FA1(1,i)=k1(1,i)*A(1,i);
257         FA1(2,i)=k1(2,i)*A(2,i);
258         FA1(3,i)=k1(3,i)*A(3,i);
259         FA1(4,i)=0;
260         FB1(1,i)=k1(1,i)*B(1,i);
261         FB1(2,i)=k1(2,i)*B(2,i);
262         FB1(3,i)=k1(3,i)*B(3,i);
263         FB1(4,i)=0;
264     end
265     %Total moments and forces in x y and z directions
266     Msum=0;FX=0;FY=0;FZ=0;
267     Msum=cross(PA(1:3,1)',FA1(1:3,1)')+cross(PA(1:3,2)',FA1(1:3,2)')...
268     +cross(PA(1:3,3)',FA1(1:3,3)')+cross(PB(1:3,1)',FB1(1:3,1)')...
269     +cross(PB(1:3,2)',FB1(1:3,2)')+cross(PB(1:3,3)',FB1(1:3,3)');
270     MX=Msum(1)+Mxc;MY=Msum(2)+Myc;
271     FC1=FA1+FB1;
272     FX=FC1(1,1)+FC1(1,2)+FC1(1,3)+FC1(1,4)+Fxc;
273     FY=FC1(2,1)+FC1(2,2)+FC1(2,3)+FC1(2,4)+Fyc;
274     FZ=FC1(3,1)+FC1(3,2)+FC1(3,3)+FC1(3,4)+Fzc;
275     b1=MX;b2=MY;b3=FX;b4=FY;b5=FZ;
276     B=[b1;b2;b3;b4;b5];
277     C=A1\B;
278     C1=[C(1)*1000;C(2)*1000;C(3)*1000;C(4)/radasec;C(5)/radasec];
279     dx10=C1(1);dy10=C1(2);dz10=C1(3);
280     ex10=C1(4);ey10=C1(5);
281     end

```

E. Monte Carlo Simulation for Rotary Bearings Accuracy Analysis

```
1  %Setting Error Boundaries
2  a0=-3/1000;
3  b0=3/1000;
4  p=10000; %Number of solution
5  dx10=zeros(1,p);dy10=zeros(1,p);dz10=zeros(1,p);
6  ex10=zeros(1,p);ey10=zeros(1,p);ez10=zeros(1,p);
7  for r=1:p
8      [dx10(r),dy10(r),dz10(r),ex10(r),ey10(r)]=rotarybalance4(a0,b0);
9  end
10 close all
11 figure(1)
12     hist(dx10,100)
13     xlabel('\delta_x [\mum]'); ylabel('Frequency')
14     title(['2\sigma = ' num2str(2*std(dx10)) ' \mum'])
15     figure(2)
16     hist(dy10,100)
17     xlabel('\delta_y [\mum]'); ylabel('Frequency')
18     title(['2\sigma = ' num2str(2*std(dy10)) ' \mum'])
19     figure(3)
20     hist(dz10,100)
21     xlabel('\delta_z [\mum]'); ylabel('Frequency')
22     title(['2\sigma = ' num2str(2*std(dz10)) ' \mum'])
23     figure(4)
24     hist(ex10,100)
25     xlabel('\epsilon_x [arcsec]'); ylabel('Frequency')
26     title(['2\sigma = ' num2str(2*std(ex10)) ' arcsec'])
27     figure(5)
28     hist(ey10,100)
29     xlabel('\epsilon_y [arcsec]'); ylabel('Frequency')
30     title(['2\sigma = ' num2str(2*std(ey10)) ' arcsec'])
31 end
```

F. Center Forces

```
1  function
   [Mxc,Myc,Mzc,Fxc,Fyc,Fzc]=CenterForces(Fxt,Fyt,Fzt,Rx,Ry,Rz,Weight)
2  %Amplitude of the forces
3  a = -Fxt;b = Fxt;F1 = (b-a).*rand(1,1) + a;
4  a = -Fyt;b = Fyt;F2 = (b-a).*rand(1,1) + a;
5  a = -Fzt;b = Fzt;F3 = (b-a).*rand(1,1) + a;
6  B1=[F1 F2 F3];
7  %Location of the forces R1,R2,R3
8  a = -Rx;b = Rx;R1 = (b-a).*rand(1,1) + a;
9  a = -Ry;b = Ry;R2 = (b-a).*rand(1,1) + a;
10 a = 0;b = Rz;R3 = (b-a).*rand(1,1) + a;
11 A1=[R1 R2 R3];
12 %Amplitude of the Weight
13 a = 0;b = Weight;W3 = (b-a).*rand(1,1) + a;
14 B2=[0,0,-W3];
15 %Location of Weight R1,R2,R4
16 R4=R3/2;
17 A2=[0,0,R4];
18 %Total moments and forces in x y and z directions
19     Mtot=0;
20     Mtot=cross(A1,B1)+cross(A2,B2);
21     Mx=Mtot(1);My=Mtot(2);Mz=Mtot(3);
22     Fx=F1;
23     Fy=F2;
24     Fz=F3-W3;
25     Mxc=Mx;Myc=My;Mzc=Mz;Fxc=Fx;Fyc=Fy;Fzc=Fz;
26 end
```

CURRICULUM VITAE

PERSONAL INFORMATION

Surname, Name : Yılmaz, Yunus Emre
Nationality : Turkish (TC)
Date and Place of Birth : 21 October 1992, Altındağ, Ankara
Phone : +90 507 149 20 92
E-mail : e180272@metu.edu.tr

EDUCATION

Degree	Institution	Year of Graduation
MS	METU Mechanical Engineering	2019
BS	METU NCC Mechanical Engineering	2015
High School	Hürriyet Anadolu Lisesi, Ankara	2010

WORK EXPERIENCE

Year	Place	Enrollment
2019 May-Present	METU	Teaching Assistant
2018 Jan-Present	METU	Research Assistant
2017 Aug-Dec	ProMec Mühendislik Ltd. Şti.	Mechanical Design Engineer

FOREIGN LANGUAGES

Turkish (Native), Advanced English, Elementary German

HOBBIES

Scuba Diving, Swimming, Playing Volleyball and Football, Cycling